

UNIVERSITA' DEGLI STUDI DI MILANO

LA STATALE



PhD program

in Experimental Medicine and Medical Biotechnologies

XXXII cycle

PhD Thesis

**Functional genomic approaches to sensitize hematological
malignancies to proteasome inhibitors**

PhD student

Tutor

Cecilia Bandini

Prof. Antonino Neri

September 2019

Index

1. Abstract	6
2. Introduction	7
2.1. Multiple myeloma: an overview	7
2.1.1. Multiple myeloma and microenvironment	9
2.1.2. Genomic and epigenomic complexity of multiple myeloma	12
2.2. Existing and novel therapies for the management of multiple myeloma	16
2.2.1. Proteasome inhibitors	17
2.2.2. Immunomodulatory drugs (IMiDs)	20
2.2.3. Monoclonal antibodies (mAbs)	22
2.2.4. Epigenetics drugs	23
2.3. Resistances in multiple myeloma	25
2.3.1. Proteasome inhibitors: different resistance-driving mechanisms	25
2.3.2. IMiD resistances	26
2.3.3. Resistance to mAbs	27
2.4. Synthetic lethality approach: finding novel therapeutic targets with functional screenings.....	27
3. Aim of the study	31
4. Materials and Methods.....	32
4.1. Cell culture conditions and reagents	32
4.2. Lentivirus production and in vitro transduction	32
4.3. Plasmids constructs and cloning of gRNAs.....	33
4.4. SIRT3 construct	34
4.5. IDH2 and LSD1 constructs	34
4.6. shSIRT3	34
4.7. Generation of inducible cell lines	35
4.8. shRNA screening	35

4.9.	Purification of total RNA and Reverse Transcription-quantitative Polymerase Chain Reaction (RT-qPCR)	36
4.10.	DNA sequencing	36
4.11.	Western Blotting	37
4.12.	Gene Expression Profiling	37
4.13.	Analysis of apoptosis, cell cycle and cell differentiation	38
4.14.	Reactive oxygen species (ROS) production	38
4.15.	Mitochondria isolation	38
4.16.	NF- κ B activity	39
4.17.	Tricarboxylic acid (TCA) cycle measurement.....	39
4.18.	IDH enzymatic activity	39
4.19.	Measurement of complex I–III activity	40
4.20.	ATP measurement.....	40
4.21.	Xenograft models.....	40
4.22.	Drug synergy.....	41
4.23.	Statistical analysis.....	41
5.	Results.....	42
5.1.	Generation of PI-resistant MM cell lines.....	42
5.2.	shRNA screening in multiple myeloma cell lines identifies 3 synthetic lethal targets to the proteasome inhibitor carfilzomib	44
5.3.	IDH2 inhibition sensitize PI-resistant MM cell lines to carfilzomib.....	45
5.4.	AGI-6780 selectively impairs IDH2 enzymatic activity in MM cells.....	48
5.5.	Pharmacological inhibition of IDH2 enhances sensitivity to CFZ in MM cell lines.....	49
5.6.	CFZ/AGI-6780 regimen elicits significant changes converging in cell cycle and apoptotic pathways	52
5.7.	IDH2 inhibition synergizes with first- and second-generation PIs in multiple myeloma cells	54
5.8.	IDH2 inhibition synergizes with PI in B-cell hematological malignancies.....	55
5.9.	IDH2 overactivity is able to decrease sensibility to CFZ treatment	57

5.10. CFZ/AGI-6780 combinatorial treatment decreases TCA cycle activity and mitochondrial ATP production.....	59
5.11. Combinatorial treatment with CFZ and AGI-6780 acts through the inhibition of the NAMPT/SIRT3/IDH2 pathway	61
5.12. Generation of inducible shIDH2 MM cell lines for in vivo studies	65
5.13. Targeting IDH2 and proteasome activities triggers synergistic inhibition of human MM cells growth ex-vivo and in vivo with low toxicity to normal human cells.....	67
5.14. LSD1 silencing sensitizes PI-resistant MM cells to carfilzomib treatment.....	72
5.15. Synthetic lethal interaction between LSD1 silencing and CFZ treatment is recapitulated in MM-sensitive cell lines.....	74
5.16. LSD1 inhibitors are effective in MOLM-13 AML cell line	76
5.17. LSD1 pharmacological inhibition enhances sensitivity to CFZ treatment in MM cell lines	79
5.18. GSK LSD1 inhibitors are not able to sensitize MM cells to CFZ treatment.....	81
5.19. Overexpression of endogenous and exogenous LSD1 as in vitro models to access SP2509 specificity	82
6. Discussion.....	86
7. References	91

1. Abstract

Proteasome inhibitors (PIs) are extensively used for the therapy of multiple myeloma (MM) and mantle-cell lymphoma (MCL). Nevertheless, patients continuously relapse or are intrinsically resistant to PIs.

Here, to identify druggable targets that synergize with PIs, we carried out a functional screening in MM cell lines using a shRNA library targeting cancer driver genes. The Isocitrate Dehydrogenase 2 (IDH2) and Lysin Specific-Demethylases 1 (LSD1) genes were identified as top candidates, showing a synthetic lethal activity with the PI Carfilzomib (CFZ). We first validated the role of IDH2 in mediating PIs sensitivity. Combinations of the pharmacological IDH2 inhibitor AGI-6780 with FDA approved PIs significantly increased apoptotic cell death in ten MM cell lines, both sensitive and resistant to PIs. Combined treatments triggered synergistic cytotoxicity also in others hematological malignancies, such as Burkitt's lymphoma, mantle cell lymphoma and diffuse large B-cell lymphoma. Importantly, CFZ/AGI-6780 treatment increased death of primary MM cells from nine patients and exhibited a favorable cytotoxicity profile towards normal human cells. Mechanistically, CFZ/AGI-6780 combination decreased TCA cycle activity and ATP levels, due to enhanced IDH2 enzymatic inhibition. Specifically, CFZ treatment decreased nicotinamide phosphoribosyltransferase (NAMPT) expression, a rate-limiting enzyme required for IDH2 activation, through the NAD⁺-dependent deacetylase SIRT3. Consistently, combination of CFZ with either NAMPT or SIRT3 inhibitors impaired IDH2 activity and increased MM cells death, thus phenocopying CFZ/AGI-6780 effects and putting the proteasome in a direct link with IDH2 inhibition. Moreover, inducible IDH2 knock-down enhanced the therapeutic efficacy of CFZ in xenograft mouse models of MM, resulting in inhibition of tumor progression and extended survival.

Finally, preliminary results also showed that LSD1 may represent a potential therapeutic target to combine with PIs. Indeed, genetic inhibition of LSD1 increased sensitivity to CFZ in MM cell lines, both sensitive and resistant to PIs. Remarkably, treatment with the non-competitive LSD1 inhibitor SP2509 significantly increased CFZ efficacy in eighth out of ten MM cell lines, both sensitive and resistant to PIs. However, GSK2879552 and GSK-LSD1, two LSD1 enzymatic inhibitors, did not display synergistic activity with CFZ, thus establishing the basis for future research of non-canonical functions of LSD1 or alternative SP2509 targets.

In conclusion, our data demonstrate that IDH2 inhibition increases the therapeutic efficacy of PIs, thus providing compelling evidence for treatments with lower and less toxic doses and broadening the application of PIs to other malignancies. Moreover, preliminary results suggest LSD1 targeting as an alternative promising strategy to enhance PIs sensitivity in multiple myeloma.

2. Introduction

2.1. Multiple myeloma: an overview

Multiple myeloma, (MM) also known as plasma cell myeloma, accounts for 1,8% of all tumors worldwide and it is the second most common hematological cancer after non-Hodgkin lymphoma. Each year, in the United States, the newly diagnosed cases are more than 32.000 and above 13.000 are the myeloma-related deaths¹. The United States and other highly developed countries such as Western Europe and Australia show the highest incidence of the disease.

Interestingly, the ethnic origin defines differences in the risk of myeloma development: people with African roots have a two-to-three-fold increased chance to show the disease respect to Caucasian people². Notably, the risk of myeloma development is also related to pesticides usage³, obesity, pre-existing immunological disorders (e.g. ankylosing spondylitis), exposure to radiations and chemicals (e.g. formaldehyde, acrolein, hair dyers). The disease is more frequent in males rather than in females and the average age of diagnosis is around the seventh decade of life⁴.

Multiple myeloma usually develops starting from a subset of benign conditions known as monoclonal gammopathy of undetermined significance (MGUS)⁵ (Fig. 1). MGUS affects 3% of general population over 50 years of age, while in black people the incidence rate is around 5-8%⁶. Usually, MGUS dyscrasia is diagnosed as a side result of blood tests performed for the evaluation of unrelated clinical conditions. MGUS is characterized by minimum plasmacytosis in the bone marrow and the presence of serum monoclonal protein (M-protein or paraprotein), without any other observed impairment. It is estimated that 15% of MGUS patients progress toward multiple myeloma⁷. In a certain portion of patients, multiple myeloma is preceded by an intermediate stage known as smoldering multiple myeloma (SMM), which can progress to multiple myeloma in time-dependent manner. Specifically, the annual risk of SMM-myeloma progression is 10% per year for the first 5 years, 5% per year during the subsequent 5 years and 1% per year after 10 years⁸. SMM is a pre-cancer condition characterized by higher paraprotein levels and enriched plasma cell population in the bone marrow respect to MGUS, without manifested alterations in the patient.

In addition, 1-4% of myeloma patients could develop a rare and aggressive condition known as plasma cell leukemia (PCL), probably upon clonal transformation. PCL is characterized by peripheral blood plasmacytosis, with splenomegaly and hepatomegaly related to plasma cell accumulation in these organs. PCL is accompanied by severe anemia and thrombocytopenia. The calculated survival is very poor, limited to few months after diagnosis⁹.

Plasma cell myeloma arises from terminally differentiated post-germinal center B cells. Initially, tumor cells are localized in the bone marrow. Subsequently, in advanced stages of the disease, they circulate in the peripheral blood and home to distal tissues and organs. Functional tissue alterations are due to the massive M-protein production and secretion. IgG are overproduced in more than half of the patients, followed by IgA (20% of diagnosed cases), while IgD and IgM are uncommon (2% and 0,5%, respectively). Around 15% of patients display excess of free monoclonal light chains, while a minority of cases are characterized by bi-clonal gammopathy¹⁰. The accumulation of monoclonal proteins in nerves, heart and renal district causes severe organ damages. In the distal nephron, protein accumulation overcomes filtration capacity and leads to renal failure. Considering these events, renal functional impairment is included in the so-called “myeloma-defining events” or CRAB features: hypercalcemia (C), renal insufficiency (R), anemia (A) and bone lytic lesions (B). Other symptoms that can be observed in patients are fatigue, dyspnea, and neurological deficits related to blood hyper viscosity or spinal cord lesions⁷ essential to understand the clinical phase of the disease, in order to follow the best therapeutic protocol. The staging systems today available are the Durie-Salmon System (DSS) and the International Staging System (ISS). The DSS approach was developed starting from 1975 and considers blood values as monoclonal immunoglobulin, calcium, hemoglobin, number of bone lesions and kidney functionality. On the other hand, ISS is based on the quantitation of sera albumin and β_2 -microglobulin. Nowadays, a revised (R) version of ISS, considering genetic alterations and additional hematic parameters, is the most widely used. For instance, standard-risk MM patients are characterized by the translocations t(4;14)(p16;q32) or t(14;16)(q32;q23), and the absence of del(17p), with an average patient survival around 50 months. In high-risk disease, there is at least one of the previously mentioned alterations and the mean survival at diagnosis is reduced at 24,5 months. The R-ISS system also includes the serum level of lactate dehydrogenase (LDH) as a biomarker for high cell proliferation, the aggressiveness of the pathology, presence of extra-medullary and extra-osseous disease. In the case of elevated LDH, the predicted survival is minor than in all other clinical conditions¹¹. According to R-ISS, multiple myeloma staging is described as:

- ❖ stage I: serum β_2 -microglobulin < 3.5 mg/L and serum albumin \geq 3.5 g/dL; normal LDH levels; standard-risk chromosomal abnormalities;
- ❖ stage II: intermediate condition between stages I and III;
- ❖ stage III: β_2 -microglobulin \geq 5.5 mg/L; very low or any albumin; either high LDH or high-risk chromosomal abnormalities¹¹.

Of course, in the analysis of the single patient, the staging is informative, but several other factors must be considered and taken into account as potential prognostic factors. Among them, the number of circulating plasma cells and their proliferative rate, renal status, plasmablastic morphology and

different co-morbidities (e.g. hypertension, diabetes mellitus) are some of the many elements to analyze regarding the single patient disease evolution.

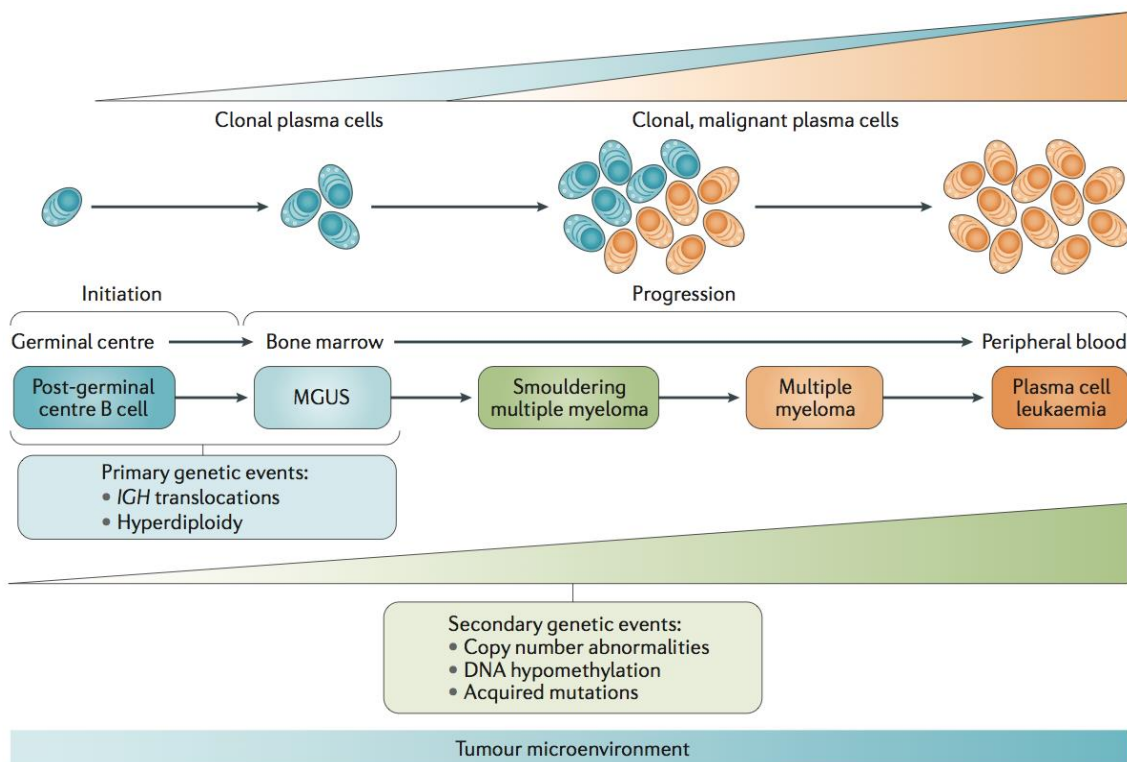


Figure 1. Clonal evolution of monoclonal gammopathies. The conversion between normal post germinal center B cell and pre-malignant or malignant phenotypes involves different genetic events and clonal evolution. In this context MGUS, asymptomatic and symptomatic multiple myeloma and finally plasma cell leukemia disorders are observed. All these states show peculiar features, even if the basis characteristics are shared⁷.

2.1.1. Multiple myeloma and microenvironment

The reason behind hypercalcemia and multiple skeletal lesions can be explained by the crosstalk between multiple myeloma cells and bone marrow stromal population. A variety of extracellular matrix proteins and cellular populations are located in the bone marrow microenvironment. Their interplay with malignant cells can explain tumor homing, support migration and resistance to treatments and local damages¹². Particularly relevant is the role of bone marrow stromal cells (BMSCs) that express vascular cell adhesion molecule 1 (VCAM-1), a ligand for VLA-4 (very late antigen 4 or $\alpha 4\beta 1$ integrin) found on the surface of myeloma cells. The interaction VCAM-1-VLA-4

is one of the mechanisms that allow myeloma cells to home in the bone marrow¹³. The connection of tumor cells with BMSCs also triggers the production of cytokines and mediators that sustain tumor fitness and impair bone homeostasis. One of the altered systems is the OPG:RANK ratio. In normal tissue, osteoclast progenitors express receptor activator of nuclear factor (NF)- κ B (RANK), a transmembrane protein belonging to tumor necrosis factor (TNF) superfamily. RANK ligand (RANKL) is expressed by BMSCs of osteoblastic lineage and activated T-lymphocytes. The binding RANK-RANKL induces osteoclast activity and their genesis. On the other hand, BMSCs and osteoblasts secrete osteoprotegerin (OPG), another TNF cytokine. OPG is defined as a decoy receptor for RANKL: if OPG binds RANKL, it blocks pro-osteoclast events¹⁴. This system is completely deregulated in plasma cell myeloma, where the OPG:RANK ratio is in favor of bone reabsorption (Fig. 2).

Other mediators that induce bone lytic disease via osteoclast stimulation are interleukins (IL-3, 6, 17), TNF- α and MIP1 α . IL-3 and IL-6 are relevantly involved in osteoclast activity promotion. Interleukin 6 (IL-6) is produced by BMSCs, osteoclasts and myeloid precursor cells and its overexpression supports osteoclast activation and tumor cell proliferation¹⁵. IL-3 is also upregulated in myeloma microenvironment: the stimulation on bone marrow macrophages induces activin A production, which favors osteoclasts maturation¹⁴. Additionally, IL-3 has a direct inhibitory effect on osteoblasts formation¹⁶. Moreover, MIP1 α (macrophage inflammatory protein 1- α or CCL3) is secreted by multiple myeloma cells and is known to be a strong inducer of osteoclastogenesis¹⁷, independently on RANKL system (Fig. 2).

Furthermore, osteoblast activity is relevantly impaired in multiple myeloma patients. Key mediators that lead to osteopenia are e.g. RUNX2 and DKK. In addition to bone marrow stromal cells, VCAM-1 can be expressed also by osteoblast progenitors. Therefore, MM cells can interact directly with osteoblastic lineage. In pre-osteoblasts, the cell contact via VCAM-1- α 4 β 1 downregulates the expression of the transcription factor runt-related transcription factor 2 (*RUNX2*). RUNX2 is a transcription factor belonging to the non-canonical WNT signaling pathway and is known to be crucial for osteoblast differentiation and skeletal morphogenesis¹⁸. Osteoblast activity is dramatically impaired by WNT inhibitor Dickkopf-1 (DKK1). DKK1 is secreted by multiple myeloma cells in the bone marrow and blocks the canonical WNT/ β -catenin pathway in BMSCs, preventing their differentiation in mature osteoblasts. Moreover, those immature cells produce IL-6, establishing a positive feedback on MM cells secreting DKK1¹⁹. Furthermore, DKK1 exerts an indirect stimulatory effect on osteoclastogenesis, via increasing the RANKL:OPG ratio²⁰.

Taken together, all those mediators and signaling pathways explain the reason why one of the most relevant manifestations in around 90% of multiple myeloma patients are the severe alterations at the

bone level. Usually, investigation with radiographic imaging is performed in order to define the number and the extension of focal lesions and this information can be used as a prognostic marker. As described, the interplay between myeloma cells and bone marrow microenvironment has consequences in bone metabolism. This relationship also affects tumor growth, survival, migration and drug resistance¹². In addition to VCAM-1-VLA-4, many other mediators promote the homing of MM cells to the bone marrow niche, such as CD44, syndecan 1 (CD138), CD166, and CXCR4 (C-X-C chemokine receptor type 4). CD166 is expressed by myeloma cells and is crucial to allow tumor cell homing in the bone marrow, through homophilic and heterophilic interactions. In addition, CD166 induces a reduction of RUNX2 expression in BMSCs, promoting osteolysis²¹. The axis CXCR4-SDF1 α (stromal cell-derived factor-1 α) is also involved in tumor homing but most importantly it is related to cell motility (Fig. 2). CXCR4, also known as CD184, is expressed on the MM cell surface and binds the SDF1 α chemokine. Upon this interaction, CXCR4 is internalized, cytoskeleton is reconstructed, and the cell is polarized. This leads to the extrusion of pseudopodia, which establishes the chance for malignant cells to migrate²². Once out of the bone marrow, tumor cells can circulate in peripheral blood and colonize all body districts, such as skin, liver, lung, and kidneys.

Another relevant event related to the crosstalk between malignant plasma cells and bone marrow microenvironment is the stimulation of angiogenesis. Cancer cells secrete pro-angiogenic factors as VEGF, FGF-2²³ and proteases able to activate hepatocyte growth factor (HGF), a potent pro-angiogenic mediator that sustains also cell survival²⁴. Importantly, VEGF secretion by MM cells induces an overproduction of IL-6 by BMSCs and microvascular endothelial cells (MVECs), suggesting a paracrine action for VEGF in tumor-stroma interactions²⁵. IL-6 triggers an increment in VEGF release and acts also in the bone remodeling context. In clinics, neovascularization and microvessel density at bone marrow level are used as prognostic markers of adverse significance that correlates with plasma cell proliferation, infiltration and disease progression.

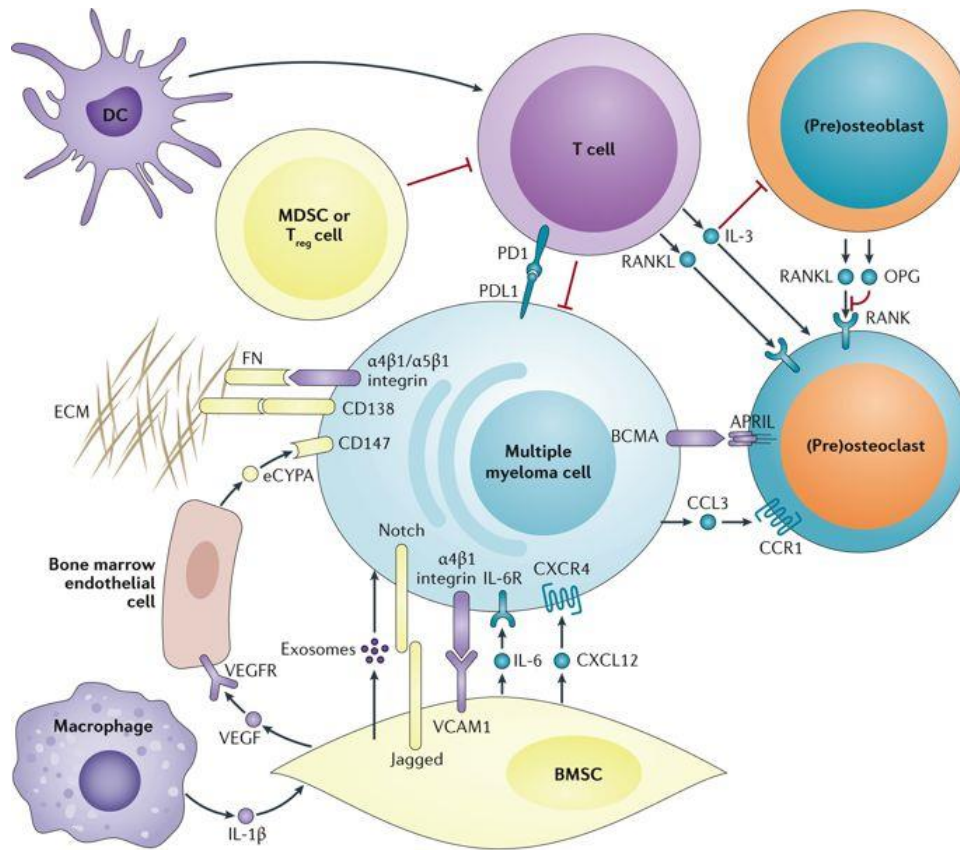


Figure 2. Multiple myeloma cell crosstalk with the tumor microenvironment. The interplay between cancer cells, resident bone marrow cells and secreted factors is crucial to sustain malignant homing in bone niches, cancer proliferation and migration. Bone marrow stromal cells (BMSCs) are the most relevant players, secreting CXCL12 (SDF1 α), which interacts with CXCR4 and contributes to cell mobility. BMSCs expose on the cell surface VCAM1, receptor for α 4 β 1 (VLA-4), contributing to tumor cell homing in bone marrow. Also, IL-6 is secreted by BMSCs, contributing to tumor cell proliferation and osteoclast activation. Myeloma cells are able to stimulate osteoclastogenesis by secreting CCL3 (MIP1 α), further enhanced by dysregulations of the OPG:RANK ratio. The tumor microenvironment is moreover characterized by neoangiogenesis, with release of VEGF by BMSCs and myeloma cells⁷.

2.1.2. Genomic and epigenomic complexity of multiple myeloma

Multiple myeloma is characterized by an extremely variegated set-up of alterations, observed at chromosomal level, at single gene loci, and at epigenetic level. For this reason, MM should be considered a collection of conditions characterized by different genetic make-ups that converge to same phenotypes. The definition of the genetic alterations in a MM patient is instrumental for the classification of the disease and has consistent prognostic and therapeutic implications.

The total chromosome number in myeloma cells can vary non-randomly between 38 and 92. Approximately 55-60% of myeloma patients show hyperdiploidy with trisomies, of chromosomes 9, 15, 19, 5, 3, 11, 7, or 21 (in order of occurrence), and co-occurrence of up to five trisomies in the same karyotype²⁶. The hyperdiploid status has on average 53 chromosomes. Non-hyperdiploid cases are classified as pseudodiploid (less than 48 chromosomes), hypodiploid (on average 44,6 chromosomes) and near-tetraploid (80-93 chromosomes per cell)²⁷. In rare cases myeloma cells are characterized by 30-33 chromosomes, with disomies of 18 and odd-numbered chromosomes or monosomies of chromosomes 1, 13 and even-numbered ones. Considering the disease outcome related to numeric alterations, patients with hypodiploidy show the worst outcome, followed by pseudodiploidy and hyperdiploidy states.

In plasma cell myeloma, several alterations in chromosomal structure can be observed. Translocations and chromosomes arm loss/gain are very frequent. Chromosomal translocations mainly involve *IGH* gene (14q32.3), and less frequently the *IgL* loci (2p12 and 22q11). Immunoglobulin loci are characterized by strong enhancers. Following translocation, Ig enhancers trigger the overexpression of the partner gene. In particular, t(4;14)(p16.3;q32) is observed in almost 15% of myeloma patients. This chromosomal rearrangement leads to the upregulation of fibroblast growth factor receptor 3 (FGFR3) and the myeloma SET domain (MMSET) proteins, which precise roles in myelomagenesis remains to be elucidated. Dysregulated MMSET can be responsible for epigenetic and DNA repair alterations, while the role of FGFR3 is not clear, also because in 30% of patients it is not expressed upon translocation. Very often translocations induce the overexpression of cyclins, as in case of t(6;14) and t(11;14). t(6;14)(p21;q32) is rare and elicits the constitutive expression of cyclin D3 (*CCND3*). On the other hand, the t(11;14)(q13;q32) rearrangement that prompts to cyclin D1 (*CCND1*) overexpression occurs in approximately 17% of myeloma cases. As a consequence of cell cycle overactivation, numerous downstream cellular effectors are deregulated, thus leading to tumor transformation. Other chromosomal rearrangements highlighted in the 5-10% of cases are t(14;16)(q32;q23) and t(14;20)(q32;q11). These events force the expression of *MAF* family oncogenes (*MAF* and *MafB*, respectively), which are related to myeloma cell proliferation through cyclin D2 expression and augmented adhesion to bone marrow stromal cells. In terms of prognosis, the worst outcome is associated to t(14;16) and t(4;14) translocations, while longer survival is coupled to t(11;14). Another indicator of poor prognosis is the overexpression of *MYC* protein as a consequence of t(8;14), an event observed in late stage disease²⁸. Because *MYC* is a master transcription factor gene in B-cells, its dysregulation is reflected by alterations in a large pool of downstream effectors involved in cellular events as metabolism and proliferation²⁹.

Partial chromosomal losses and gain are other peculiar features of multiple myeloma patients. The most frequent and relevant chromosomal alterations are observed in chromosomes 1, 13 and 17, even if also chromosomes 6 and 8 can be altered due to deletions. Approximately 50% of MM cases show deletions of chromosome 13 (del(13q)), with the downregulation of *RBI* tumor suppressor gene³⁰. Chromosome 1 is damaged by gain or amplifications of the big arm in 35-40% of cases³⁰. The genes located in the amplified region of chromosome 1 are not completely explored, even if overexpression of B-cell lymphoma 9 (*BCL-9*) is seen in patients. This leads to an aberrant WNT- β -catenin signaling, giving tumor progression, metastasis and angiogenesis³¹. Considering the short arm of the same chromosome, part of it can be deleted reducing the expression of genes hosted here. Among them, it is possible to find cyclin-dependent kinase inhibitor 2C (*CDKN2C* or *P18*), and *FAF1*, which encodes for a protein involved in apoptosis regulation through the Fas pathway²⁸. A less frequent chromosomal loss is in chromosome 17p, where *TP53* gene is located. In patients, *TP53* expression is reduced³⁰ and this correlates, together with *MYC* translocations in late pathology, to refractory disease and negative outcomes. Not simply entire or parts of chromosomes are altered in MM, but also single gene loci. Tumor suppressor genes are recurrently mutated in many diagnosed cases, leading to deep alterations in downstream pathways. Some examples of altered signaling systems are the RAS/MAPK pathway, mutated in above 40% of patients with alterations on *NRAS*, *KRAS* and *BRAF*. Moreover, the NF- κ B cascade is dysregulated because of alterations on *TRAF3*, *CYLD* and *LTB*. Other examples of altered genes are *TP53*, *FAM46C*, *DIS3*, *HIST1H1E*, *IRF4*, and *MAX*³². Another interesting altered feature of multiple myeloma is its epigenetic set-up. In MGUS and myeloma phases, a general hypomethylation of several genomic regions is observed, when compared to healthy plasma cell controls. This tendency is reverted in case of relapsed tumor, where hypermethylation predominates, mainly at tumor suppressor genes. In MM patients, methylation alterations mainly focus away from CpG islands and are related to genes controlling the expression of targets involved in cell cycle and proliferation. Among hypomethylated loci there are *CEBPa*, interleukins and cognate receptors; considering hypermethylation, this alteration is seen at *CDKN2A*, *CDKN2B*, *CCND2*, *HOX* elements, *SOX*, and *WNT* family members. The reason behind those alterations in the epigenetic status of myeloma cells can be found in a significant dysregulation of the cellular machines responsible for methylation features of the genome. An example is the hypermethylation of *DNMT3a* promoter, followed by a decreased expression of this enzyme in myeloma cells. This allows establishing a hypomethylated status that is connected to a significant impact on survival³³. Apart from methylation, another epigenetic feature that is altered in plasma cell myeloma is histones acetylation. Multiple myeloma is dependent, for its growth and survival, on the activity provided by

histone deacetylases on non-histonic targets. An example is represented by the stabilization elicited by HDAC3 on multiple cellular targets such as MYC, STAT3 and DNMT1; this stabilization is related to the enhanced fitness and apoptosis suppression in tumor cells³⁴.

As described, MM has an extremely variegated pattern of alterations at genetic level. This complexity is related to disease progression and prognosis and the patient's characterization is important in order to define the best and most proficient therapeutic approach.

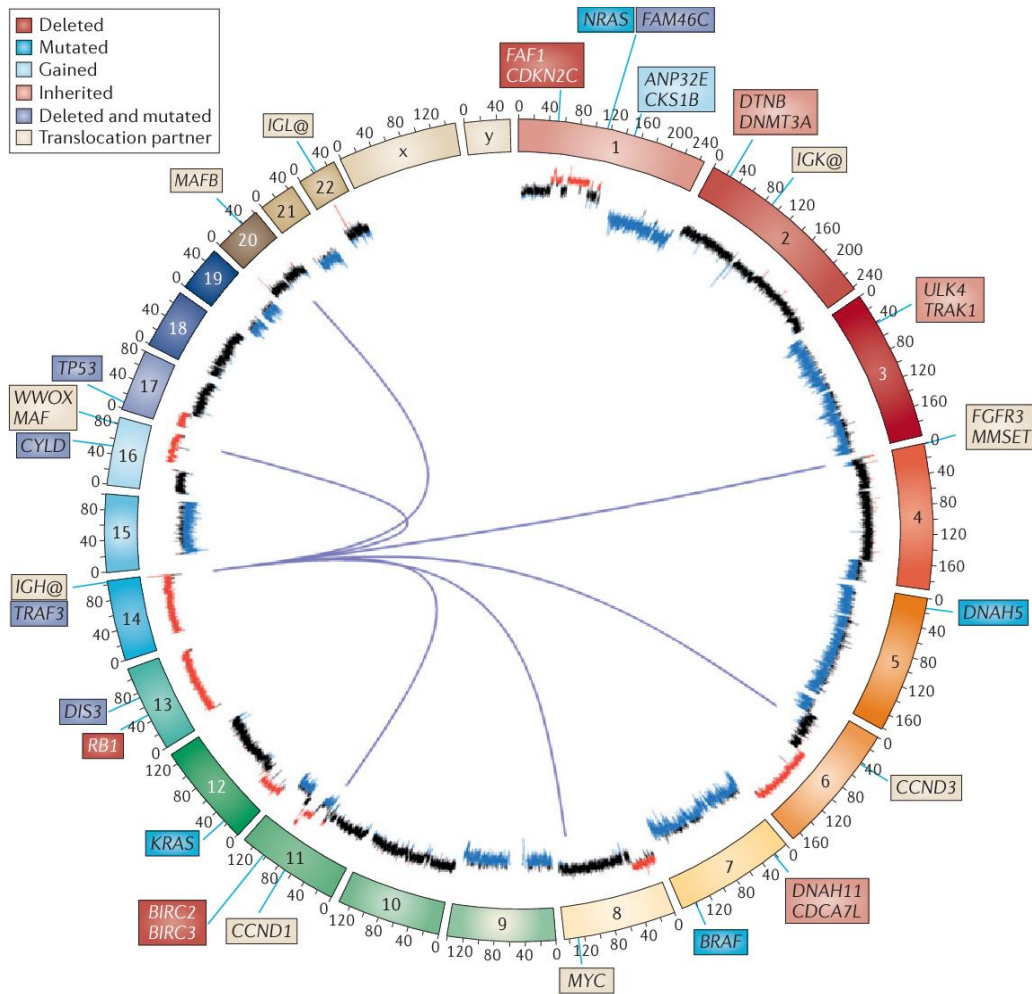


Figure 3. The genetic alterations in multiple myeloma. In the Circos plot translocations, copy number abnormalities and mutations in myeloma are reported. The chromosomes are arranged around the circle. IGH@ translocations are shown as lines emerging from chromosome 14 to the partner chromosomes. Copy number data are reported inside of the circle, showing deletions (red) and gains (blue) as well as normal copy number (black). Genes targeted by deletions and/or mutations are labelled outside the circle and colored according to the abnormality³⁵.

2.2. Existing and novel therapies for the management of multiple myeloma

When a diagnosis of plasma cell alteration is performed, it is necessary to define the best management approach considering the single patient status and its characteristics. In the case of asymptomatic MGUS or SMM usually is adopted a “watch-and-wait” approach, with recurrent evaluations of the clinical status. On the contrary, if MGUS or SMM are defined at high risk of cancer progression, early treatment can be started.

When multiple myeloma is diagnosed, a therapeutic protocol is generally activated, and many options exist to direct the therapies. A classical treatment protocol consists of initial therapy, stem cell transplantation (if eligible), consolidation/maintenance therapy and relapse treatment. The initial or induction therapy has the aim to target and eliminate as much as possible of malignant cells and different drug combinations can be used: lenalidomide plus dexamethasone (Rd); bortezomib, lenalidomide and dexamethasone (VRD); bortezomib, thalidomide and dexamethasone (VTD); bortezomib, cyclophosphamide, and dexamethasone (VCD). This initial therapy is repeated generally four times before autologous stem cell transplantation (ASCT). In recent years, tandem ASCT is also possible by repeating the treatment, with a better prognosis for patients³⁶. Considering transplants, also allogenic cell transfer is a chance, even if its effectiveness is debated^{37,38}. To prepare for ASCT, patients undergo peripheral blood stem cell collection with growth factor support (granulocyte colony-stimulating factor treatment) with or without chemotherapy, followed by myeloablative conditioning and reinfusion of collected stem cells⁷. Melphalan remains the most widely used chemotherapeutic agent in preparative regimens for hematopoietic stem-cell transplantation. Briefly, melphalan is a dialkylating agent, which attaches an alkyl group to the guanine base of DNA, thus producing DNA damage and cell ablation. Melphalan is also used in combination with other alkylating agents and corticosteroids³⁹.

The third treatment step is consolidation or maintenance therapy, a long-lasting treatment of about two years. Usually, it consists in a prolonged therapy with lenalidomide or bortezomib, especially for intermediate and high-risk myeloma cases. During this phase, novel proteasome inhibitors can replace bortezomib, such as ixazomib and carfilzomib. For patients that are not good transplant candidates, direct administration of standard drugs for 12-18 months is the better option, with lenalidomide/bortezomib only or Rd/VRD therapy. Recently, the MPR approach was also tested, by combining melphalan, prednisone, lenalidomide (MPR) followed by lenalidomide maintenance, with promising results⁴⁰. All these prolonged therapies can be protracted until tolerated; only in the final phases of disease, supportive therapy is recommended. Importantly, it is preferable to maintain the initial chosen approach in the following consolidation step³⁶.

Until today, multiple myeloma is not curable: the pathology can be monitored and go in remission but almost all patients develop drugs resistance and relapse. Different rounds of remission and relapse typically characterize plasma cell myeloma. Today, the discovery of novel cellular targets and new treatment options are an urgent need and a research first goal.

2.2.1. Proteasome inhibitors

Proteasome inhibition has emerged as an important therapeutic strategy in multiple myeloma, establishing as one of the standard cares. Proteasome is a cellular machine deputed to the maintenance of proteostasis. Before entering for degradation, the target protein is tagged by a polyubiquitin tag, added in a three-step process. A first ubiquitin-activating enzyme E1 activates ubiquitin in an ATP-dependent manner, creating a high-energy thiol ester intermediate named E1-S-ubiquitin. Subsequently, one among the many E2 enzymes translocates the ubiquitin moiety to the substrate, which is already bound by an E3 enzyme (ubiquitin-protein ligase family). The process is repeated until a polyubiquitin chain is formed (Fig. 4A)⁴¹. The 26S proteasome is composed of a 20S proteasome core particle capped on one or both ends by the 19S regulatory particle (Fig. 4A). It degrades proteins by a multistep process; the 19S regulatory particle binds ubiquitinated substrates, opens a substrate entry gate in 20S, and unfolds its substrates by linearly translocating them into the 20S catalytic chamber, where they are degraded to peptides (Fig. 4A)⁴². Indeed, the eukaryotic 20S proteasome contains six proteolytically active β subunits, three on each β ring, that exhibit different substrate preferences. The chymotrypsin-like site ($\beta 5$) preferentially cleaves after hydrophobic residues, the trypsin-like site ($\beta 2$) preferentially cleaves after basic residues, and the caspase-like site ($\beta 1$) preferentially cleaves after acidic residues^{43,44}.

Proteasome activity is crucial to create fragments starting from full-length proteins that are old, not working, useless or misfolded and that will be subsequently fully degraded to free amino acids. A well operating proteasome machine is crucial to guarantee cellular homeostasis and protein components recycling. In the case of tumor cells, the proteasome activity is particularly important due to the degradation of proteins that would trigger apoptosis in malignant cells. The possibility to block proteasome activity emerged, at the beginning of 2000, as a very promising strategy to induce tumor cells death. As a consequence of proteasome inhibition, the upregulation of pro-apoptotic factors, NF- κ B inhibition, cell cycle arrest and accumulation of polypeptides that lead to endoplasmic reticulum stress are frequent events observed in cells⁴⁵.

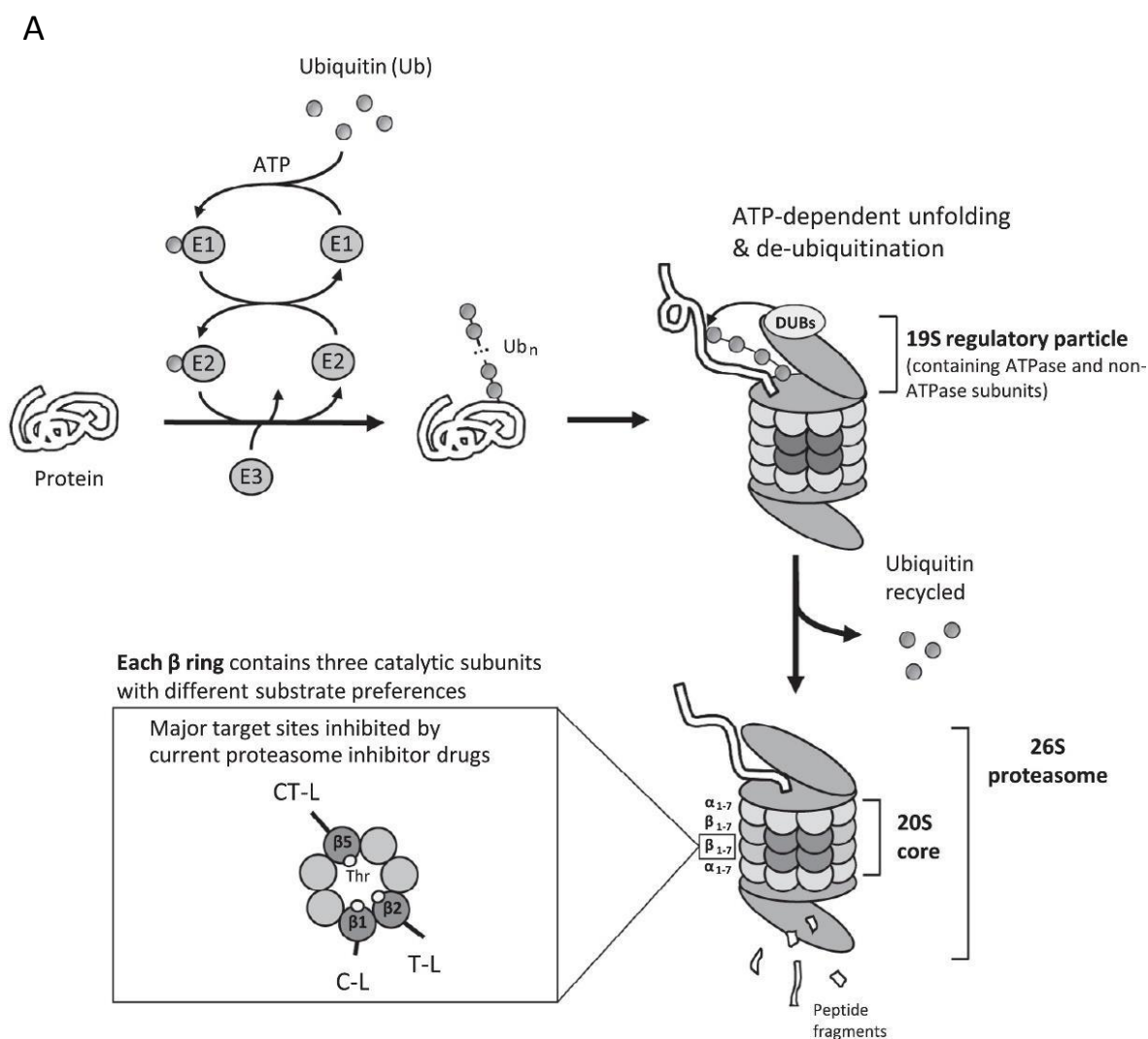
The first FDA approved proteasome inhibitor for the treatment of plasma cell myeloma was bortezomib, in 2003 (Fig. 4B)⁴⁶. The approval was accelerated considering the patient's benefits and

the enhanced survival respect to the existing therapies. This represented a milestone in the management of multiple myeloma. Bortezomib (BTZ) is a boronic acid dipeptide that acts as a reversible inhibitor of the chymotrypsin-like activity of the 26S proteasome ($\beta 5$ subunit). Bortezomib is today used as a front-line agent for novel myeloma diagnosis in combination with immunomodulatory drugs and steroids but it is also useful in the treatment of relapsed and refractory cases⁴⁷. However, the development of widespread resistance to bortezomib and its side effects highlighted the necessity to find alternative compounds able to inhibit proteasome activity. In fact, adverse events are very common and include peripheral neuropathy, thrombocytopenia, neutropenia, anemia, fatigue and diarrhea. The mechanism behind resistance is related to augmented proteasome activity and metabolic adaptation to the selective pressure represented by the drug, as discussed above. Resistant cells show enhanced pentose phosphate pathway, antioxidant capability and serine synthesis pathway⁴⁸.

A good alternative to bortezomib is represented by carfilzomib (CFZ), a second-generation proteasome inhibitor (Fig. 4B). Carfilzomib was developed starting from epoxomicin, a naturally occurring compound able to inhibit the proteasome machine⁴⁹ and approved for myeloma therapy in 2012. Chemically, carfilzomib is a tetrapeptide with an epoxyketone moiety and binds irreversibly to the proteasome $\beta 5$ catalytic subunits in the core region⁴⁷. Its capability to block proteasome chymotrypsin-like activity is much more intense if compared to bortezomib, with an enhanced duration of the effect. Carfilzomib treatment induces apoptosis by increasing caspase 3, 8 and 9 and reduces multiple myeloma cell viability in a dose-dependent manner. It is also able to overcome bortezomib and other antitumor drug resistance both *in vitro* and *ex vivo*⁵⁰. However, it also possesses some aftereffects. Carfilzomib does not induce peripheral neuropathy but can eventually provoke hypertension and heart failure⁵¹.

Another FDA approved second-generation proteasome inhibitor used in plasma cell myeloma management is ixazomib (IXZ), a reversible boronic acid proteasome inhibitor (Fig. 4B). Ixazomib triggers apoptosis in myeloma cell lines, inhibits human myeloma cell growth *in vivo* and prolongs survival in xenograft mouse; moreover, it restrains BMSCs-induced proliferation of tumor cells⁵². In 2015 ixazomib received the FDA approval and, until today, is the only orally administered compound. It is part of the second-line therapy, administered to patients with relapsed or refractory multiple myeloma, whom previously received one of the available therapies⁵¹. Compared to bortezomib and carfilzomib, ixazomib has a better safety profile, and does not induce peripheral neuropathy, thanks to its inability to block neuronal cell survival protease HtrA2/Omi⁵². Classical ixazomib-related side effects are low blood counts, transient rashes and diarrhea. These side effects are limited if compared to those given by previous proteasome inhibitors.

Today, novel third-generation proteasome inhibitor candidates are under evaluation, but still not available for standard human therapy. An example is marizomib; a phase I clinical trial was completed in 2017⁵³ and a phase II is ongoing (NCT00461045) for relapsed/refractory multiple myeloma, while today this compound is in phase III for glioblastoma therapy (NCT03345095). Nonetheless, marizomib administration can lead to few but severe side effects: its capability to pass the blood-brain barrier is significant⁵⁴, with concomitant central nervous system toxicity.



B

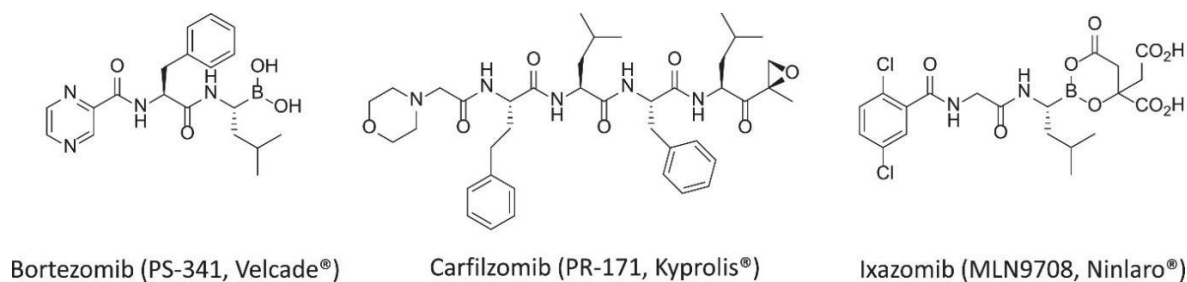


Figure 4. Structure and function of 26S proteasome in the ubiquitin-proteasome system. (A) Proteins targeted for proteasome-mediated degradation are tagged by a polyubiquitin chain, thanks to the action of E1, E2 and E3 enzymes. Ubiquitinated proteins are recognized by the proteasome, unfolded, and de-ubiquitinated by the lid of 26S proteasome (19S regulatory particle). The proteolysis takes place at the inner chamber inside the 20S core, generating short peptide fragments of 2-24 residues⁴⁷. (B) Structures of proteasome inhibitors approved for clinical use⁴⁷.

2.2.2. Immunomodulatory drugs (IMiDs)

In 1998 FDA approved a controversial drug in the management of multiple myeloma: thalidomide. Thalidomide administration was very common in late 50s to treat pregnancy, sickness and anxiety⁵⁵. Once this compound was correlated to newborns malformations, it was withdrawn from market and prohibited. In the 90s the interest about the possibility to restrict tumor angiogenesis allowed to discover thalidomide as a potent blocker of new vessel formation⁵⁶. Thalidomide was the first among the immunomodulatory drugs (*IMiDs*) used in the management of multiple myeloma, followed in recent years by thalidomide analogues lenalidomide (2006) and pomalidomide (2013)⁵⁷ (Fig. 5A). Usually IMiDs are coupled to corticosteroid administration, to enhance their effectiveness. IMiDs show both direct and indirect effects on myeloma cells: direct events are related to the intracellular alterations provoked by the pharmacological compounds, while the indirect results are linked to microenvironmental and immune modulation⁵⁸.

The teratogenicity exerted by thalidomide is related to the drug target cereblon (CRBN, cerebral protein with ion protease). CRBN is part of a DCX (DDB1-CUL4-X-box) E3 protein ligase complex, a system that mediates ubiquitination and proteasomal degradation of different target proteins. Thalidomide teratogenic effects are related to the deregulations of key development signaling pathways such as BMP and FGF8⁵⁹. CRBN-IMiD complex is also responsible for the observed antitumor effect in myeloma treatment. Myeloma cells viability and proliferation is dependent on CRBN, as demonstrated in silencing experiment⁶⁰. The IMiDs molecular mechanism of action is the inhibition of the auto-ubiquitination activity of the CRBN, thus leading to stabilization of the protein and consequent degradation of its numerous targets, such as the zinc finger transcription factors Ikaros (IKZF1) and Aiolos (IKZF3). Thus, IMiDs lead to an indirect downregulation of IKZF1/3 targets, of which the most characterized are IRF4 and MYC^{61,62} (Fig. 5B). Myeloma cells are addicted to IRF4 aberrant network activity⁶³, while IKZF1 and IKZF3 are fundamental transcription factors for plasma cell development and proliferation⁶¹. The binding of IMiD to CRBN is therefore able to alter some

of the most important pathways for multiple myeloma wellness (Fig. 5B). Notably, IMiDs also exert an immunomodulatory effect, by enhancing T cell activation⁶⁴ and NK-mediated myeloma cytotoxicity⁶⁵. Other effects observed upon IMiDs administration, are significant reductions in the release of pro-inflammatory mediators as TNF α , IL-6, IL-1 and IL-12⁶⁶, VEGF and bFGF by BMSCs⁶⁷. A low level of these and other mediators is connected to reduced adhesion of tumor cells in the bone marrow, limited neoangiogenesis, restricted osteoclastogenesis and the establishment of a generally negative condition for the tumor⁶⁷. Moreover, among IMiDs effects it is observed an increment in tumor death via caspase 8 activation and inhibition of anti-apoptotic proteins in myeloma cells⁶⁸, together with permeabilization of mitochondrial membranes.

The second- and third-generation immunomodulatory drugs, lenalidomide and pomalidomide, show a stronger interaction with CRBN respect to thalidomide and, moreover, have an enlarged spectrum of effects. In particular, lenalidomide and pomalidomide upregulate *P21^{WAF}* expression. P21^{WAF} is a CDK2 (Cyclin Dependent Kinase 2) inhibitor and, through retinoblastoma protein-dependent mechanism, it blocks cells in G1 phase.

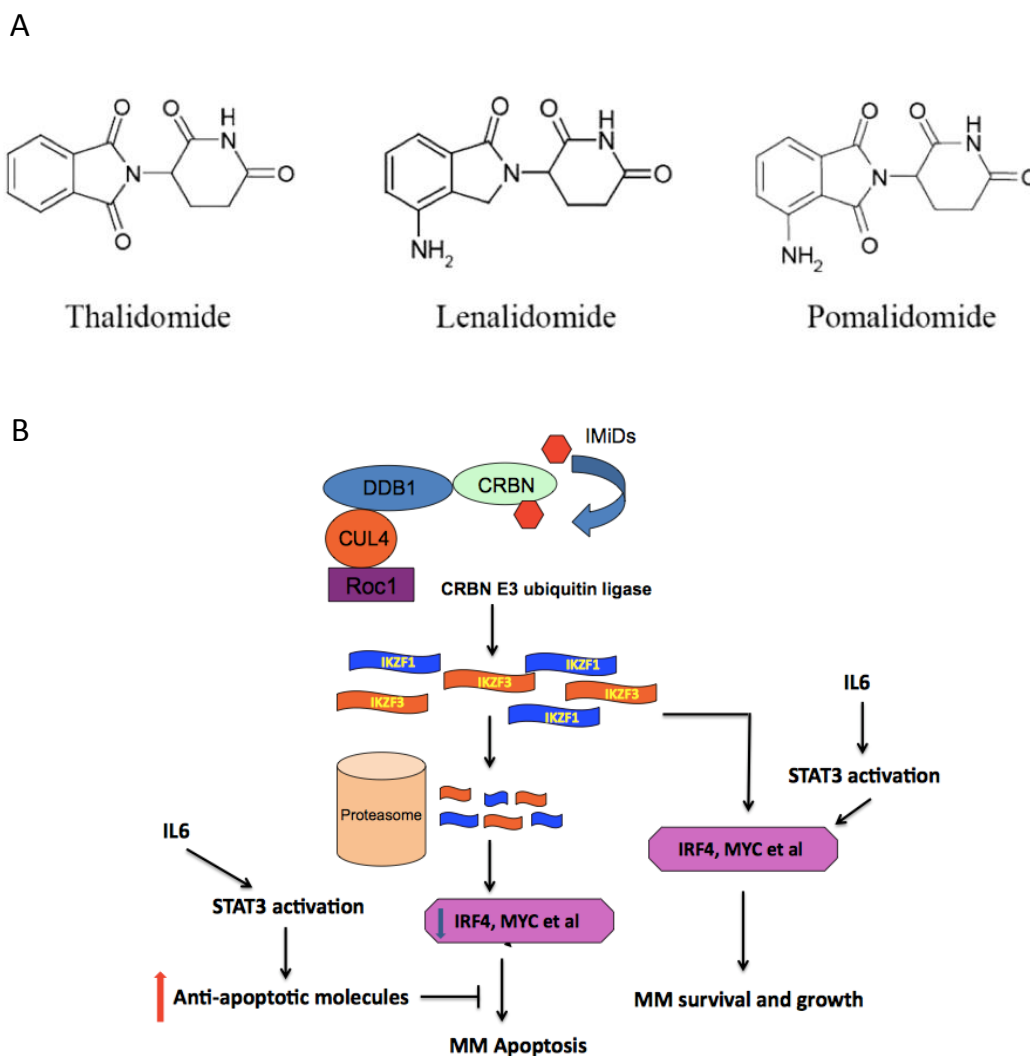


Figure 5. Proposed mechanism of action of IMiDs in myeloma cells. (A) Structural formulas of IMiDs: thalidomide, lenalidomide, pomalidomide⁶⁹. (B) IKZF1/IKZF3 regulate *IRF4*, *MYC*, and other genes to support myeloma cell proliferation and survival. Upon IMiDs treatment, IKZF1/IKZF3 are recognized by CRBN E3 ubiquitin ligase, degraded in the proteasome, resulting in downregulation of IRF4, MYC, and other targets that further induce inhibition of tumor growth and favor apoptosis. Autocrine IL6 activates STAT3 pathway to upregulate anti-apoptotic molecules so to antagonize the apoptotic signals induced by IMiD-mediated IKZF1/IKZF3 and IRF4 downregulation⁷⁰.

2.2.3. Monoclonal antibodies (mAbs)

In recent years, research interest has focused on discovering or design new therapeutic approaches. Immunotherapy has emerged as a promising strategy to fight cancer and today represents one of the main researches in the field of anticancer treatments.

In the treatment of multiple myeloma two FDA approved monoclonal antibodies (mAbs) are applied: daratumumab (DARA) and elotumumab (Elo)⁷¹. Daratumumab is a fully humanized IgG1 κ , targeting CD38⁺ cells. CD38 is a single transmembrane glycoprotein that acts as a surface receptor and as ectoenzyme with cyclic ADP ribose hydrolase activity. It is involved in cell adhesion and regulation of intracellular calcium mobilization. CD38 is normally expressed at low levels by lymphoid and myeloid cells, as well as by non-hematopoietic tissues as epithelia, striated muscle and nerve cells; in multiple myeloma cells it is reported an increased presence of this surface molecule⁷². The application of DARA to myeloma cell lines, primary tumors and xenograft models resulted in significant tumor cell death, via antibody-dependent cell mediated cytotoxicity (ADCC), antibody-dependent cellular phagocytosis (ADCP) and complement-dependent cytotoxicity (CDC)⁷³. Moreover, DARA induces helper and cytotoxic T cell expansion⁷⁴. For these reasons, the anti-CD38 monoclonal antibody was approved for patients who failed at least three previous therapies with immunomodulators and a proteasome inhibitor. Today, two additional anti-CD38 monoclonal antibodies are under clinical evaluation: MOR202 and isatuximab⁷⁵.

Another mAb used in myeloma treatment is elotuzumab, able to target SLAMF7⁺ cells (self-ligand receptor of the signaling lymphocytic activation molecule (SLAM) family member 7). SLAMF7, also called CS1, is a cell surface glycoprotein receptor expressed by normal plasma cells, B and T lymphocytes and by natural killers (NKs). Non-lymphoid tissues are SLAMF7 negative, while it is overexpressed in myeloma, favoring tumor adhesion to bone marrow stromal cells. Elotuzumab is humanized IgG1 mAb that exerts myeloma-cell lysis thanks to the effector activity of NK cells⁷⁶. Additionally, the Elo-CS1 binding on NK surface enhances granzyme release, mediating a direct cancer killing effect independent on the ADCC process⁷⁷. It is important to note that, in 30% of multiple myeloma stage III patients, a significant amount of soluble SLAMF7 is detected in serum and this must be considered as a potential reducing agent in anti-CS1 regimen⁷⁸.

2.2.4. Epigenetic drugs

The last family of anti-myeloma drugs under investigation includes the epigenetic drugs, acting on DNA and histones acetylation and methylation. The only approved compound is panobinostat (LBH589), a hydroxamic acid derivative (Fig. 6). Panobinostat acts as non-selective histone deacetylase inhibitor (pan-HDACi), active against class I (HDACs 1, 2, 3, 8), class II (HDACs 4, 5, 6, 7, 9, 10), and class IV (HDAC 11) deacetylases⁷⁹. In multiple myeloma cell lines and patient-derived cells it was reported a deregulated expression of all classes of histone deacetylase, with a significant overexpression of class I enzymes. Moreover, in patients this feature usually correlates to

a poor outcome⁸⁰. Panobinostat treatment of cell lines, primary samples and mice bearing xenografts, showed reduction in cell viability, mitochondrial alterations and limited cell growth *in vivo*; diminished bone damage was also seen in model animals⁸¹.

The mechanism of action of HDACs as panobinostat is the re-activation of epigenetically silenced genomic regions, corresponding to tumor suppressor genes such as P21⁸².

Panobinostat is able to restrict viability in various myeloma cell lines, also resistant to conventional chemotherapies. The reduced cell survival is related apoptosis activation given by drug-induced cleavage of caspase 8, 9 and 3, as well as PARP⁸³.

Given the pan-HDAC inhibitor action, panobinostat is capable to block the activity of HDAC6, a cellular enzyme crucial for the formation of pericentriolar microtubule-based structure known as aggresome⁸⁴. These structures are involved in the cellular response to the excessive accumulation of misfolded/unfolded proteins; therefore, HDAC6 inhibition can result in failed protein aggregate clearance and reduced cell fitness. This aspect is of note considering the deadly outcome observed *in vitro* upon treatment with panobinostat and bortezomib: in this case a synergistic effect is established between the two drugs⁸³.

Panobinostat treatment is able to upregulate CD38 expression in myeloma cells. Considering that CD38 surface molecule is targeted by daratumumab, an overexpression of the mAb target enhances the immunotherapeutic effect via increased ADCC process. The combination daratumumab-panobinostat is a synergistic anti-myeloma effect⁸⁵.

Other HDACi are not yet approved but in clinical trials for myeloma therapy. Suberoylanilide hydroxamic acid (SAHA) and trichostatin A enhance apoptosis via death receptors, pro-apoptotic proteins upregulation and arrest cell cycle in G1 phase⁸⁶.

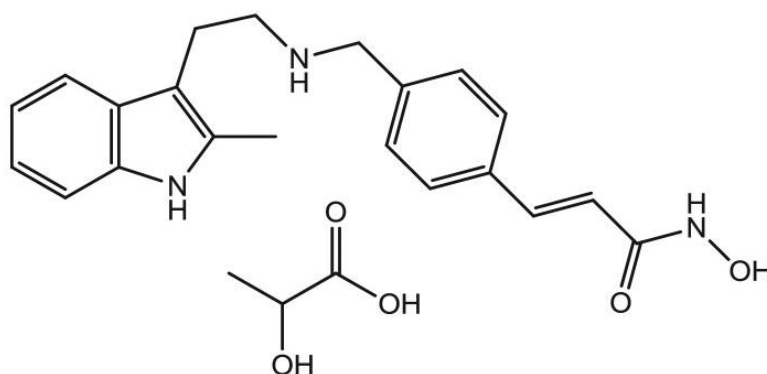


Figure 6. Chemical structure of panobinostat⁸⁷.

2.3. Resistances in multiple myeloma

Many patients initially respond to treatments but, in a second phase, drug-resistant clones emerge and disease relapses, with refractory characteristics. Different are the mechanisms that are behind a resistance; some are related to gene expression modifications, while others are given by altered drug targets. The first known mechanism responsible for resistance in multiple myeloma is the upregulation of multidrug resistance proteins⁸⁸. An example is represented by P-glycoprotein (P-gp), an efflux pump capable to avoid drug accumulation in tumor cells. Other examples of active exporting systems are BCRP and MRP1. P-gp is a transmembrane protein that is part of the ATP-binding cassette transporter family (ABC). It is expressed by a wide range of tissues and its role is to avoid internalization of xenobiotics and toxins, as well as regulation of endogenous material transport. In response to the presence of chemotherapeutics, P-gp expression is upregulated, as demonstrated in patient-derived samples⁸⁹. To overcome the developed resistance, it is possible to apply anti-refractory protocols based on pump blockers or chemosensitizers. The efficacy of those compounds was established but the low specificity and the high cytotoxicity on normal tissues limit their applications⁹⁰. Another ABC transporter involved in the development of resistance is breast cancer resistance protein (*BCRP*). The expression of this surface pump on myeloma cells is enhanced by various chemotherapeutic compounds and contributes to the refractoriness of the disease. In particular, BCRP expression is high in a subpopulation of tumor cells known as side population, which exhibit stem-like properties. Moreover, BCRP levels tend to increase during disease progression⁹¹.

Considering the genes that codify efflux pumps, they are highly polymorphic. Depending on the observed single-nucleotide polymorphisms and haplotypes it is possible to observe different outcomes in MM patients⁹².

2.3.1. Proteasome inhibitors: different resistance-driving mechanisms

Multiple myeloma cells can exhibit resistance to proteasome inhibitors by different mechanisms, intrinsically related to proteasome components or due to cell adaptation systems.

Overexpression of heat shock proteins (HSP) by tumor cells, following proteasome inhibitors treatment, is one of the well-known mechanisms to escape cell death. Proteasome inhibition triggers cellular stress, which is counteracted by overexpression of *HSP27*, *HSP40β*, *HSP70* and *HSP105*. A strategy to bypass this cytoprotective response could be the use of heat shock response inhibitors. Several compounds have been tested in trials, but none received the approval, because of their low

potency. Many HSP inhibitors are necessary to obtain some effects, and this is not applicable for human treatments. On the other hand, the targeting of heat shock factor 1 (HSF1), the master transcription factor of the heat shock response seems promising to sensitize cells to BTZ treatment⁹³. Another stress-induced resistance mechanism is the overexpression of anti-stress factors, such as the nuclear factor erythroid 2 [NF-E2]-related factor 2 (NRF2). This transcription factor is expressed in myeloma cells and regulates hundreds of targets involved in detoxification, pro-tumoral phenotype and inflammation⁹⁴. In several multiple myeloma cell lines, *NRF2* expression is high and its silencing reduces cell viability. Upon either CFZ or BTZ treatment, *NRF2* transcription dramatically increases, thus leading to a modulation of redox homeostasis that reduce sensitivity to proteasome inhibitors⁹⁵. Myeloma cells can also overcome proteasome inhibitors cytotoxicity by becoming less dependent on unfolded protein response (UPR). UPR is a cellular response required to adapt to stress conditions and rely on mediators such as ATF6 and XBP1⁹⁶. Comparing bortezomib sensitive and resistant myeloma cells, it is observed a reduction in *ATF6* and *XBP1* expression in resistant cells, consistent with a reduced dependence on UPR for cell survival^{97,98}. In addition, endoplasmic reticulum dimensions are reduced in resistant cells, indicating a diminished UPR pathway activity⁹⁹. In particular, XBP1 reduction is related to a single nucleotide polymorphism in a splicing residue that impinges the activation of XBP1 and UPR pathway¹⁰⁰.

Other strategies adopted by multiple myeloma cells to acquire resistance to proteasome inhibitors include the alteration of drug targets. The majority of proteasome β subunits were found mutated in relapsed/refractory patients (*PSMA1*, *PSMB5*, *PSMB8*, *PSMB9*, and *PSMG2*), as well as variants in 19S proteasome subunit *PSMD1*. In particular, *PSMB5* gene, encoding for a 20S core component of the proteasome was observed enriched in point mutations in the binding pocket for BTZ, conferring treatment resistance *in vitro*. Notably, some of the discovered mutations were also able to decrease cell line sensitivity to newer proteasome inhibitors carfilzomib and ixazomib¹⁰¹. In addition, a recent study showed that, upon BTZ and CFZ treatments in some MM patients, the expression of proteasome subunits increases, leading to a positive feedback that try to restore proteasome stability after its inhibition¹⁰².

2.3.2. IMiD resistances

The appearance of resistances in multiple myeloma patients is also seen in the case of immunomodulatory drugs treatment combined with proteasome inhibitors. Many are the genes found mutated in patients' cohorts and among them, *CRBN* is frequently altered. As mentioned, cereblon is the key responsible to allow the anti-tumor effects provided by IMiDs. In significant percentages of patients *CRBN* is either truncated, differs in splicing sites or has altered sequence in the drug-binding

region, leading to lenalidomide and pomalidomide refractoriness. In addition, components of the cereblon pathway are observed mutated in patients that do not respond to therapy, as *CUL4B*, *IRF4*, and *IKZF1*¹⁰³. Those data are also confirmed *in vitro*, where not simply mutations but also downregulation of CRBN and CRBN-related partners can establish resistant phenotype⁷⁰.

The resistance to IMiDs can also being achieved by altering various RAS pathway components. Mutations in *NRAS*, *KRAS*, and/or *BRAF* are responsible for MAPK cascade activation and downstream signaling which can provide cell survival, proliferation and cytoskeletal re-organization. For example, mutations on *KRAS* gene can lead to MEK/ERK activation¹⁰⁴.

2.3.3. Resistance to mAbs

The new era of immunotherapy seemed really promising at the beginning, also for the treatment of resistant/relapsed multiple myeloma cases. However, myeloma cells can adapt and escape this therapeutic approach by modifying the availability of mAb targets.

CD38 is one of the most relevant surface targets for multiple myeloma immunotherapy. In cells derived from patients treated with daratumumab, CD38 expression is reduced during the therapeutic window; upon DARA suspension, high levels of CD38 are recovered. This suggests that the adaptation mechanism consists in a reduction of the drug target, which renders myeloma cells not visible for the mAb. Furthermore, in daratumumab regimen, myeloma cells increase the levels of complement inhibitory proteins CD55 and CD59, contributing to resistance by depressing the complement-dependent cytotoxicity triggered by α -CD38¹⁰⁵.

Another approved anti-myeloma mAb is elotuzumab. In the case of anti-SLAMF7 regimen, resistant tumor clones arise, but resistance is related to the release of soluble SLAMF7 (sSLAMF7). sSLAMF7 is produced by unknown cleavage mechanisms and introduced in serum; in blood, sSLAMF7 represent a decoy target for elotuzumab, reducing the chances for the drug to bind CS1 on tumor cells. Interestingly, the levels of sSLAMF7 positively correlate in time and dose-dependent manner with Elo administration¹⁰⁶.

2.4. Synthetic lethality approach: finding novel therapeutic targets with functional screenings

Tumor therapies are based on a variety of different approaches and mechanisms of action. They can restrict cancer cells growth and progression, but sometimes are not sufficiently specific. Therefore, systemic toxicity and drug-related side effects are observed in patients. In order to reduce negative

events related to treatments, it is therefore crucial to identify molecular candidates or pathways that are altered in tumors and that, upon targeting, can induce accurately tumoral cells death.

One of the anticancer approaches, related to target and drug discovery, is known as synthetic lethality. This concept is actually very old and first described by C. Bridges in 1922¹⁰⁷. Bridges observed that just the concomitant presence of specific mutations in *Drosophila melanogaster* led to lethality. The term synthetic lethality was coined later in 1946, with the word *synthetic* to mean “the combination of two entities to form something new”, coming from its Greek original meaning¹⁰⁸. In the tumor context, synthetic lethality involves two genes which are, for examples, required for cellular survival. The alteration/inhibition of a gene alone is not sufficient to trigger cell death, while the contemporaneous targeting of both genes results in tumoral cell death, while sparing normal cells¹⁰⁹. This targeting can be done either via genetic alterations, for instance through RNA interference (RNAi), mutations, deletions, epigenetic changes, or with chemical inhibitors (Fig. 7).

The identity of synthetic lethals can be often rationalized based on the functions of their protein products. They might be uniquely redundant with respect to an essential function (as occurs in some paralogues), be two subunits of an essential multiprotein complex, be two interconnected components in an essential linear pathway or participate in parallel pathways that are together essential for survival (for example, a crucial metabolic pathway and an alternative or salvage pathway)¹¹⁰.

The identification of candidate targets is not a trivial process; therefore, it is possible to start by using hypothesis-driven approaches or functional screening approaches. In the first case, the selection of a candidate derived from the knowledge of its alterations, that should be associated with a particular disease. Thus, if the gene is frequently over-expressed within cancer type, it could be target by using RNAi or chemical compound. On the other hand, screening-based strategy is a high throughput methodology that can help to find unknown targets beforehand.

Functional screening can be distinguished in chemical libraries and genome-wide interference. Chemical libraries are based on testing thousands of drugs, with known or unknown targets. On the other hand, genome-wide interference screenings are based either on siRNA, shRNA or CRISPR-Cas9 libraries that can interfere with the expression of a specific gene¹⁰⁹.

Of note, a modern approach in synthetic lethal targets identification is the use of in silico supports. Starting from cancer genomic data analysis, algorithms integrate several information in order to infer synthetic lethal interactions. The algorithm's performances are at present not yet optimized, since the false discovery rate is high. *In vitro* validation of computationally identified candidates remains crucial¹⁰⁹.

Considering siRNA/shRNA screenings, they are particularly useful to define crucial genes for cell survival. They are based on loss-of-function principle: if the expression of a gene is essential for cell

survival/proliferation/metabolism, its silencing will affect cancer cell fitness. The application of this technology in cancer investigation, allowed the identification of cancer drivers that can also represent candidate drug targets. A relevant detail to consider with the use of shRNA screenings is the necessity of more than one interfering RNA that targets the expression of the same gene, so to reduce false positive rates. This is explained by the variation in the shRNA individual level of efficacy, shRNA design and possibility to have off-targets¹⁰⁹.

One of the first siRNA screenings performed, allowed clarifying the addiction of multiple myeloma to IRF4 transcription factor and its role in conferring survival advantage to tumor cells⁶³. By using the same idea but extended to a high throughput approach, other key survival myeloma genes were identified. Among deadliest molecular targets, there are spliceosome components and mRNA processing elements (e.g. *SF3A1*, *SNRPA1* and *PRPF8*), ribosome assembly factors (e.g. *WBSCR22*), as well as regulators of protein degradation (e.g. *TRIM21*, *USP8*) and cell division genes (e.g. *CDK11A*, *CDK11B*)¹¹¹.

The importance of this type of screenings is not simply limited to identify tumor drivers or pure therapeutic targets. As discussed above, upon results analysis it is possible to find synthetic lethal relations and select candidates that can act as sensitizers in presence of a specific treatment. An example is represented by *RSK2* and lenalidomide. *RSK2* is a kinase that activates MAPK signaling pathway and is involved in the control of cell growth and differentiation¹¹². *RSK2* silencing through siRNA is capable to sensitize multiple myeloma cell lines to lenalidomide-mediated cytotoxicity¹¹³. In the same year, a paper reported that the genetic depletion of almost any 19S proteasome components de-sensitized myeloma cell lines to carfilzomib administration, while 20S subunits depletion strongly sensitizes cells to the same drug. This result was unexpected, considering the concerted activity of the two proteasome constituents. A possible explanation for this phenotype is a change in the levels of protein degradation factors upon 19S factors depletion. This mechanism may represent a homeostatic feedback loop in which the upregulation of protein turnover pathways may reduce cellular dependence on the proteasome¹¹⁴.

RNA-guided CRISPR-Cas9 has become an efficient and precise tool to introduce mutations at specific sites in the genome. In past years, genome-scale CRISPR-Cas9 library was developed to interrogate gene function on a wide scale^{115,116}, with several advantages relative to RNA interference technology. Since then, many discoveries have been made concerning cancer hallmarks, including drug resistances. For instance, by applying a CRISPR-Cas9 knockout genome-wide screening in an IMiDs-sensitive MM cell line, it was recently demonstrated that almost all CSN9 signalosome subunits, are required for cell sensitivity to IMiDs, by regulating CRBN expression levels¹¹⁷. Moreover, by using a CRISPR-Cas9 loss-of-function screening in BTZ-resistant MM cell line, other

study showed that proteasome regulatory subunit PSMC6 is one of the most prominent gene associated with BTZ resistance¹¹⁸.

A more applicable high throughput strategy to find new effective drugs or drug synthetic lethal combinations, is represented by annotated or non-annotated chemical compound libraries. These have been used to find synthetically lethal interactions in a number of different cancers^{119–121}. In multiple myeloma, a panel of small molecule inhibitors was used to identify the bromodomain inhibitor CPI203 as an agent that showed intriguing effectiveness in BTZ resistant cell lines¹²².

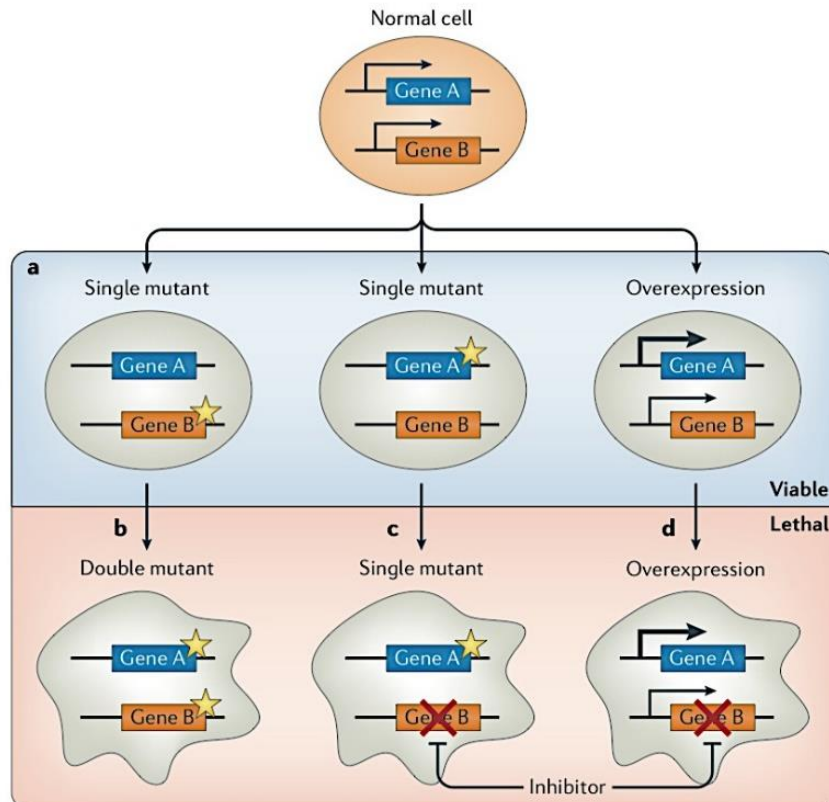


Figure 7. Synthetic lethality principle. The patterns of alterations in a cell can comprise mutations or differential gene expression at level of genes that are e.g crucial for cell survival. If a single gene is mutated (star) or its action is impinged no phenotype is observed. When another crucial gene is targeted by inhibition or mutations the lack of two co-essential genes defines cell lethality¹²³.

3. Aim of the study

To identify druggable targets which inhibition sensitize MM cells to PIs, we have previously performed a short hairpin RNA functional screening targeting 152 cancer driver genes in two MM cell lines resistant to PIs. The screening revealed that the silencing of isocitrate dehydrogenase 2 (IDH2) or lysine-specific demethylase 1 (LSD1) has a synthetic lethal activity with carfilzomib (CFZ). This means that tumor cells death is observed only with the simultaneous inhibition of the proteasome and IDH2 or LSD1.

Isocitrate dehydrogenase protein family consists of three self-regulating enzymes (IDH1, IDH2, IDH3). IDH1 and IDH2 are both nicotinamide adenine dinucleotide phosphate (NADP)-dependent enzymes, whereas IDH3 is a NAD-dependent enzyme. IDH2 and IDH3 are located in the mitochondria, whereas IDH1 is located in the cytosol and peroxisome. They all catalyze the oxidative decarboxylation of isocitrate to alpha-ketoglutarate (α -KG), with the consequent production of NADPH by IDH1 and IDH2, and the generation of NADH by IDH3^{124,125}. Mutations in IDH2 have been demonstrated in different malignancies, such as low grade gliomas¹²⁶, acute myeloid leukemia¹²⁷, chondrosarcoma¹²⁸, and cholangiocarcinoma¹²⁹. These hotspot mutations cause loss of IDH1/2 canonical activity and an enzymatic gain of function that catalyzes the conversion of α -KG to (R)-hydroxyglutarate (2-HG) with severe consequences on epigenetic, metabolism, and other cellular processes¹²⁵. However, the role of wild-type IDH2 in tumors has been poorly investigated.

Histones demethylases comprise two different family of proteins. The bigger one includes Jumonji C family (JMJs) that are dependent on α -ketoglutarate and Fe²⁺ and acts on tri-, di-, or mono-methylated lysine residues. The smaller LSD family consists of only two members LSD1, and its paralog LSD2 which are FAD-depend enzymes that only recognize di- and mono-methylated lysine residues¹³⁰. LSD1 acts as transcriptional co-repressor or co-activator, depending on its interacting partners and it is involved in the regulation of several biological processes, such as embryonic development, adult tissue homeostasis and cellular differentiation¹³¹. Interestingly, it was found to be overexpress in several hematological and solid tumors (Harris et al., 2012) where it plays a pivotal role in regulating stem cell potential^{133,134}, metabolic reprogramming¹³⁵⁻¹³⁷ and epithelial-to-mesenchymal transition, thus orchestrating cellular motility and invasiveness¹³⁸⁻¹⁴⁰. However, LSD1 functions in cancer remains heterogeneous and cell-context specific, thus difficult to completely understand. Moreover, its roles in multiple myeloma remains mostly unknown.

The aim of the present study is to: a) confirm the synthetic lethal activity of IDH2 and LSD1 with CFZ in multiple myeloma and others hematological malignancies; b) to characterize the molecular mechanisms through which IDH2 and LSD1 inhibition could enhance the efficacy of proteasome inhibitors.

4. Materials and Methods

4.1. Cell culture conditions and reagents

Human multiple myeloma (MM) cell lines KMM-1, U266, KMM-1^{PIR}, U266^{PIR}, RPMI-8226, KMS-18, KMS-27, SK-MM-1, NCI-H929, CMA-03, KMS-26, KMS-28, KMS-11, KMS-34, OPM-2, LP1, AMO-1; human chronic myelogenous leukemia cell line K-562; human acute myeloid leukemia MOLM-13; human mantle cell lymphoma (MCL) cell lines JeKo-1, SP-49, Mino, Granta-519; human Burkitt's lymphoma (BL) cell lines HS-Sultan and Raji; human diffuse large B-cell lymphomas (DLBCL) SU-DHL-2, RIVA, U2932 (ABC-DLBCL), OCI-LY8, SU-DHL-6, DoHH2 and KARPAS-422 (GCB-DLBCL) were obtained from DSMZ (German Collection of Microorganisms and Cell Cultures), ATCC (American Type Culture Collection), or generated in our lab and authenticated by DNA fingerprinting using GenePrint system (Promega). Cell lines were maintained in RPMI 1640 medium (EuroClone), supplemented with 2 mM of L-glutamine, 100 U/mL of penicillin, 100 µg/mL of streptomycin (Gibco), 10-20% fetal bovine serum (FBS; Sigma-Aldrich), and grown at 37°C in humidified atmosphere with 5% CO₂. CMA-03 cells were supplemented with 10 ng/mL IL-6. 293T cells obtained from DSMZ were cultured under standard conditions (37°C in humidified atmosphere, with 5% CO₂) in DMEM supplemented with 10% FBS. For experiments with glucose deprivation, RPMI 1640 medium without glucose (Corning), supplemented with 100 U/mL of penicillin, 100 µg/mL of streptomycin (Gibco), and 10% FBS was used. Cells were seeded at 1-2 x 10⁵ cells/mL before treatments. Peripheral blood mononuclear cells (PBMCs) from healthy blood donors were provided by the local Blood Bank (Fondazione Strumia) and isolated on a Ficoll-Hypaque density gradient. Bone marrow white cells (containing more than 20% of myeloma cells) were obtained from routine BM aspirates of myeloma patients. They were collected by buffy coat, incubated with Red Blood Cell Lysing Buffer (Sigma), suspended in RPMI-10% FBS medium and seeded (10⁶ cells/mL) on a 50% confluent HS-5 cell monolayer. Informed consent was obtained from all enrolled patients after the procedures were approved by the local ethical committee. Carfilzomib (PR-171) and AGI-6780 were obtained from Selleckchem, bortezomib (PS-341) from Millennium Pharmaceuticals, ixazomib (MLN9708), GSK-LSD1, GSK2879552 and SP2509 from MedChemtronica, FK866 from Sigma, and AGK7 from Cayman Chemical.

4.2. Lentivirus production and in vitro transduction

High titer lentiviral stocks were produced in 293T cells by co-transfecting all expression vectors and packaging vectors (pCMV-dR8.74 or psPAX2 and VSVG/ pMD2.G) with the Effectene Transfection Reagent (Qiagen), according to the manufacturer's instructions. Supernatants were harvested over 36

to 60 hours, filtrated (0.22 μm pore), and used directly or concentrated by ultracentrifugation for 2 h at 50,000 rcf, and then resuspended in cold phosphate-buffered saline (PBS). Aliquots of virus, plus 4-8 $\mu\text{g}/\text{mL}$ polybrene, were used to infect KMM-1, KMM-1^{PIR}, U266, U266^{PIR}, KMS-27, KMS-28, KMM-1 and AMO-1 cells ($1 \times 10^5/\text{mL}$). Fresh medium was supplemented 2 hours after infection. Stable cell lines expressing indicated constructs were selected by treatment with 1,5-2,5 $\mu\text{g}/\text{mL}$ puromycin (Sigma-Aldrich) for 24 or 48 hours.

4.3. Plasmids constructs and cloning of gRNAs

Two gRNAs were used together to obtain the deletion of the whole region spanning from exon 2 to exon 11 of IDH2 locus. gRNAs were designed using the CRISPR DESIGN (crispr.mit.edu) and the CHOPCHOP (chopchop.rc.fas.harvard.edu) web tools. To maximize on target and minimizing off target activities, four top ranking candidate gRNA sequences were selected and coupled to obtain four different plasmids. gRNAs were cloned in SpCAS9 (BB) 2A Pure (PX459) V2.0 plasmid according to the PrecisionX™ Multiplex gRNA Cloning (SBI) kit and protocol (U6-H1 construct).

gRNAs	IDH2 gRNA sequences (5' to 3')	Target
1	GATCAAGGTGGCGAAGCCCG TGG	Exon 2
2	ATGAGATGACCCGTATTATC TGG	Exon 2
3	TTTCCCCTCATGGTGACGTG AGG	Exon 11
4	CGAGGAAGTCCGTGGTGTTTC AGG	Exon 11

To induce LSD1 over-expression, the plasmids lenti sgRNA(MS2)_puro backbone [Plasmid #73795], lenti dCAS9-VP64_Blast [Plasmid #61425], and lenti MS2-p65-HSF1_Hygro [Plasmid #61426] were obtained from Addgene, gifted by, Feng Zhang. gRNAs targeting LSD1 promoter region were selected from CRISPRi library of Jonathan Weissman¹⁴¹. To maximize on target and minimizing off target activities, three top ranking candidate gRNA sequences were selected. Sequences were cloned via BsmBI site into lenti sgRNA(MS2)_puro backbone. The vector was digested with BsmBI, purified with a QIAquick Gel Extraction Kit (Qiagen) and dephosphorylated. Equal amount (100 μM) of complementary oligonucleotide was mixed in T4 DNA ligase buffer with T4 polynucleotide kinase (PNK) enzyme for annealing and phosphorylation. These annealed seed pairs were ligated into the BsmBI-digested lentiviral vector using T4 ligase. The ligation mixture was transformed into Stab13 competent cells. Positive clones were identified by Sanger sequencing.

gRNAs	LSD1 gRNA sequences (5' to 3')
1 top	caccGAACGCCGGGGAGACGCTCT
1 bottom	aaacAGAGCGTCTCCCCGGCGTTC
2 top	caccGAGGAAATGGTCACCTTCGG
2 bottom	aaacCCGAAGGTGACCATTTCCTC
3 top	caccGTCTCCCCGGCGTTTGGAGT
3 bottom	aaacACTCCAAACGCCGGGGAGAC

4.4. SIRT3 construct

pCW57.1-SIRT3-FLAG vector was constructed by replacing the Cas9 of the pCW57.1- Cas9 vector (Addgene plasmid # 50661) with the SIRT3-Flag cassette from pcDNA3.1+ (Addgene plasmid # 13814), using the NheI-BamHI sites. Stable cell lines expressing the construct were selected by treatment with 2 µg/mL puromycin (Sigma-Aldrich) for 24 hours. SIRT3 expression was induced by doxycycline treatment (1 µg/mL) for 72h.

4.5. IDH2 and LSD1 constructs

IDH2 was amplified by PCR from KMM-1^{PIR} using specific primers and cloned into pENTR1A no ccdB vector (Eric Campeau, <http://ericcampeau.com/>). Lentiviral expression vector pLX304-IDH2-FLAG was generated by Gateway recombination (Gateway System, Invitrogen). KMM-1^{PIR} cells expressing the construct were selected by treatment with 7.5 µg/mL blasticidin (Sigma-Aldrich) for 48 hours. Lentiviral expression vector pLX304-hLSD1-V5 was obtained from DNAsu plasmid repository (ID HsCD00438895).

4.6. shSIRT3

Five different shRNAs glycerol stocks were purchased (Sigma-Aldrich: TRCN0000331109, TRCN0000038893, TRCN0000038892, TRCN0000038890, TRCN0000038889). High titer lentiviral stocks were produced as described above. Stable cell lines expressing the shRNA were selected by treatment with 2 µg/mL puromycin for 24 hours.

4.7. Generation of inducible cell lines

pLVTHM-GFP-shIDH2 and pLVTHM-GFP-shLSD1 vectors was constructed by subcloning the U6 promoter–shIDH2-A4, shLSD1-D6, shLSD1-D9, shLSD1-D10 cassette into the EcoRI-ClaI sites of the pLVTHM vector¹⁴², kindly provided by D. Trono (University of Geneva, Geneva, Switzerland). For conditional RNAi, KMS-27, KMS-28 and AMO-1 cells were transduced at high efficiency with pLV-DsRed-tTRKRAB plasmid, expanded, and used for transduction with pLVTHM-GFP-shIDH2 and pLVTHM-GFP-shLSD1 lentiviral particles. Next, cells were treated with doxycycline (1 µg/mL) for 12 hours, double GFP+DsRed+ cells were flow sorted (FACS Aria III, BD Bioscience, Milan, Italy) and expanded. shIDH2, shLSD1 expression was induced by doxycycline treatment (1 µg/mL).

4.8. shRNA screening

The shRNA library targeting 152 cancer driver genes (supplemental Table S1) was assembled with 684 lentiviral shRNA (pLKO backbone) from The RNAi consortium (TRC - <https://www.broadinstitute.org/rnai-consortium/rnai-consortium-shrna-library>) (supplemental Table S2). Lentiviral infections were optimized in U bottom 96-well plates for growth conditions, plate types, viral dose, and assay time points. KMM-1^{PIR} cells were seeded at a density of 20 000 cells/well, incubated for 24 hours, and infected using viral volumes of shRNA lentiviral supernatants sufficient to transduce 30% of cells (day -3). After 24h the cells were selected with puromycin (2.5 µg/mL) (day -2). Infected cells were detected using Cell Titer Glo (Promega) luminescence assay performed in duplicate two days after selection (day 0). Percentage of transduction (T) was defined as: (average luminescence value of puromycin selected samples/average luminescence of unselected samples) x 100 (supplemental Table S4). As controls, we used samples infected with different doses of empty shRNA (CTRL_PURO), non-targeting shRNA (CTRL_67C), GFP empty vector (CTRL_GFP), or non-infected cells (NT) with or without puromycin selection (supplemental Table S4). Samples with T<10% were excluded from subsequent analysis. At day 0 KMM-1^{PIR} cells were splitted and treated with 2.5 nM carfilzomib (CFZ) or with control diluent (DMSO) every 72 hours. Cell Titer Glo was performed 3 and 7 days posttreatment. Luminescence value were used to calculate Cell Growth (CG), Growth Rate (GC), and Z-Score for each time point. CG was calculated as the ratio between day 3 (or day 7) and day 0 luminescence values, adjusted for dilution factor. GR was calculated as follow: GR = (CG shRNA infected cells/CG control cells) x 100 (supplemental Table S5). Z-score was calculated using the following formula:

$$Z = \frac{(X - \mu)}{\alpha}$$

X: GR at a given time point (day 3 or day 7);

μ : average GR of controls;

σ : standard deviation of controls (supplemental Table S6).

We selected samples with Z-score lower than -0.75 (162 shRNAs) at day 3, and -0.8 (195 shRNA) at day 7. Within these groups candidate genes were selected according to the following criteria: more than one shRNA sequence per gene determine growth inhibition in presence of CFZ; shRNA reduces target gene expression by at least 60%; positive hits are present both at day 3 and day 7 (19 genes), or within the top 5 at day 7 (5 genes) (Supplemental Table S7). Top 24 scoring genes were validated in U266PIR cell line using similar protocol for the primary screening, scaled up to 6 cm dishes (data not shown; Figure 1C). Correlation analysis between gene silencing and phenotype was used to define top three candidates.

4.9. Purification of total RNA and Reverse Transcription-quantitative Polymerase Chain Reaction (RT-qPCR)

Total RNA was extracted using Magmax 96 Total RNA isolation kit (Ambion) or RNeasy Mini Kit (Qiagen) according to the manufacturer's instructions. cDNA was obtained from total RNA, previously treated with RQ1 RNase-free DNase (Promega), using iScript RT (Bio-Rad Laboratories) or Superscript III reverse transcriptase (Invitrogen), following the manufacturer's instructions. Quantitative PCR reactions were performed in 384-well plates with a Thermal iCycler (Bio-Rad) using the Bio-Rad iQ SYBR Green Supermix according to the manufacturer's instructions. The PCR cycling conditions were as follows: 95°C for 5 minutes followed by 40 cycles at 94°C for 10 seconds and 60°C for 30 seconds. The oligonucleotide primer pairs used for RT-qPCR were designed with PrimerBLAST

(<http://www.ncbi.nlm.nih.gov/tools/primer-blast/>), and available upon request. To confirm the amplification specificity, the PCR products were subjected to the analysis of melting curve. All PCR assays were performed in triplicate and the average Ct (cycles to threshold) was used for the comparative Ct method¹⁴³. Quantification of GAPDH levels served as an endogenous control. Control infections with scrambled shRNA, empty vector, or noninfected cells were used to define 100% expression.

4.10. DNA sequencing

Genomic DNA of KMM-1, U266, KMM-1^{PIR}, and U266^{PIR} cell lines was extracted using DNeasy Blood & Tissue Kit (Quiagen). Exon 4 of the IDH2 gene was analyzed by PCR amplification and

bidirectional direct sequencing using the ABI PRISM 3100 Genetic Analyzer (Applied Biosystems, Foster City, California, USA). Primer sequences are available upon request.

4.11. Western Blotting

Protein extracts were prepared using Lysis Buffer containing 20 mM Tris-HCl (pH 7.4), 150 mM NaCl, 5 mM EDTA, 1% Triton X-100, 1 mM PMSF, 10 mM NaF, 1 mM Na₃VO₄, and Protease Inhibitor Cocktail (Roche, Basilea, Switzerland). Total protein concentrations were measured using Bio-Rad DC protein assay kit (Bio-Rad). Equal amounts of protein lysates were resolved by SDS-PAGE, transferred to nitrocellulose membrane, and probed with the following primary antibodies: rabbit PARP-1 (H-250; sc-7150, Santa Cruz Biotechnology, Dallas, Texas, USA), mouse actin (clone C4; MAB1501, Merck Millipore, Burlington, Massachusetts, USA), mouse IDH2 (ab55271, Abcam, Cambridge, UK), mouse vinculin (SAB4200080, Sigma), mouse cyclin E (HE12; sc-247, Santa Cruz Biotechnology), rabbit cyclin A (H-432; sc-751, Santa Cruz Biotechnology), rabbit cyclin B1 (H433; sc-752, Santa Cruz Biotechnology), mouse p21 (610233, BD Biosciences), mouse p27 (610241, BD Biosciences), rabbit cleaved PARP-1 (5625, Cell Signaling Technology, Leiden, The Netherlands), rabbit cleaved caspase-9 (7237, Cell Signaling Technology), rabbit cleaved caspase-7 (8438, Cell Signaling Technology), rabbit cleaved caspase-3 (9664, Cell Signaling Technology), rabbit sirtuin 3 (D22A3; 5490, Cell Signaling Technology), mouse α -tubulin (clone B-5-1-2, T5168, Sigma), rabbit GFP (2555S, Cell Signaling Technology), rabbit LSD1 (C69G12, 2184, Cell Signaling Technology), rabbit NF- κ B p65 (D14E12, 8242, Cell Signaling Technology), mouse Cas9 (7A9-3A3, 14697 Cell Signaling Technology).

4.12. Gene Expression Profiling

Total RNA samples were processed according to manufacturer's procedure for global gene expression profiling onto GeneChip® Human Gene 2.0 ST arrays (Affymetrix Inc., Santa Clara, CA). Normalized expression values were obtained using Robust Multi Array Average (RMA) procedure. A custom annotation pipeline was applied that combined GENCODE v25 (Ensembl v87) annotations with the CDF (Chip Definition File) version 21 for gene annotations freely available at <http://brainarray.mbni.med.umich.edu/Brainarray/Database/CustomCDF/21.0.0/genecodeg.asp>. The expression levels of 18.642 Ensembl genes were obtained. Probes mapping to regions with ambiguous detection due to transcript overlapping were discarded. Hierarchical agglomerative clustering based on the most variable genes (genes whose average change in expression levels varied at least two fold from the mean across the entire panel) was performed using Pearson's correlation and average as distance and linkage methods, respectively, by means of DNA-Chip Analyzer software¹⁴⁴. Supervised

analyses were carried out using the Significant Analysis of Microarrays software version 5.00¹⁴⁵ using the web application provided in the shiny package of the R software (<https://github.com/MikeJSeo/SAM>). The cut-off point for statistical significance (at a qvalue 0) was determined by tuning the Δ parameter on the false discovery rate and controlling the q-value of the selected probes. Functional annotation clustering using DAVID 6.8 (<https://david.ncifcrf.gov/>) was applied at high stringency on gene-ontology terms and significant clusters (Enrichment Score, ES>1.3) were selected for each list of differentially expressed genes.

4.13. Analysis of apoptosis, cell cycle and cell differentiation

Apoptosis was measured by flow cytometry after staining with tetramethylrhodamine methyl ester (TMRM; Molecular Probes, Eugene, Oregon, USA) or Annexin V-FITC Kit (Miltenyi Biotec, Bergisch Gladbach, Germany), according to the manufacturer's instructions. CD138+ cells were identified by anti hCD138-FITC antibody (clone: 44F9; 130-098-197, Miltenyi Biotec). Cell cycle was measured by propidium iodide (PI) staining – flow cytometry. Briefly, cells were washed in PBS, treated with RNase (0.14 mg/mL) and incubated with propidium iodide (28.57 μ g/mL). Data were acquired using FACSCalibur or FACSCanto II cytofluorimeters and processed with FACSDiva 8.0 software (BD Biosciences). MOLM-13 cell differentiation was measured with CD11b-PE antibody staining (clone: M1/70.15.11.5, 130-113-235, Miltenyi Biotec), according to the manufacturer's instructions.

4.14. Reactive oxygen species (ROS) production

ROS production was detected by flow cytometry using 20 μ M 2',7'-Dichlorofluorescein diacetate (Sigma-Aldrich) incubated for 30 minutes at 37°C. Mitochondrial ROS production was detected by flow cytometry using the MitoSOX Red mitochondrial superoxide indicator (Thermo Fisher Scientific, Waltham, Massachusetts, USA), according to the manufacturer's instructions.

4.15. Mitochondria isolation

To isolate mitochondrial fractions, cells were washed twice in ice-cold PBS, then lysed in 0.5 mL mitochondria lysis buffer (50 mM Tris, 100 mM KCl, 5 mM MgCl₂, 1.8 mM ATP, 1 mM EDTA pH 7.2), supplemented with protease inhibitor cocktail III (Calbiochem), 1 mM PMSF, and 250 mM NaF. Samples were clarified by centrifuging at 650 \times g for 3 min at 4°C; the supernatant was collected and centrifuged at 13 000 \times g for 5 min at 4°C. The cytosolic extract was transferred to a new series of tubes and stored at -80°C after protein quantification. The pellet containing mitochondria was washed once with lysis buffer and re-suspended in 0.25 mL mitochondria resuspension buffer (250 mM

sucrose, 15 mM K₂HPO₄, 2 mM MgCl₂, 0.5 mM EDTA). A 50 µL aliquot was sonicated and used for the measurement of protein content.

4.16. NF-κB activity

Protein extracts were prepared using Lysis Buffer containing 20 mM Tris-HCl (pH 7.4), 150 mM NaCl, 5 mM EDTA, 0.1% Triton X-100, 1 mM PMSF, 10 mM NaF, 1 mM Na₃VO₄, and Protease Inhibitor Cocktail (Roche). NF-κB activity was assessed using the TransAM™ Flexi NF-κB Family kit (Active Motif, Carlsbad, California, USA). Briefly, total protein extracts (5 µg) were incubated with biotinylated probe containing the κB consensus site 5'-GGGACTTCC-3' (1 pmol). Binding of NF-κB subunits to the κB target sites was detected using specific primary antibodies against NF-κB p50, p52, p65, c-Rel, and RelB, according to the manufacturer's instructions. Absorbance at 450 nm was measured with a Packard EL340 microplate reader (Bio-Tek Instruments, Winooski, Vermont, USA). For each set of experiments, a blank was prepared with bi-distilled water, and its absorbance was subtracted from that obtained in the presence of protein extracts. Data obtained are absorbance units·mg⁻¹ cell proteins.

4.17. Tricarboxylic acid (TCA) cycle measurement

The glucose flux through TCA cycle was measured by radiolabeling cells with 2 µCi/mL [6-¹⁴C]-glucose (55 mCi/mmol; PerkinElmer, Waltham, Massachusetts, USA). Cell suspensions were incubated for 1 hour in a closed experimental system to trap the ¹⁴CO₂ developed from [¹⁴C]-glucose, and the reaction was stopped by injecting 0.5 mL of 0.8 N HClO₄. The amount of glucose transformed into CO₂ through the TCA cycle was calculated as described,¹⁸ and expressed as pmoles CO₂/h/mg cell proteins.

4.18. IDH enzymatic activity

Isocitrate Dehydrogenase Activity was measured using the IDH assay kit (Sigma-Aldrich, St. Louis, Missouri, USA), according to the manufacturer's protocol. IDH activity was determined using isocitrate as a substrate of the reaction, which results in a colorimetric (450 nm) product proportional to the enzymatic activity present. One unit of IDH is the amount of enzyme that generates 1.0 µmole of NADH or NADP per minute at pH 8.0 at 37°C. To evaluate IDH2 and IDH1 activities, mitochondrial or cytoplasmic extracts were respectively used.

4.19. Measurement of complex I–III activity

Mitochondria were extracted as described above. The electron flux from complex I to complex III was measured in 50 μ L non-sonicated mitochondrial extracts, resuspended in 120 μ L buffer A (5 mM KH₂PO₄, 5 mM MgCl₂, 5% w/v BSA) in a 96 well plate. Then, 100 μ L buffer B (25% w/v saponin, 50 mM KH₂PO₄, 5 mM MgCl₂, 5% w/v BSA, 0.12 mM cytochrome c-oxidized form, 0.2 mM NaN₃) was added for 5 min at room temperature. The reaction was started with 0.15 mM NADH and was followed for 6 min, reading the absorbance at 550 nm by a Lambda 3 spectrophotometer (PerkinElmer). Results were expressed as nmoles cytochrome c reduced/min/mg mitochondrial proteins.

4.20. ATP measurement

The amount of ATP was measured in 50 μ L mitochondrial extracts with the ATPlite assay (PerkinElmer), using a Synergy HT Multi-Mode Microplate Reader (Bio-Tek Instruments, Winooski, Vermont, USA). ATP was quantified as arbitrary light units; data were converted into nmoles/mg mitochondrial proteins, using a calibration curve previously set.

4.21. Xenograft models

KMS-27-TK-IDH2-A4 cells (5×10^5) suspended in phosphate-buffered saline (PBS)–50% Matrigel (BD Biosciences, San Jose, California, USA) were injected into the left and right flanks of NOD/SCID/IL2R γ ^{-/-} (NSG) mice, previously anesthetized intramuscularly with xylazine and tiletamine/zolazepam. Tumor growth was monitored over time by determining the volume of tumor masses. Mice with tumor masses of 0.5 cm diameter (~3 weeks after the injection) were randomized and treated for 3 weeks with doxycycline by oral administration (0.1 mg/mL biweekly), CFZ i.v. (4 mg/kg biweekly), or the combination with the same dosing regimen used for the individual agents. Doxycycline was administrated in a 0.5% sucrose solution in light-proof bottles, for 48h. CFZ was dissolved in 3% DMSO, 10% Captisol (CYDEX Pharmaceuticals Inc., Lenexa Kansas, USA), 10 mM sodium citrate pH 3.5, and administrated after doxycycline removal. The control group received the carriers alone at the same schedule as the combination group. Mice were euthanized in a carbon dioxide chamber, after the tumor masses reached a volume of approximately 1 500 mm³, or at early signs of distress. Tumor volume was calculated using the ellipsoid formula $\frac{4}{3} \times \pi \times \frac{1}{2} \times (\text{length} \times \text{width} \times \text{depth})$. Animals were housed in the animal facility of the Molecular Biotechnology Center (Torino, Italy), in accordance with guidelines approved by the local Ethical Animal Committee. Experimental approval was obtained from the Italian Ministry of Health.

For systemic MM mouse model KMS-28-TK-IDH2_A4 (1×10^7) cells were intravenously injected (i.v; tail vein) in 8-week old NOD/SCID/gamma chain $-/-$ (NSG) mice and left to engraft for ten days before starting treatment. Mice were treated with DOXY (0.1 mg/mL biweekly) by dissolving it in drinking water and CFZ (4 mg/kg biweekly), or control diluents by intravenously (i.v.) injection. At the end of treatment, mice were euthanized, organs collected and dismantled to obtain single cell suspension. KMS-28-TK-IDH2_A4 cell distribution in the different organs was analyzed by flow cytometry, after staining single cell suspensions with anti-human-CD138FITC and/or CD38APC antibodies to identify multiple myeloma cells.

4.22. Drug synergy

The Compusyn software and program was used to determine the effect of drug combinations and general dose effects and is based on the median effect principle and the Chou–Talalay Combination Index–Isobologram Theorem.⁴⁴ The Chou–Talalay method for drug combination is based on the median-effect equation, derived from the mass-action law principle, which provides the common link between single entity and multiple entities, and first-order and higher-order dynamics. The resulting combination index (CI) theorem of Chou–Talalay offers quantitative definition for additive effect ($CI = 1$), synergism ($CI < 1$) and antagonism ($CI > 1$) in drug combinations.

4.23. Statistical analysis

Statistical analyses were performed with GraphPad Prism 5.01 (GraphPad Software Inc.). Statistical significance of differences observed (in both in vitro and in vivo experiments) was determined by Student t test, one way or two-way ANOVA analysis; differences were considered significant when P value was $< .05$ (*), $< .01$ (**), or $< .001$ (***). Survival curves were estimated with the Kaplan-Meier method. The log-rank test was used for statistical analysis.

5. Results

5.1. Generation of PI-resistant MM cell lines

In order to identify potential targets that could synergize with PI, we first generated two multiple myeloma cell line models resistant to PI (KMM-1^{PIR} and U266^{PIR}). Parental cell lines were grown in the presence of increasing concentrations of Bortezomib (BTZ) for 6 months. After drug treatment release, KMM-1^{PIR} and U266^{PIR} cells were evaluated for PI resistance. Analysis of cell viability demonstrated that both cell lines displayed a significant BTZ resistance (Fig. 8A-B, top panels). Interestingly, KMM-1^{PIR} and U266^{PIR} cells revealed cross-resistant to Carfilzomib (CFZ) and Ixazomib (IXA) (Fig. 8A-B, middle and bottom panels). PI resistance was confirmed by analysis of PARP-1 cleavage (Fig. 8C-D). The EC₅₀ in parental and resistant KMM-1 and U266 was calculated with the AATBioquest software (Table 1).

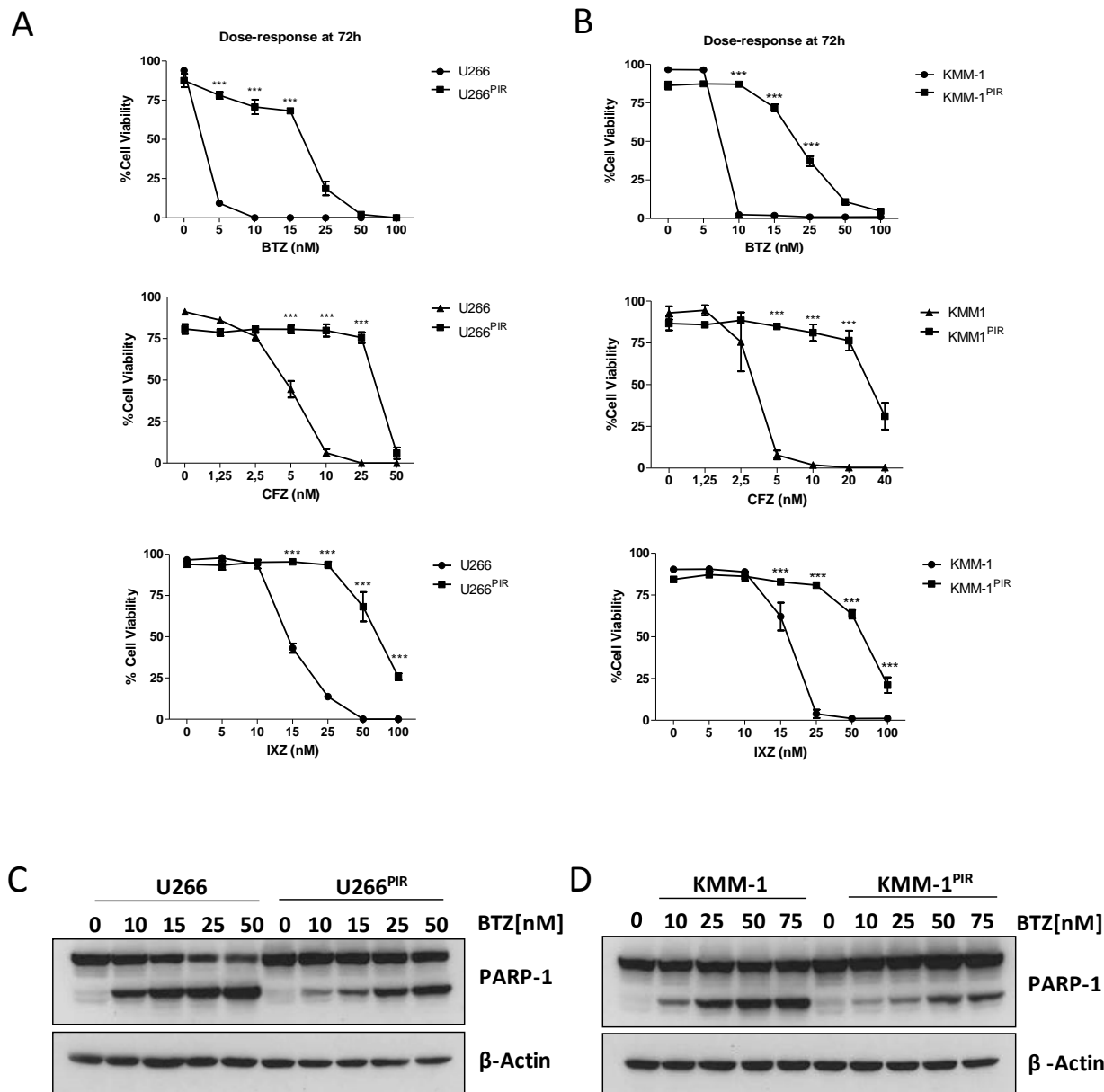


Figure 8. The multiple myeloma cell lines KMM-1^{PIR} and U266^{PIR} are cross-resistant to different generations of proteasome inhibitors. KMM-1^{PIR} and U266^{PIR} cells were generated from the parental cell lines cultured in presence of increasing concentrations of BTZ. (A-B) U266, U266^{PIR}, KMM1 and KMM-1^{PIR}, cells were treated with the indicated concentrations of BTZ, CFZ or IXZ. Cell viability was measured by TMRM staining-flow cytometry 72 hours post-treatment. (C-D) U266, U266^{PIR}, KMM1 and KMM-1^{PIR}, and cells were treated with the indicated concentrations of BTZ. Levels of PARP-1 cleavage were analyzed by western blotting 24 hours post-treatment. Actin protein expression was included for protein loading normalization.

Table 1. EC₅₀ of U266, U266^{PIR}, KMM-1 and KMM-1^{PIR} cells. Effects of selected drugs on both cell lines. Data represents mean± s.d. of at least three separate experiments

Drug	EC ₅₀ (mean ± s.d.)			
	U266	U266 ^{PIR}	KMM-1	KMM-1 ^{PIR}
VLD(nM)	3,991±0,09	20,093±0,76	7,846±0,82	22,164±1,06
CFZ (nM)	4,944±0,41	39,643±13,39	3,215±0,52	35,545±5,33
IXZ (nM)	12,283±0,55	73,531±7,47	16,525±0,62	73,067±5,87

5.2. shRNA screening in multiple myeloma cell lines identifies 3 synthetic lethal targets to the proteasome inhibitor carfilzomib

To unravel druggable targets that synergize with PIs, a functional screening using a short hairpin RNA library targeting 152 cancer driver genes, highly representative of all signaling pathways, was carried out in the KMM-1^{PIR} cell line treated with sub-lethal concentrations of CFZ (Fig. 9A-B). The primary screening was validated in the U266^{PIR} cell line, by targeting the top 24 genes. Analysis of the correlation between gene silencing efficacy and growth inhibition in presence of CFZ led to the identification of 3 synthetic lethal target genes (Fig. 9C). The first part of the present study was focused on isocitrate dehydrogenase 2 (IDH2), a NADP⁺ dependent mitochondrial enzyme which catalyzes the oxidative decarboxylation of isocitrate to α -ketoglutarate in tricarboxylic acid (TCA) cycle.

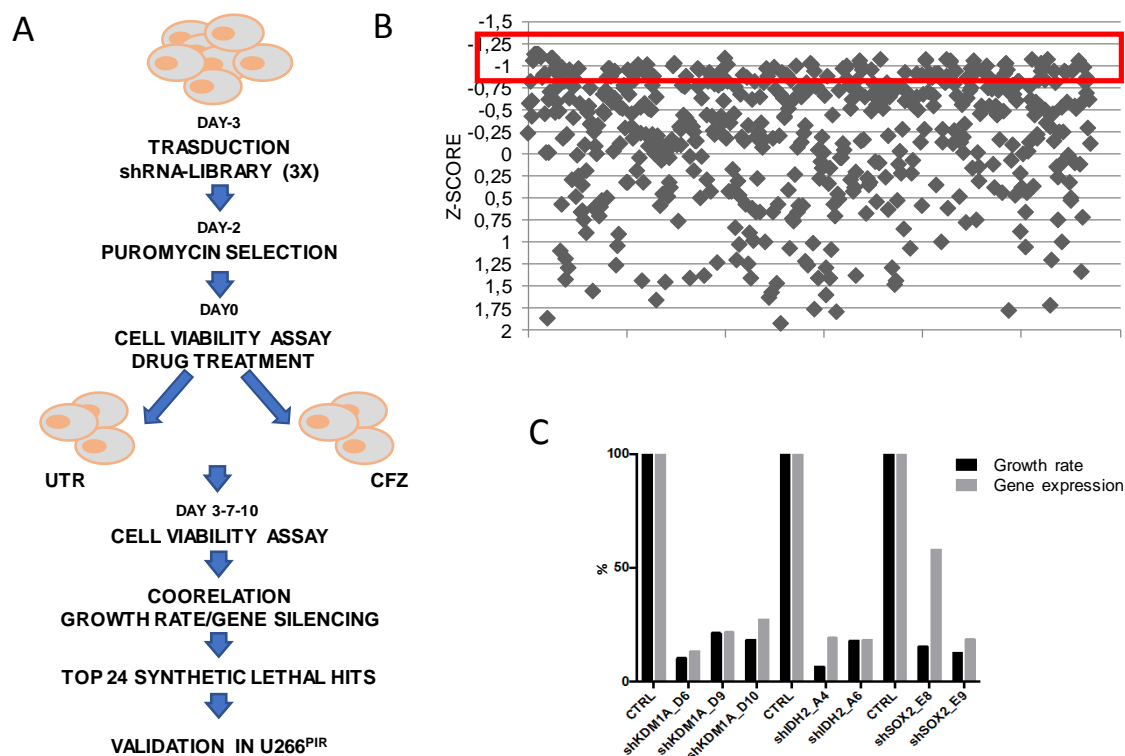


Figure 9. shRNA screening in multiple myeloma cell lines identifies 3 top synthetic lethal genes to the proteasome inhibitor carfilzomib. A) Experimental design of the shRNA screen to identify genes conferring sensitivity to carfilzomib (CFZ) in multiple myeloma cells. KMM-1^{PIR} cells were infected with 684 shRNAs targeting 152 cancer driver genes (day -3) and incubated in presence or absence of puromycin (day -2). KMM-1^{PIR} cells were then splitted and treated with 2.5 nM CFZ or with control diluent (DMSO) (day 0). Growth rate was calculated at day 3 and 7 post-treatment, and positive hits selected according to the Z-score. Top 24 selected genes were validated in a secondary screening performed in U266^{PIR} cells. (B) Representation of the Z-score (y-axis) for every shRNA (x-axis) calculated on growth rate reduction for each shRNA. Red box highlights candidates with Z-score below -0.8 (day 7). (C) Correlation between percentage of gene silencing and percentage of growth inhibition in presence of CFZ for top 3 candidate genes (IDH2, LSD1, and SOX2) in U266^{PIR} cells.

5.3. IDH2 inhibition sensitize PI-resistant MM cell lines to carfilzomib

To validate screening results, two shRNA sequences (A4 and A6) directed against human IDH2 were individually transduced into KMM-1^{PIR} and U266^{PIR} cells. IDH2 silencing was confirmed by RT-qPCR (Figure 10A-B) and western blot (Fig. 10C). IDH2 knockdown did not affect viability of KMM-1^{PIR} and U266^{PIR} cells. In contrast, IDH2 depletion was dramatically cytotoxic in cells treated with a sub-lethal dose of CFZ (Fig. 10D-E). These findings prompted us to verify whether IDH2

knockdown could synergize with CFZ also in PI-sensitive cell lines. Accordingly, IDH2 silencing considerably enhanced sensitivity to CFZ in parental KMM-1 and U266 cell lines (Fig. 10F-G). Taken together these data established that IDH2 knockdown is synthetic lethal to CFZ treatment in both PI resistant and sensitive MM cell lines. We excluded that IDH2 mutations or its aberrant expression were associated to PIs resistance in MM cells (Fig. 11).

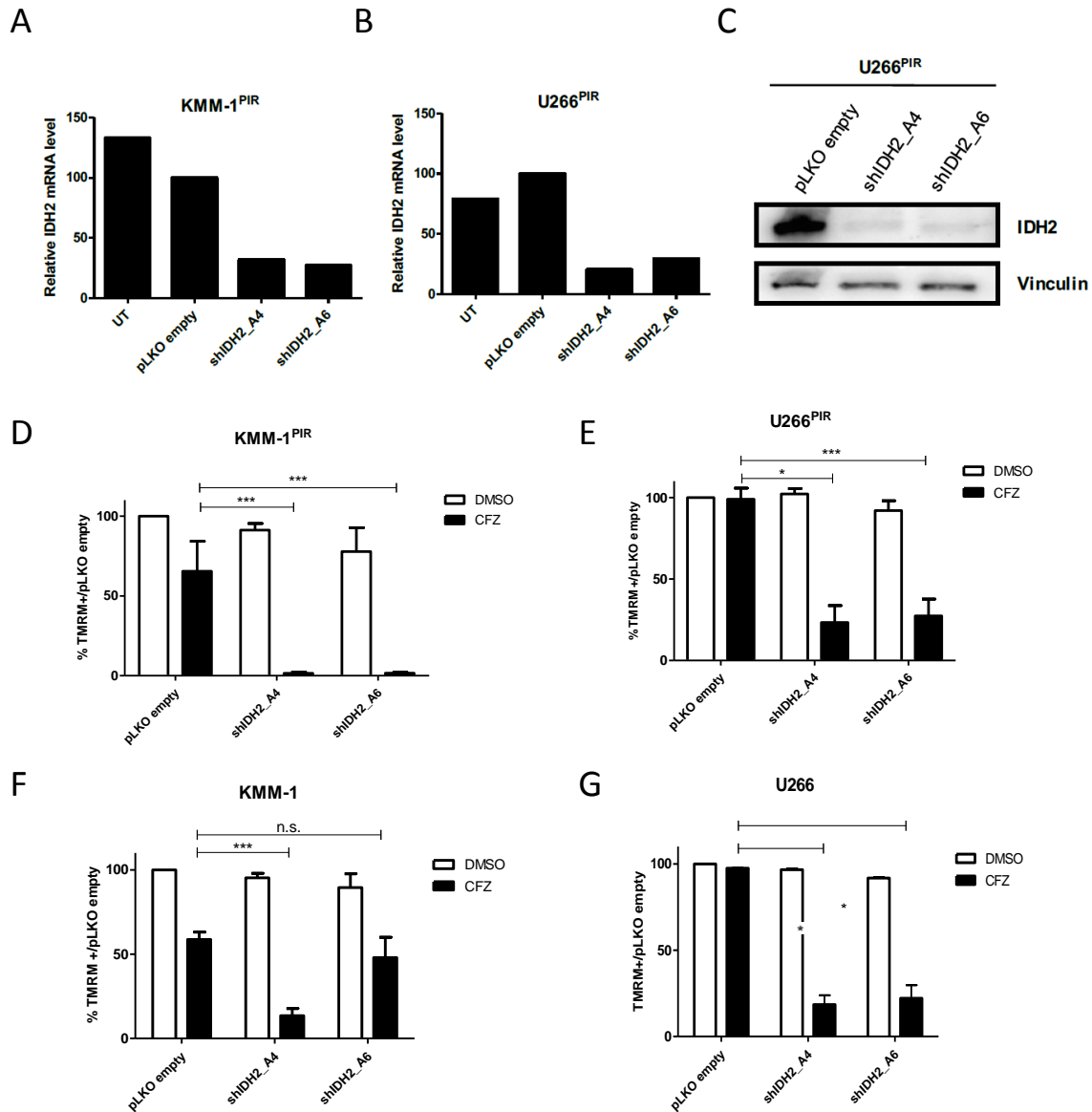


Figure 10. IDH2 inhibition synergizes with carfilzomib treatment. (A) KMM-1^{PIR} and (B) U266^{PIR} cells were transduced with lentiviral particles expressing two shRNA (shIDH2_A4, shIDH2_A6) targeting IDH2, empty vector (pLKO empty) or left untransduced (UT). IDH2 silencing was monitored by RT-qPCR after puromycin selection. (C) Representative western blot showing IDH2 expression levels in U266^{PIR} cells

transduced with lentiviral particles expressing the empty vector (pLKO empty) or the shRNAs targeting IDH2: shIDH2_A4 and shIDH2_A6. Vinculin protein expression was included for protein loading normalization. KMM-1^{PIR}, (D) U266^{PIR}, (E) KMM-1, and (F) U266 cell lines were transduced with the empty vector or shRNAs targeting IDH2 (shIDH2_A4, shIDH2_A6) and treated with CFZ (KMM-1^{PIR} and U266^{PIR}: 5 nM; KMM-1 and U266: 2.5 nM) or DMSO every 48h. Cell viability was measured by TMRM staining-flow cytometry 96 hours post-treatment (hpt) for KMM-1^{PIR} and U266^{PIR}, 48 hours post-treatment (hpt) for KMM-1 and U266. Data are the means \pm s.d. of three independent experiments (*P<.05; **P<.01).

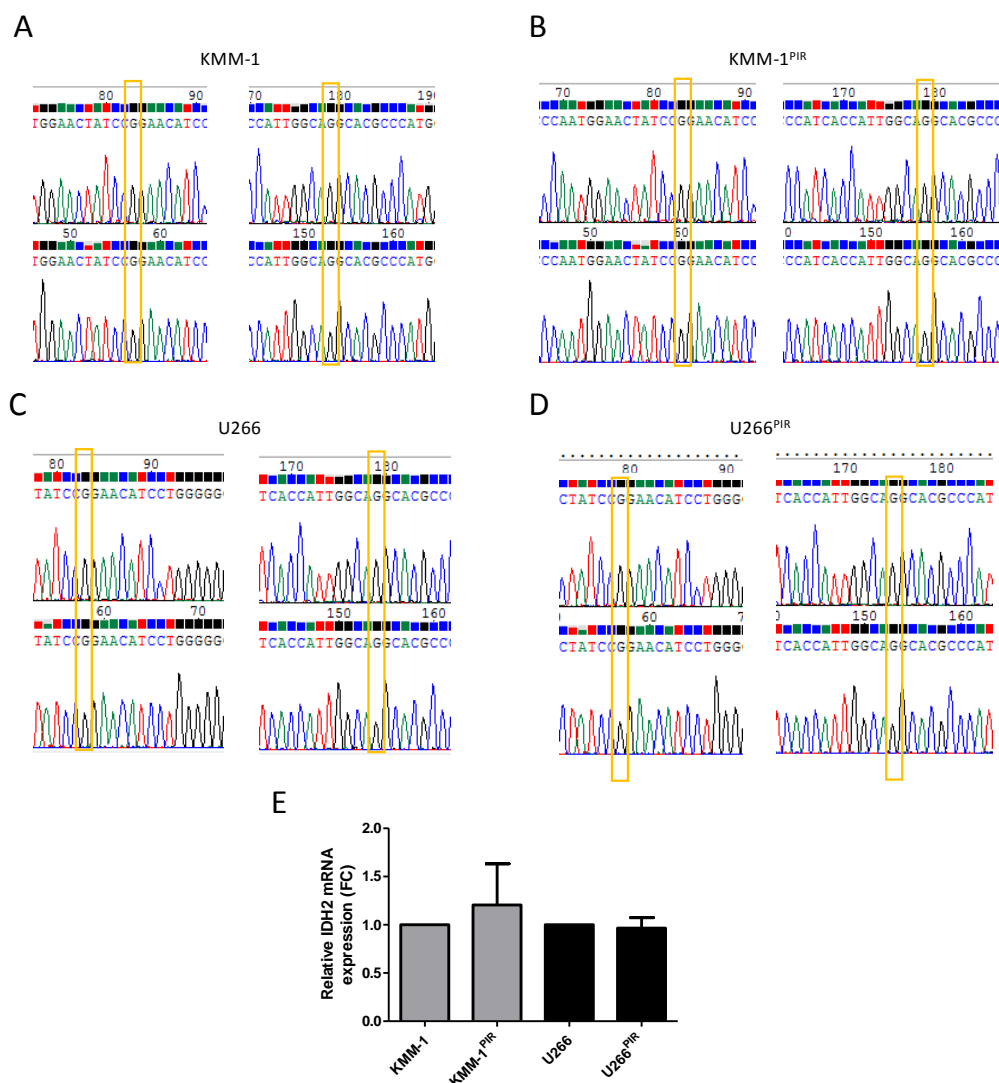


Figure 11. PI resistance of MM cell lines is not associated to IDH2 mutations or aberrant expression. (A-D) Sanger-sequencing showing wild-type IDH2 codon 140 (CGG, R140) and wild-type IDH2 codon 172 (AGG, R172) of (A) KMM-1, (B) KMM-1^{PIR}, (C) U266, and (D) U266^{PIR} cells (yellow rectangles). (E) IDH2 mRNA expression

levels monitored by RT-qPCR in KMM-1, KMM-^{1PIR}, U266, and U266^{PIR} cells. Data are represented as fold change (FC) over the sensitive counterpart.

5.4. AGI-6780 selectively impairs IDH2 enzymatic activity in MM cells

To define whether pharmacological inhibition of IDH2 recapitulates the synthetic lethal phenotype, we verified whether AGI-6780, an allosteric inhibitor of mutant IDH2, could also reduce the activity of wild type IDH2, as previously described^{146,147} (Fig. 12A). First, we demonstrated that AGI-6780 selectively impaired IDH2 enzymatic activity in multiple myeloma cells in a dose-dependent manner (Fig. 12B). We selected 5 μ M for subsequent experiment. Then, we investigated

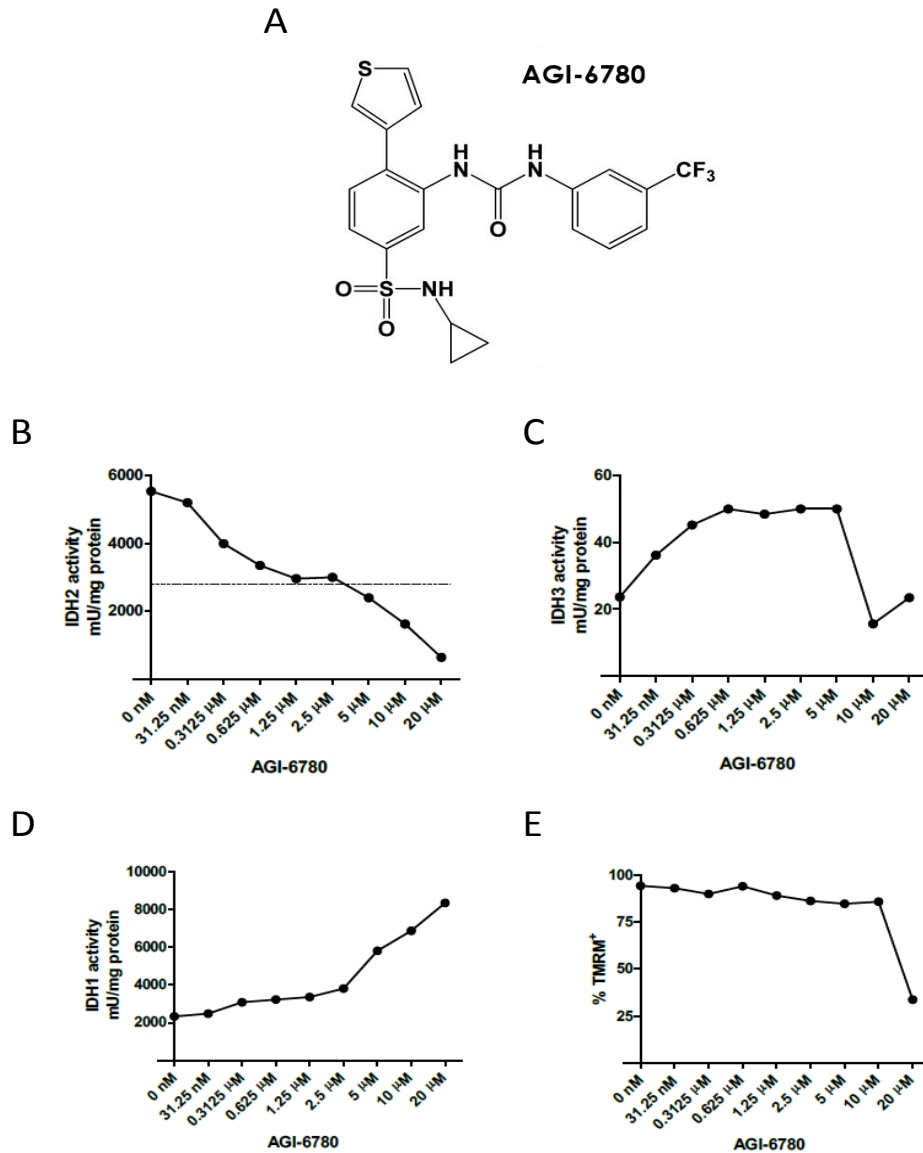


Figure 12. AGI-6780 selectively impairs wt IDH2 enzymatic activity in MM cells. (A) Chemical structure of AGI-6780¹⁴⁷. KMS-27 treated with increasing doses of AGI-6780 were analyzed for (B) IDH2, (C) IDH3, (D) IDH1 activity 6 hours post-treatment, (E) and for cell viability measured by TMRM staining-flow cytometry 48 hours post-treatment.

the effect of AGI-6780 on the other related IDH enzymes, IDH1 and IDH3. AGI-6780 did not show inhibitory effect on NAD⁺ dependent IDH3 enzyme (Fig. 12C). On the contrary, a slight increase of cytoplasmic IDH1 activity was detected, probably as a compensatory effect of IDH2 inhibition (Fig. 12D). Importantly, IDH2 inhibition with AGI-6780 (up to 10 μ M) did not affect MM cell viability (Fig. 12E).

5.5. Pharmacological inhibition of IDH2 enhances sensitivity to CFZ in MM cell lines

Next, the PIs resistant MM cell lines KMM-1^{PIR} and U266^{PIR} were treated with either CFZ, AGI-6780 alone, or the combination of the two drugs. Combinatorial treatments significantly increased cell death, compared to single drugs (Fig. 13A-B), confirming data obtained by IDH2 knockdown. This combination was effective also in MM cells resistant to very high concentrations of PIs (Fig. 13C). To prove that the combined cytotoxicity of AGI-6780 and CFZ is not restricted to PI resistant cells, eight MM cell lines with different degrees of PI sensitivity were treated with a single dose of CFZ in combination or not with AGI-6780, refreshed every 48 hours. Enhanced sensitivity to the combination treatment in comparison with either agent alone was observed in all MM cell lines (Fig. 13D). In contrast, the chronic myelogenous leukemia cell line K-562 was unresponsive to both drugs and to their combination (Fig. 13D). To elucidate mechanisms of synthetic lethality, cell cycle and apoptotic markers were analyzed. CFZ/AGI-6780 combination was associated with a down-modulation of cyclins, up-regulation of cyclin-dependent kinase inhibitors, proteolytic cleavage of the caspases substrate PARP-1, and activation of effector caspases 3, 7, and 9 (Figure 13E). To reduce the confounding effects of cell death induction, western blotting was performed 24 hours post-treatment, when cells displayed comparable levels of viability (Figure 13F-G). Moreover, an increase of G0/G1 phase was also confirmed by analysis of cell cycle with propidium iodide (PI) staining at flow cytometry (Fig. 14).

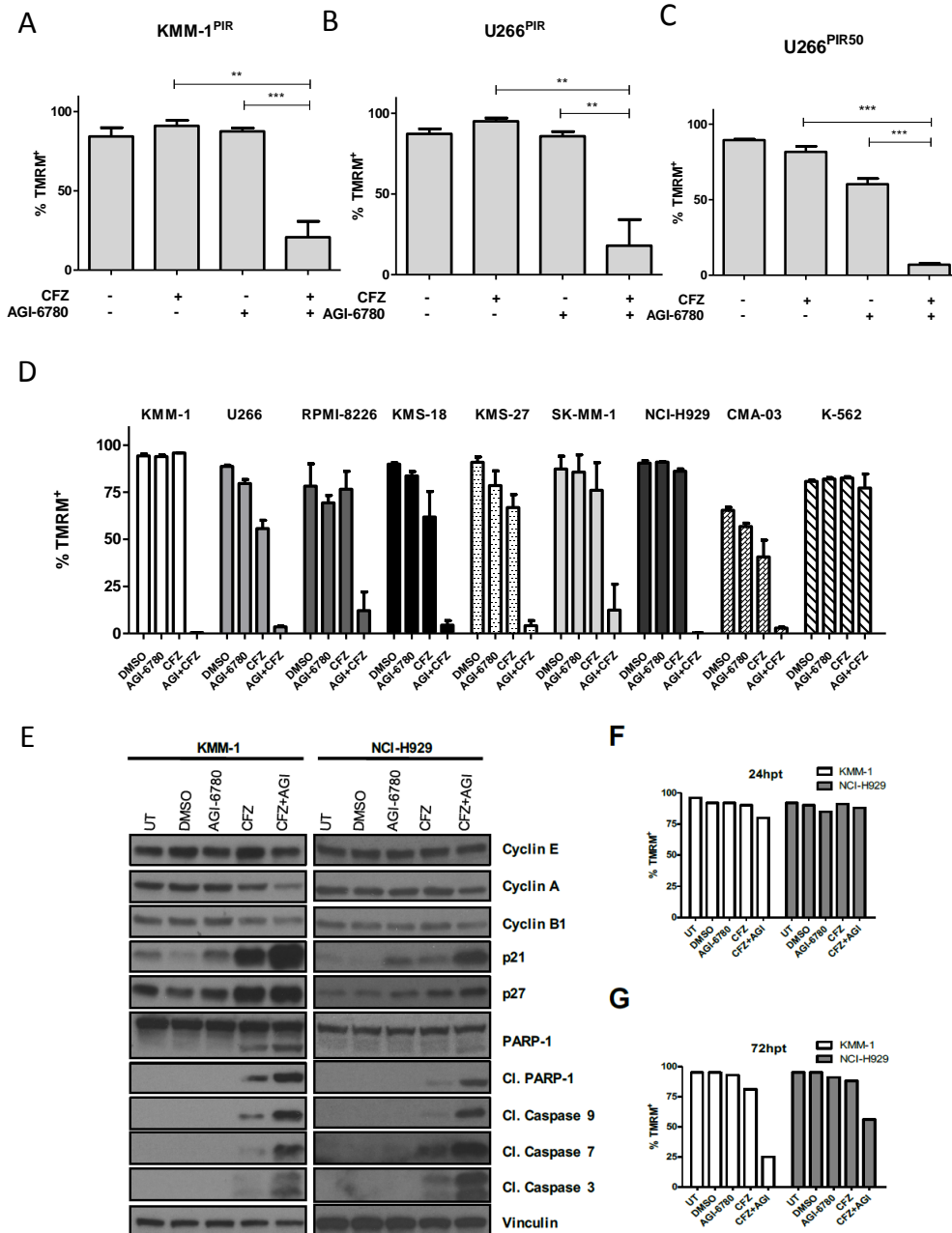
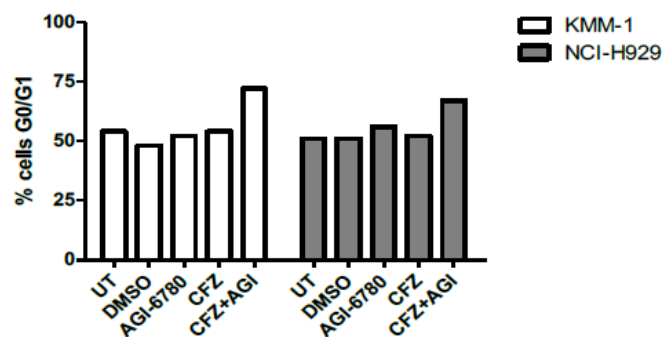


Figure 13. Pharmacological inhibition of IDH2 enhances sensitivity to CFZ in MM cell lines. (A) KMM-1^{PIR} and (B) U266^{PIR} cells were treated with 2.5 nM CFZ in combination or not with 10 μ M AGI-6780. Cell viability was measured by TMRM staining-flow cytometry 96 hours post-treatment. Data are the means \pm s.d. of four independent experiments. (C) U266^{PIR50} cells were treated with 75 nM CFZ in combination or not with 10 μ M AGI-6780. Cell viability was measured by TMRM staining-flow cytometry 72 hours post-treatment. Data are the means \pm s.d. of four independent experiments. (D) Eight MM cell lines and the K-562 cell line were treated with CFZ (1.67 nM CFZ for KMS-18; 2.5 nM for RPMI- 8226, KMS-27, SK-MM-1, and CMA-03; 5 nM for KMM-1, U266, and NCI-H929 cell lines) in combination or not with 5 μ M AGI-6780 (2.5 μ M for RPMI-8226).

Treatment was performed every 48h for AGI-6780, only at day 0 for CFZ. Cell viability was measured by TMRM staining-flow cytometry 8 days post-treatment. Data are the means \pm s.d. of three independent experiments (* $P < .05$; ** $P < .01$; *** $P < .001$; # $P \geq .05$). (E) Western blot of KMM-1 and NCI-H929 cells, untreated (UT), treated with DMSO, AGI-6780 (KMM-1: 5 μ M; NCIH929: 10 μ M), CFZ (KMM-1: 5 nM; NCI-H929: 2.5 nM), or the combination of the two drugs. Cell lysates were immunoblotted using the indicated antibodies 24 hours posttreatment. Vinculin protein expression was included for protein loading normalization. (FG) Cell viability of the experiment described above was measured by TMRM staining-flow cytometry 24 and 72 hours post-treatment (hpt), respectively.

A



B

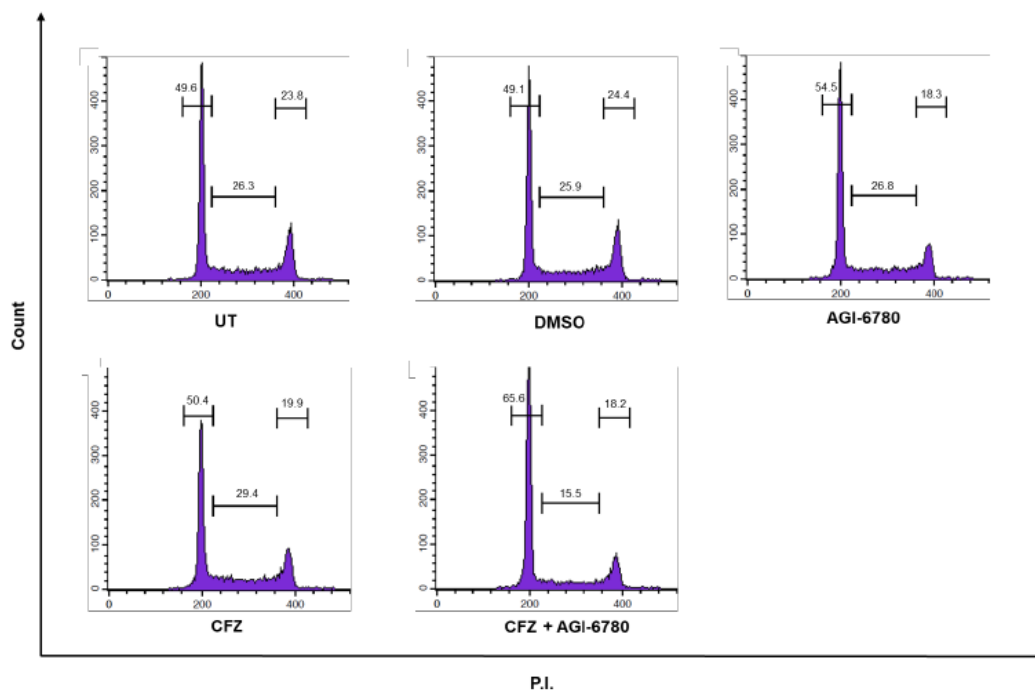
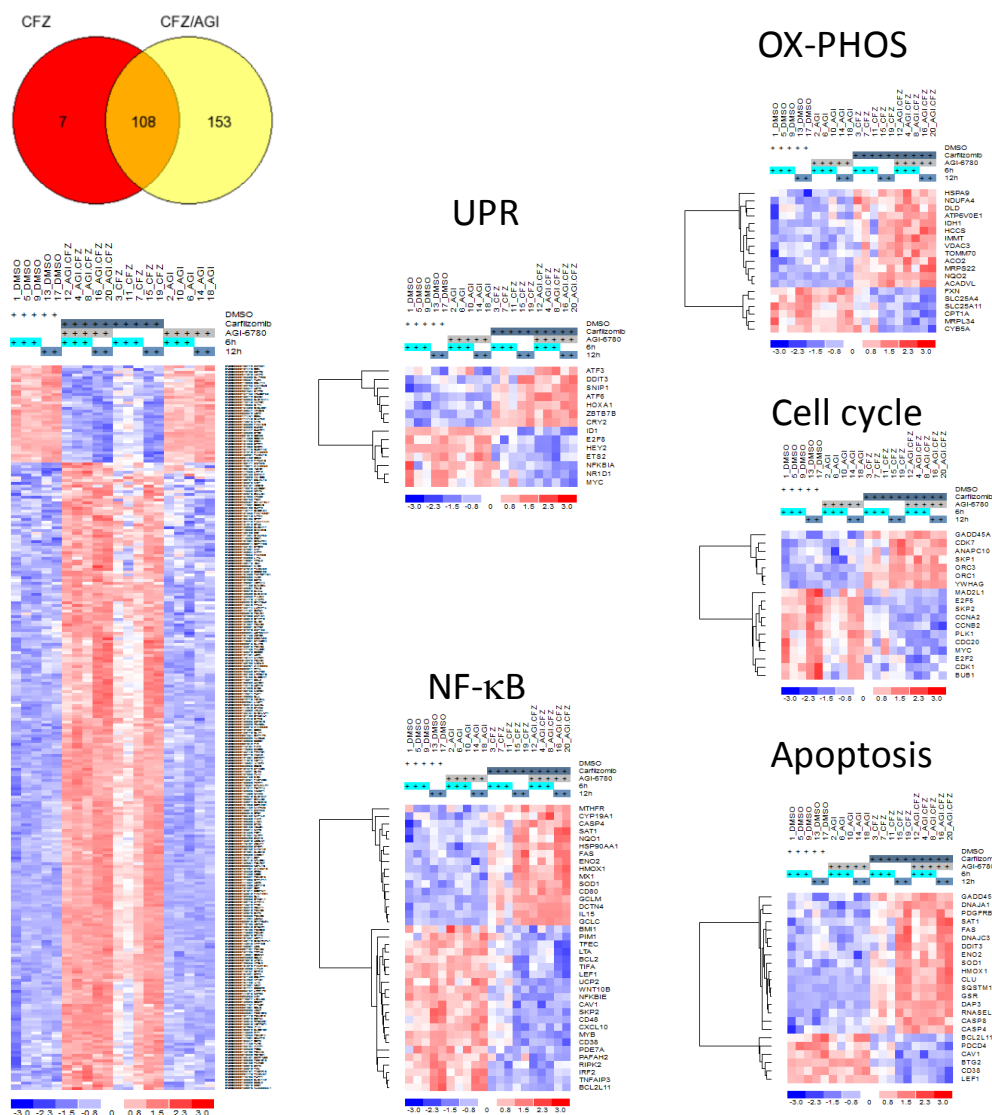


Figure 14. CFZ/AGI-6780 combination is associated with an increase of G0/G1 phase.

(A) KMM-1 and NCI-H929 cell lines were treated with AGI-6780 (5 μ M and 10 μ M, respectively) in combination or not with CFZ (5 nM and 2.5 nM, respectively). Cell cycle was measured by flow cytometry 24 hours post-treatment. (B) Representative cell cycle of NCI-H929 treated with AGI-6780 (10 μ M) in combination or not with CFZ (2.5 nM). Cell cycle was measured by flow cytometry 24 hours post-treatment.

5.6. CFZ/AGI-6780 regimen elicits significant changes converging in cell cycle and apoptotic pathways

To further define the molecular mechanisms involved and/or regulated by the synergistic activity of CFZ/AGI-6780, gene expression profiles were analyzed 6 and 12 hours after single or combination treatments and compared with untreated control samples. Supervised analysis identified 115 genes differentially regulated by CFZ, while AGI-6780 treatment had negligible transcriptional effects. Remarkably, 261 genes were differentially expressed after combined treatment, and nearly all genes modulated by CFZ (106/115) were concordantly modified to a higher degree by CFZ/AGI-6780 treatment (Fig. 15A). Pathway analyses confirmed that the classical pathway targets of PIs such as unfolded protein response (UPR), NF- κ B, cell cycle, and apoptosis, were affected in response to CFZ alone and these effects were enhanced by the combination with AGI-6780 (Fig. 15B). Collectively, these findings indicate that the CFZ/AGI-6780 regimen is effective against PI-resistant and PI-sensitive MM cells and elicits significant changes converging in cell cycle and apoptotic pathways.



Supervised analyses -> SAM q-value 0

Figure 15. Gene expression profile analysis of MM cells treated with CFZ, AGI-6780, or the combination of the two drugs. (A) KMS-27 cells were treated with DMSO, CFZ (2.5 nM), AGI-6780 (5 μ M), or the combination of the two drugs and analyzed 6 (n = 3) and 12 hours (n = 2) post-treatment using GeneChip® Human Gene 2.0 ST arrays. Expression values were normalized by Robust Multi Array Average (RMA) procedure and supervised analyses carried out using the Significant Analysis of Microarrays software (q-value = 0). (Upper panel) Venn diagram obtained overlapping genes modulated by CFZ (115) or CFZ/AGI-6780 (261) treatments. (Lower panel) Eisen plot of the expression values of 261 transcripts modulated by CFZ/AGI-6780 treatment. (B) Functional stratification of CFZ/AGI-6780-regulated genes. Genes differentially expressed in KMS-27 cells were grouped according to their functional categories. Pathway analyses of classical PIs targets such as unfolded protein response (UPR), NF- κ B, cell cycle, apoptosis,

and oxidative phosphorylation (OX-PHOS) were affected in response to CFZ alone and these effects were enhanced by the combination with AGI-6780.

5.7. IDH2 inhibition synergizes with first- and second-generation PIs in multiple myeloma cells

As described above, PI-resistant MM cells are cross-resistant to first- and second-generation proteasome inhibitors (Fig. 8). Then, to expand the clinical relevance of our observations and demonstrate that IDH2 inhibition specifically synergize with PIs, we demonstrated that MM cells treated with AGI-6780 displayed enhanced response to the FDA approved PIs bortezomib (BTZ) and ixazomib (IXA) (Fig. 16).

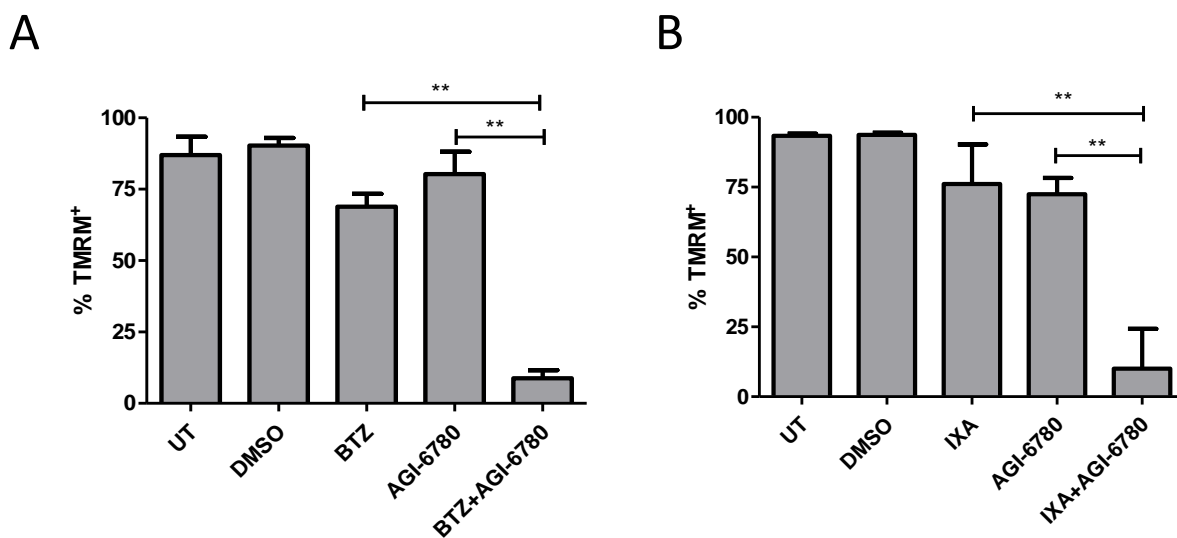


Figure 16. IDH2 inhibition synergizes with first- and second-generation PIs in multiple myeloma cells. (A) KMS-27 cells were left untreated (UT), treated with DMSO, bortezomib (BTZ; 3 nM; single administration), AGI-6780 (5 μ M; every 48 hours), or the combination of the two drugs. Cell viability was measured by TMRM staining-flow cytometry 10 days post-treatment. Data are the means \pm s.d. of three independent experiments. (B) KMS-27 cells were left untreated (UT), treated with DMSO, ixazomib (IXA; 12.5 nM; single administration), AGI-6780 (5 μ M; every 48 hours), or the combination of the two drugs. Cell viability was measured by TMRM staining-flow cytometry 10 days post-treatment. Data are the means \pm s.d. of three independent experiments.

5.8. IDH2 inhibition synergizes with PI in B-cell hematological malignancies

Since PIs have been approved also for the treatment of MCL patients and their anticancer effects have been obtained in different types of hematological malignancies^{51,148}, we tested whether IDH2 inhibition could synergize with PIs in B-cell non-Hodgkin lymphoma models. We treated four mantle cell lines JeKo-1, SP-49, Mino and Granta-519 and two Burkitt's lymphomas cell lines HS-Sultan and Raji. Remarkably, a dramatic increase of cell death was observed in all MCL and BL cell lines treated with CFZ/AGI-6780 combinations (Fig. 17). Then, we decided to test a panel of seven diffuse large B-cell lymphomas cell lines (DLBCL). We treated three activated B-cell (ABC)-DLBCL Riva, SU-DHL-2 and U2932. Enhanced sensitivity to CFZ treatment was observed in all ABC-DLBCL (Fig.17). Moreover, we treated four germinal center B-cell (GCB)-DLBCL OCI-Ly8, DoHH2, SU-DHL-6 and Karpas-422. Interestingly, we observed sensitivity to CFZ/AGI-6780 combination in OCI-Ly8 and DoHH2 cell lines. However, even if SU-DHL-6 resulted more sensitive to the combined treatment compared to either agent alone, the effects on cell death were not dramatic as compared to other cell lines. Moreover, Karpas-422 displayed resistant to both single treatments and the combination (Fig.17). It is well known that NF- κ B represents one of the main PIs target^{149,150}. Since ABC-DLBCL have been associated to aberrant NF- κ B signaling, while in GCB-DLBCL NF- κ B target genes are typically underrepresented¹⁵¹, it would be interesting to investigate possible correlation between sensitivity to CFZ/AGI-6780 combination and levels of NF- κ B activity. Further analyses are necessary to elucidate this aspect. The average of sensitivity values, in terms of percentage of cell death, were used to generate a heatmap of drugs sensitivity, by exploiting the Heatmapper software (<http://www2.heatmapper.ca/>)¹⁵² (Fig.17). Overall these results demonstrate that IDH2 could represent new therapeutic target to couple with proteasome inhibition in several B-cell hematological neoplasms.

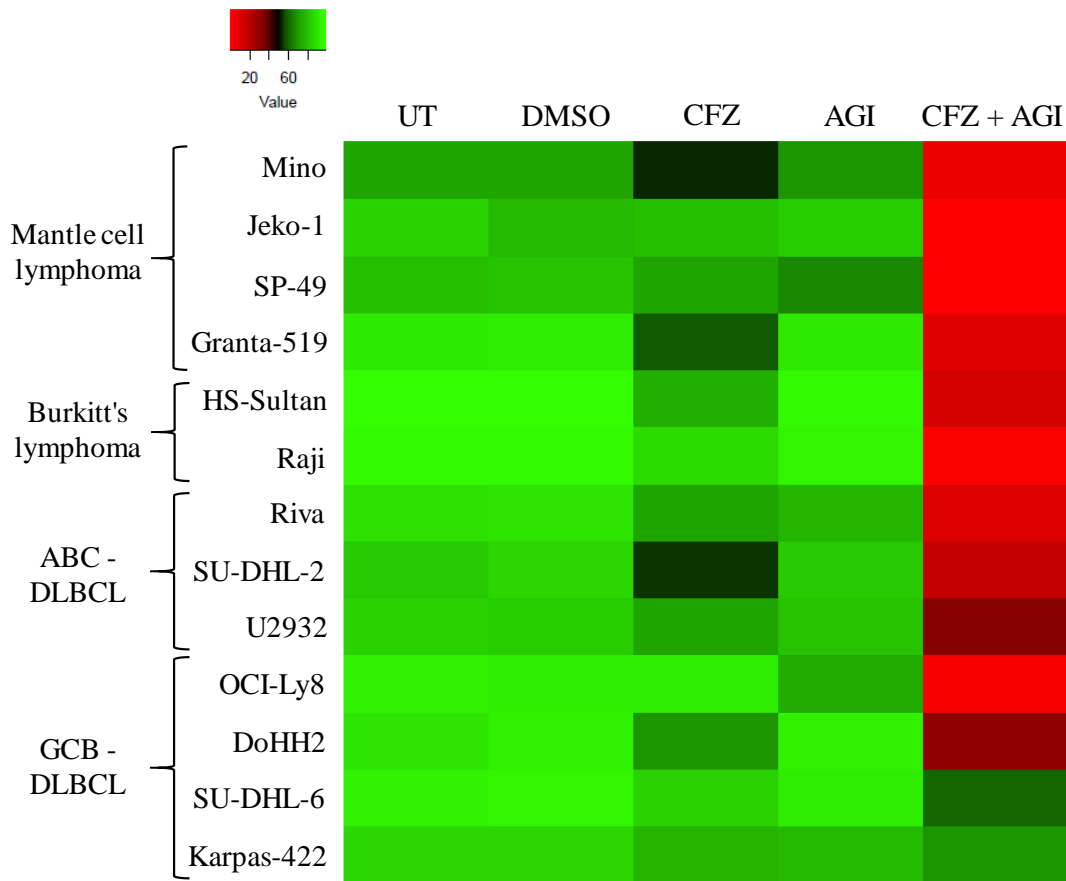


Figure 17. IDH2 inhibition increases sensitivity to CFZ in B-cell hematological malignancies. (A) Heatmap of sensitivity to DMSO, CFZ, AGI-6780, or the combination of the two drugs in a panel of B-cell lymphomas lines. JeKo-1 cells were treated at time 0, 48h, and 96h with both drugs. SP-49 cells were treated at time 0 and 48h with both drugs and at 96h with AGI-6780. Mino cells were treated with both drugs at time 0 and with AGI-6780 at 48h and 96h. Granta-519 cells were treated at time 0h and 48h with both drugs and every 48h with AGI-6780. HS-Sultan cells were treated at time 0 with both drugs and every 48h with AGI-6780. Raji cells were treated at time 0 and 48h with both drugs and every 48h with AGI-6780. ABC-DLBCL and GCB-DLBCL were treated at time 0 with both drugs. Cells were treated with 5 μ M AGI-6780 (2,5 μ M for Raji) and with different doses of CFZ (2,5 nM CFZ for Jeko-1, Granta-519, Raji, Karpas-422, OCI-Ly8, Riva and SU-DHL-2 with; 3,75 nM for U2932; 5nM for SP-49, Mino, SU-DHL-6 and DoHH2 with). Cell viability was measured by TMRM staining-flow cytometry at different time points. Data represents the means of at least three independent experiments. Heatmap was generated using the Heatmapper software, as previously descibed¹⁵².

5.9. IDH2 activation decreases sensibility to CFZ treatment

We then asked whether increased IDH2 activity could impair the cytotoxicity of PIs. As it is known that SIRT3 protein de-acetylates IDH2 and enhances its activity under glucose deprivation^{153,154}, we cultured KMM-1 cells in absence of glucose for 7 days and measured IDH1, IDH2, and IDH3 enzymatic activities. As expected, a stable induction of IDH2 activity was observed after glucose restriction (Fig. 18A). Next, we evaluated whether IDH2 activation was able to rescue MM cells from the effect of CFZ/AGI-6780 combination. KMM-1 cells were conditioned by glucose deprivation for 24 hours and subsequently treated with CFZ, AGI-6780, or with the two agents. Significantly, glucose restriction increased the viability of CFZ- and CFZ/AGI-6780-treated cells, as compared to not starved cells (Fig. 18B). Moreover, we performed a canonical rescue experiment overexpressing IDH2 and/or SIRT3 in KMM-1^{PIR} cells. We transfected cells with an inducible SIRT3-expressing vector (pCW57.1-SIRT3) and/or with a constitutive IDH2-expressing vector (pLX304-IDH2) or with its control plasmid (pLX304 empty). Next, we confirmed IDH2 expression and SIRT3 induction upon doxycycline treatment, by western blot analysis (Fig. 18C). We observed that only the combined overexpression of the two genes was able to enhance IDH2 activity (Fig. 18D). Concordantly, cells with hyperactivation of IDH2 treated with CFZ and AGI-6780 partially decrease cell death, compared to the cells with a basal IDH2 activity (Fig. 18E). Taken together these results suggest that IDH2 activity antagonizes the therapeutic efficacy of first- and second-generation PIs and that pharmacological IDH2 inhibition is a suitable strategy to enhance the therapeutic efficacy of PIs in MM and other B-cell hematological malignancies.

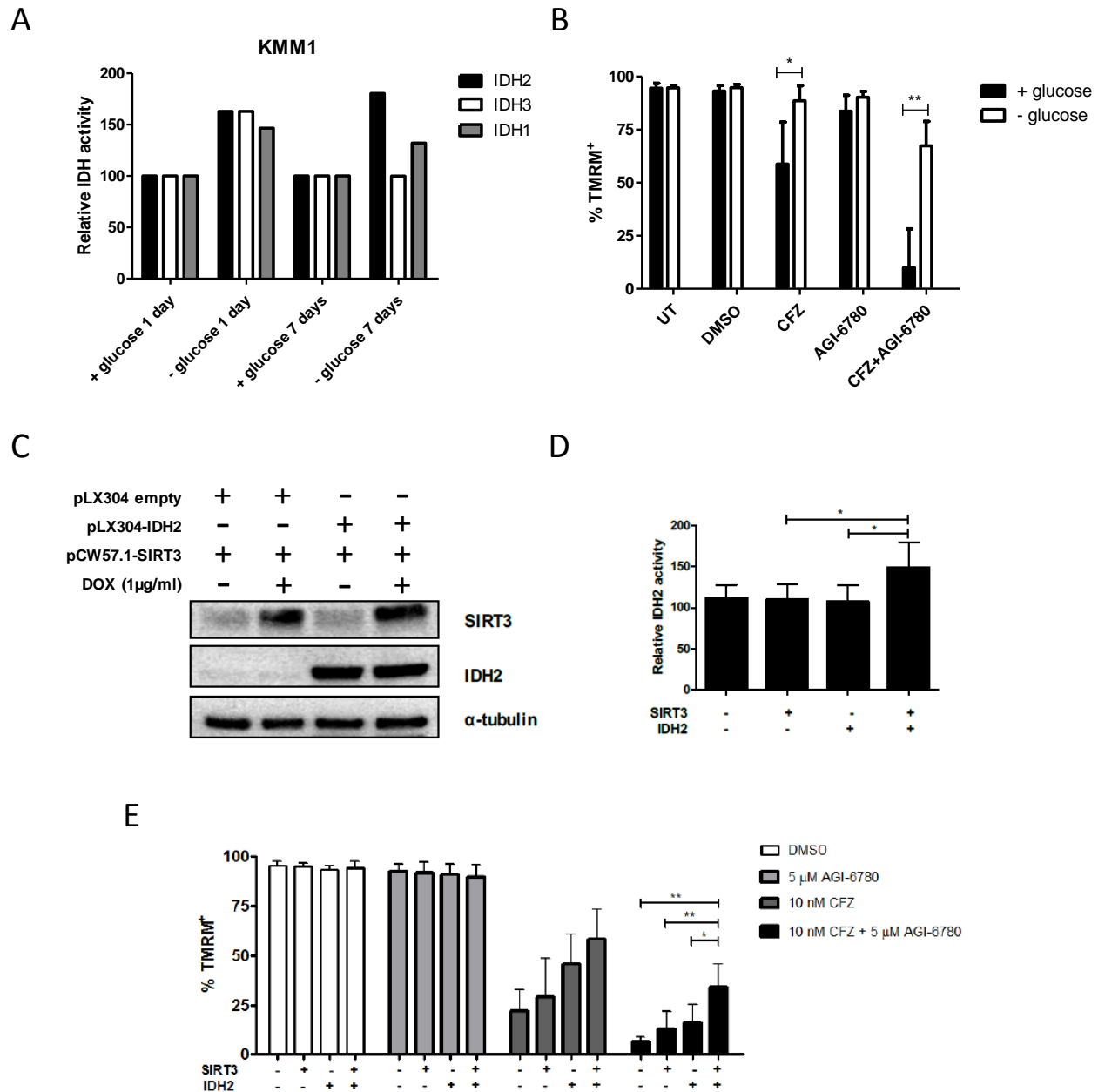


Figure 18. Enhanced IDH2 activity decreases sensitivity to CFZ. (A) KMM-1 cells were cultured in absence or presence of glucose in the medium for 7 days. IDH1, IDH2, and IDH3 activities were measured after 1 and 7 days of starvation. (B) KMM-1 cells were plated in presence or absence of glucose for 24 hours and left untreated (UT), treated with DMSO, CFZ (2.5 nM), AGI-6780 (5 µM), or the combination of the two drugs. Cell viability was measured by TMRM staining-flow cytometry 48 hours post-treatment. Data are the means ± s.d. of five independent experiments. (C) Representative western blot showing SIRT3 and IDH2 expression levels in KMM-1^{PIR} cells transduced with lentiviral particles expressing: pLX304-empty vector, pLX304-IDH2-FLAG, pCW57.1-SIRT3-FLAG. The expression of SIRT3 was induced by 72 hours of doxycycline administration.

α -tubulin protein expression was included for protein loading normalization. (D) IDH2 activity was measured in KMM-1^{PIR} cells 72 hours after doxycycline administration. Data are the means \pm s.d. of four independent experiments. (E) KMM-1^{PIR} cells expressing doxycycline-inducible SIRT3 and constitutively expressing IDH2 or empty vector control were treated with DMSO, CFZ (10 nM), AGI-6780 (5 μ M), or the combination of the two drugs. Cell viability was measured by TMRM staining-flow cytometry 48 hours post-treatment. Data are the means \pm s.d. of four independent experiments (* P <.05; ** P <.01; *** P <.001).

5.10. CFZ/AGI-6780 combinatorial treatment decreases TCA cycle activity and mitochondrial ATP production

To define the molecular mechanisms responsible for the synergy between PIs and IDH2 inhibition, we considered that targeting IDH2 activity could lead to a decrease of NADPH production, resulting in higher reactive oxygen species (ROS) levels¹⁵⁵. Taking into account that oxidative stress has been identified as an important mechanism of PI cytotoxicity in myeloma and non-myeloma cells^{156,157}, we hypothesized that CFZ/AGI-6780 combination could exacerbate ROS levels, thus leading to increased cell death. However, only a slight increase in mitochondrial ROS concentration was observed in MM cells treated with CFZ/AGI-6780 combination (Fig. 19A-B). Next, we evaluated if IDH2 inhibition could impair tricarboxylic acid (TCA) cycle activity¹⁵⁵. Notably, we observed that CFZ/AGI-6780 combination more drastically decreased IDH2 and TCA cycle activities, despite CFZ treatment was ineffective (Fig. 19C-F). In addition, electron transport chain (ETC) flux and mitochondrial ATP synthesis were accordingly down-regulated in MM cells treated with the combination of the two drugs (Fig. 19G-H).

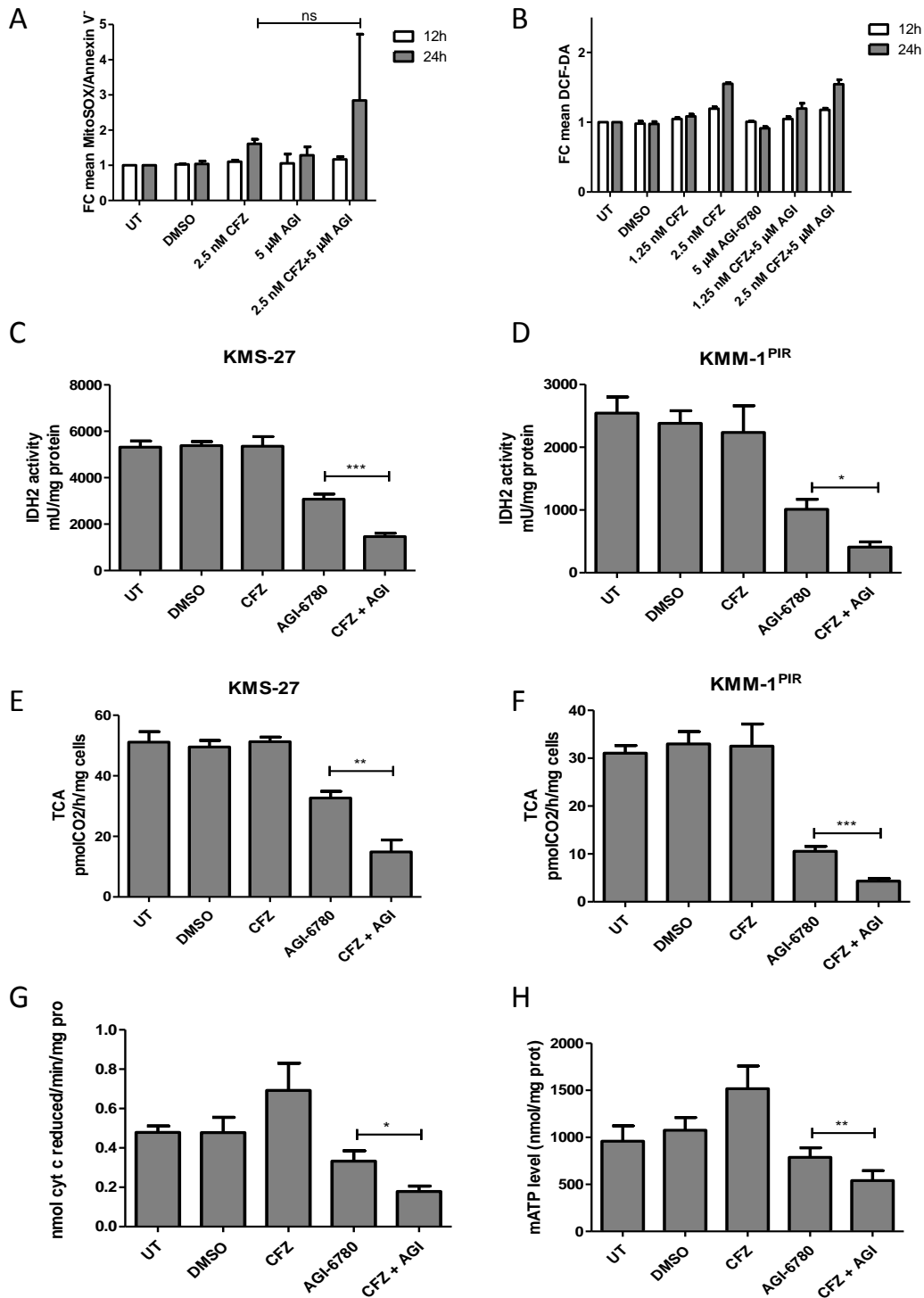


Figure 19. Combinatorial treatment with CFZ and AGI-6780 causes a reduction in IDH2 activity and mATP levels. (A) KMS-27 cells were left untreated (UT), treated with DMSO, CFZ (2.5 nM), AGI-6780 (5 μM), or the combination of the two drugs. Mitochondrial ROS concentration was measured in viable cells by MitoSOX/Annexin V staining-flow cytometry. MitoSOX mean fluorescence intensities are represented as fold change (FC) over UT cells 12 hours and 24 hours post-treatment. (B) KMS-27 cells treated as described above were analyzed for intracellular ROS by 2',7'- dichlorofluorescein

diacetate (DCF-DA) staining-flow cytometry and represented as fold change (FC) over UT cells 12 hours and 24 hours posttreatment. (C) KMS-27 and (D) KMM-1^{PIR} cells untreated (UT), treated with DMSO, CFZ (2.5 nM and 5 nM, respectively), AGI-6780 (5 μ M), or the combination of the two drugs were analyzed for IDH2 activity 6 hours post-treatment. (E) KMS-27 and (F) KMM-1^{PIR} cells treated as described above were analyzed for tricarboxylic acid (TCA) cycle activity 6 hours post-treatment. Data are the means \pm s.d. of four independent experiments. (G) KMS-27 cells treated as described above were analyzed for electron transport chain (ETC) complexes I to III 7 hours post-treatment. (H) KMS-27 cells treated as described above were analyzed for mitochondrial ATP (mATP) production 7 hours post-treatment. Data are the means \pm s.d. of three independent experiments (*P<.05; **P<.01; ***P<.001).

5.11. CFZ/AGI-6780 combinatorial treatment inhibits the NAMPT/SIRT3/IDH2 pathway

Subsequently, we examined the biochemical mechanisms whereby CFZ treatment could synergize with AGI-6780 to further decrease IDH2 activity. It is recognized that PIs inhibit NF- κ B^{149,150} and that expression of nicotinamide phosphoribosyltransferase (NAMPT), a rate-limiting enzyme in the NAD⁺ synthesis and sirtuins activation¹⁵⁸, is transcriptionally modulated by NF- κ B¹⁵⁹⁻¹⁶¹. Therefore, we reasoned that PIs could affect IDH2 activation through the NAMPT/NAD⁺/SIRT3 pathway (Fig. 20A). Consistent with this hypothesis, we demonstrated that CFZ treatment significantly reduced NF- κ B activity in KMS-27 cells (Fig. 20B). Accordingly, NAMPT expression levels were significantly downregulated by CFZ treatment (Fig. 20C). To confirm the involvement of the NAMPT/NAD⁺/SIRT3 pathway, we associated CFZ with several NAMPT inhibitors (FK866, GMX-1778, and Nampt-IN-1). As expected, combination of CFZ with NAMPT inhibitors induced synergistic down-regulation of IDH2 and TCA activity (Fig. 20D-E), followed by MM cell death, confirming the synthetic lethality previously reported by Cagnetta, et al with BTZ and FK866 (Figure 20F-H)¹⁶². Importantly, these results were phenocopied by associating CFZ treatment to SIRT3 inhibition, both using specific drugs (AGK7 and TYP-3) (Fig. 21A-D) and shRNAs targeting SIRT3 (Fig. 21E-F)¹⁶³. Taken together these data demonstrate that CFZ/AGI-6780 combination significantly decreases TCA cycle activity, as a consequence of enhanced IDH2 enzymatic inhibition. Specifically, CFZ treatment reduces NAMPT expression and thus limits IDH2 activation through the NAD⁺-dependent deacetylase SIRT3.

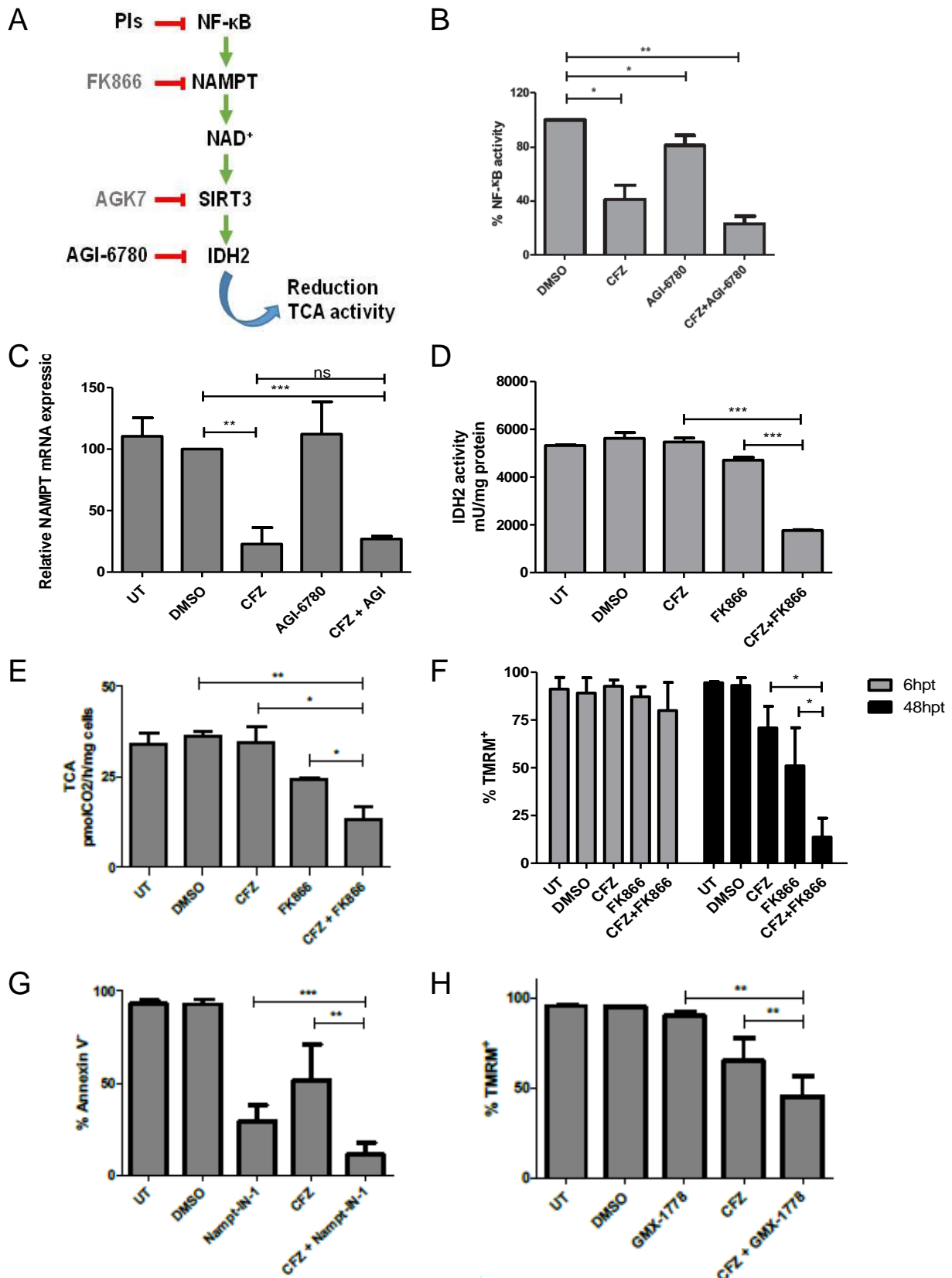


Figure 20. Combinatorial treatment with CFZ and AGI-6780 acts through the inhibition of the NAMPT/SIRT3/IDH2 pathway. (A) Schematic representation of the NAMPT/SIRT3/IDH2 pathway and inhibitors. (B) KMS-27 cells treated with DMSO,

AGI- 6780 (5 μ M), CFZ (3 nM), or the combination of the two drugs were analyzed for NF- κ B activity 6 hours post-treatment. NF- κ B activity was detected in total extracts measuring the DNA-binding capability of NF- κ B on its target sequence (see Methods). Data represent the percentage of NF- κ B binding activity normalized versus DMSO samples and are the means \pm s.d. of three independent experiments. (C) KMS-27 cells untreated (UT), treated with DMSO, CFZ (2.5 nM), AGI-6780 (5 μ M), or the combination of the two drugs were analyzed for NAMPT mRNA expression levels 24 hours post-treatment. Data are the means \pm s.d. of three independent experiments. (D-E-F) KMS-27 cells were left untreated (UT), treated with DMSO or FK866 (10 nM), for 48 hours, vehicle or CFZ (2.5 nM) were added for additional 48 hours. Cells were analyzed for (D) IDH2 activity 6 hours posttreatment with CFZ, (E) for tricarboxylic acid (TCA) cycle activity 6 hours post-treatment with CFZ and for (F) cell viability by TMRM staining-flow cytometry 6 and 48 hours post-treatment with CFZ (hpt). Data are the means \pm s.d. of three independent experiments. (G) KMS-27 cells were left untreated (UT), treated with DMSO, or Nampt-IN-1 (200 nM), for 48 hours, and then vehicle or CFZ (3.75 nM) were added for a further 48 hours. Cell viability was measured by Annexin- staining-flow cytometry 48 hours post-treatment of CFZ. Data are the means \pm s.d. of five independent experiments. (H) KMS-27 cells were left untreated (UT), treated with DMSO, or GMX-1778 (10 nM), for 48 hours, and then vehicle or CFZ (2.5 nM) were added for a further 48 hours. Cell viability was measured by TMRM staining-flow cytometry 48 hours post-treatment of CFZ. Data are the means \pm s.d. of three independent experiments.

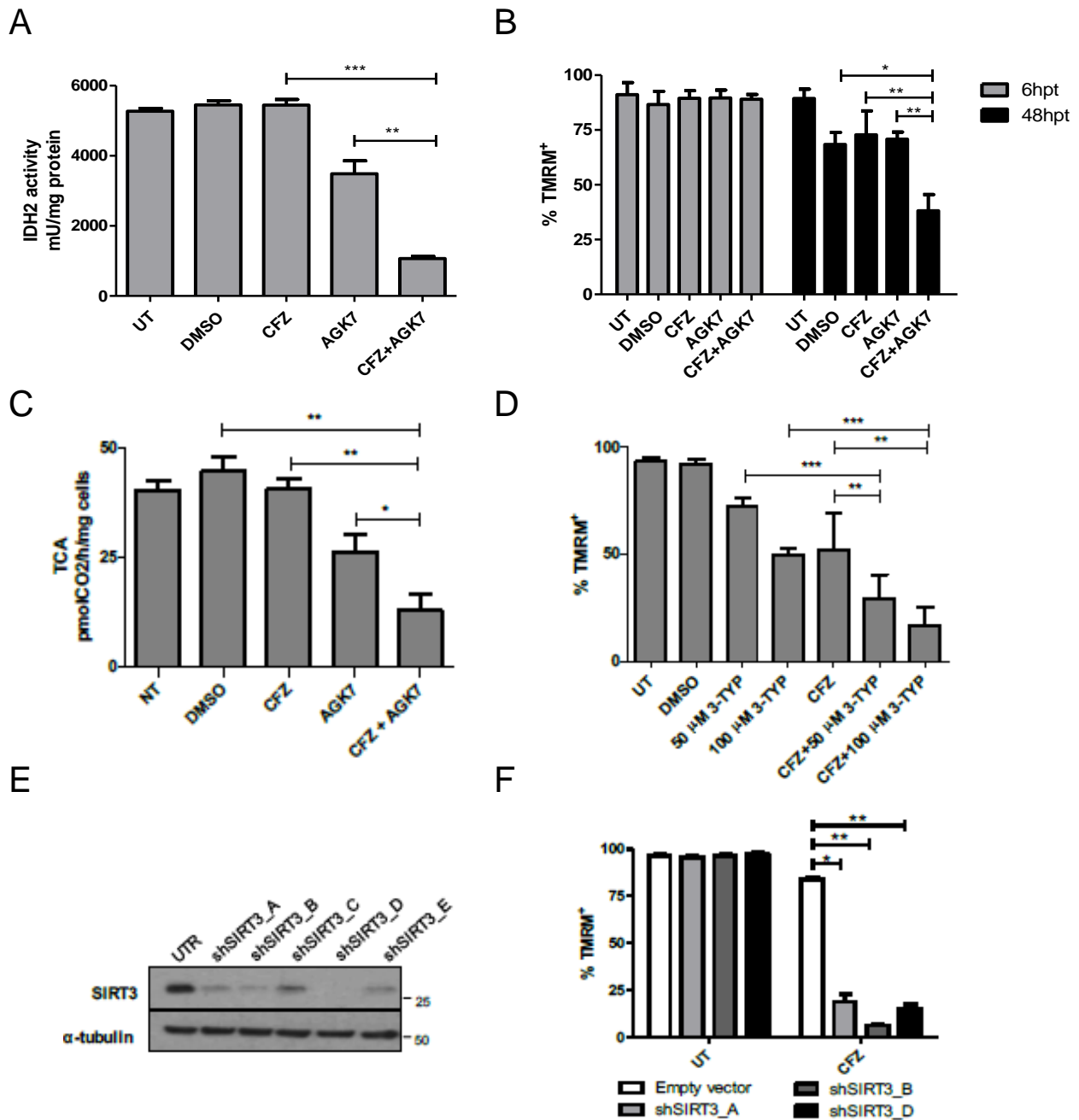


Figure 21. Combinatorial treatment with CFZ and AGI-6780 acts through the inhibition of the NAMPT/SIRT3/IDH2 pathway. (A-C) KMS-27 cells treated with DMSO, CFZ (1.25 nM), AGK7 (10 μM), or the combination of the two drugs were analyzed for (A) IDH2 activity 6 hours post-treatment, for (B) cell viability measured by TMRM staining-flow cytometry 6 and 48 hours post-treatment (hpt) and for (C) tricarboxylic acid (TCA) cycle activity 6 hours post-treatment. Data are the means ± s.d. of three independent experiments. (D) KMS-27 cells were left untreated (UT), treated with DMSO, or 3-TYP (50 or 100 μM), for 48 hours, and then vehicle or CFZ (3.75 nM) were added for a further 48 hours. Cell viability was measured by TMRM staining-flow

cytometry 48 hours post-treatment of CFZ. Data are the means \pm s.d. of five independent experiments. (E) Representative western blot showing SIRT3 expression levels in KMM-1 cells transduced with lentiviral particles expressing the shRNAs targeting SIRT3 (UTR = untransduced). α -tubulin protein expression was included for protein loading normalization. (F) KMM-1 cells were transduced with shRNAs targeting SIRT3 (shSIRT3_A, shSIRT3_B, shSIRT3_D, UTR = untransduced) and treated or not with CFZ (5 nM). Cell viability was measured by TMRM staining-flow cytometry 48 hours post-treatment. Data are the means \pm s.d. of two independent experiments (* P <.05; ** P <.01; *** P <.001).

5.12. Generation of inducible shIDH2 MM cell lines for in vivo studies

Taking into account that AGI-6780 is not suitable for in vivo studies¹⁶⁴, and that enasidenib (AG-221), the mutant IDH2 inhibitor used in the clinic, does not affect the activity of wild-type IDH2¹⁴⁶, we decided to generate IDH2 knock-out MM cell lines, by exploiting CRISPR-Cas9 technology (Fig. 22A). As previously described¹⁶⁵, we generated an all-in-one vector carrying two gRNAs targeting second and last IDH2 exons, and Cas9 protein (Fig. 22B). First, we tested the efficiency of 4 duplex gRNAs in the 293T cell line. Specifically, a consistent deletion of the IDH2 genomic locus (Fig. 22C) and a consequent reduction of IDH2 mRNA and protein levels (Fig. 22D-E) was detected in 293T cells transfected with IDH2 gRNAs and selected with puromycin. Next, we targeted the IDH2 locus in the MM cell line KMS-27 using a specific nucleofection protocol followed by puromycin selection. PCR analysis of the IDH2 locus indicated efficient IDH2 genomic deletion in the bulk cell population (Fig. 22F). Moreover, Sanger sequencing of PCR products confirmed target specificity and excluded off-target events, thus supporting the feasibility of the approach (Fig. 22G). We then plated cells by serial dilution in order to obtain one single-cell per well, thus isolating IDH2^{-/-} genotype. However, following PCR screening of almost 100 colonies we found no positive clone, but only wild type and heterozygous genotypes (Fig. 22H). As a consequence of the failure in achieving homozygous deletion of IDH2 locus in the KMS-27 cell line, we decided to exploit a conditional RNAi method to knock-down IDH2 expression^{166,167}. Therefore, to provide an *in vivo* proof of principle that IDH2 inhibition could increase the therapeutic efficacy of PIs in MM, we generated a KMS-27 cell line expressing an inducible IDH2-shRNA (IDH2-A4) under the control of the doxycycline-regulated transcriptional repressor tTR-KRAB (TK). IDH2 silencing upon doxycycline treatment was assessed by western-blot analysis in a time-course experiment (Fig. 23A). Furthermore, we confirmed that inducible IDH2 silencing increases sensitivity to CFZ treatment (Fig. 23B).

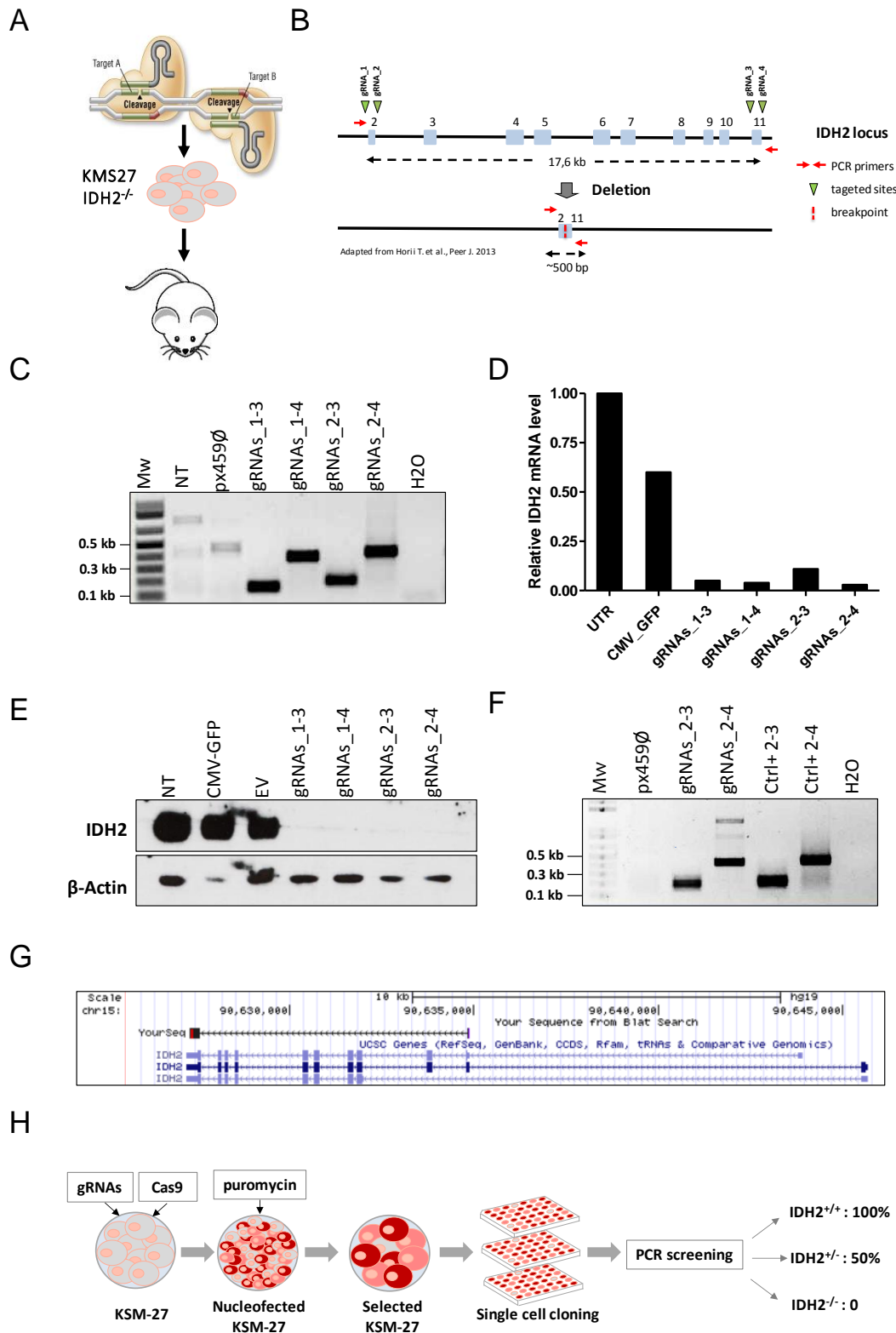


Figure 22. Inability to select IDH2^{-/-} homozygous deleted clones. (A) Representative scheme of IDH2 knock-out cells generation for *in vivo* studies. (B) Schematic representation of edited IDH2 locus. Green triangles depict four gRNAs designed targeting second and last IDH2 exons. Red arrows represent PCR primers used for screen colonies. (C) PCR products of IDH2 edited locus, detected in 293T cells transfected with two gRNAs

targeting IDH2. No PCR product was detected in untransfected cells (UTR) or transfected with empty vector (px459Ø). (D) 293T cells untransfected (UTR), transfected with control plasmid (CMV_GFP) or transfected with were analyzed for IDH2 mRNA expression levels 72 hours post-selection. (E) Western blot showing IDH2 expression levels in 293T cells untransfected (UTR), transfected with control plasmid (CMV_GFP), empty vector (px459Ø), or transfected with gRNAs targeting IDH2 locus. β -actin protein expression was included for protein loading normalization. (F) PCR products of IDH2 edited locus, detected in KMS-27 cells transfected with gRNAs targeting IDH2 locus. No PCR product was detected in cell transfected with empty vector (px459Ø). (G) Representative picture of BLAT analysis using UCSC Genome Browser. IDH2 edited locus DNA sequence were aligned on human genome (GRCh38/hg38). (H) A procedure of selection and identification of knockout clones.

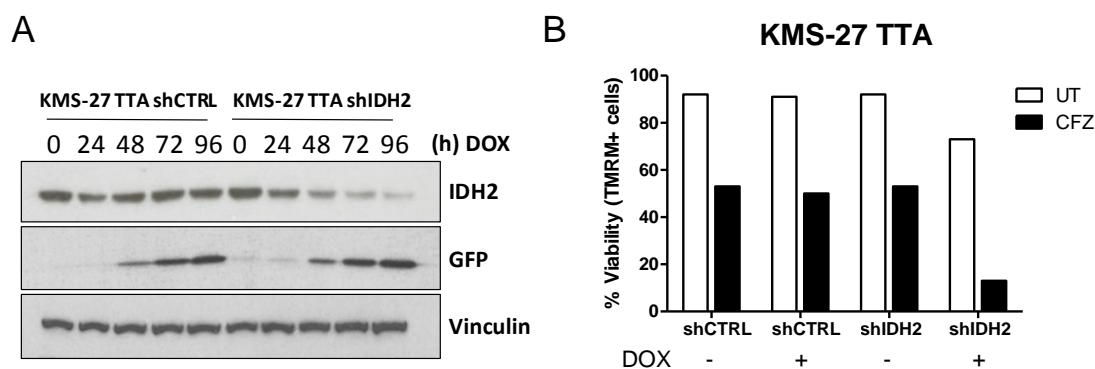


Figure 23. Generation of inducible shIDH2 KMS-27 cells. (A) Western blot analysis of IDH2 and GFP expression of inducible KMS-27. Cells were cultured in presence of 1 μ g/ml of DOX and pellet were collected at indicated points. Vinculin was included for protein loading normalization. (B) KMS-27 TTA cell line was transduced with the control vector (shCTRL) or inducible shRNA targeting IDH2 (shIDH2) and treated with 1 μ g/ml of DOX and 1,25nM CFZ. Cell viability was measured by TMRM staining-flow cytometry 72 hours post-treatment.

5.13. Targeting IDH2 and proteasome activities triggers synergistic inhibition of human MM cells growth ex-vivo and in vivo with low toxicity to normal human cells

To evaluate whether IDH2 inhibition potentiates CFZ effect in primary cells from MM patients, buffy coats derived from bone marrow aspirates of 9 MM patients were cultured on a layer of HS-5, a bone marrow stromal cell line. Ex-vivo co-cultures were treated with CFZ/AGI-6780

combination or with the single drugs for 96 hours. Combination treatment significantly decreased viability of CD138+ cells (Fig. 24A). Next, we demonstrated that CFZ/AGI-6780 treatment exhibited a favorable cytotoxicity profile towards peripheral blood mononuclear cells and bone marrow-derived stromal cells, compared to KMS-27 (Figure 24B-C). We next studied the growth patterns of KMS-27-TK-IDH2-A4 cells injected subcutaneously into the flanks of NOD/SCID/IL2R γ ^{-/-} (NSG) mice. Mice with masses of 0.5 cm in diameter were treated with doxycycline (DOXY; 0.1 mg/mL biweekly), CFZ (4 mg/kg biweekly), or control diluents. Administration of either agent had a substantial effect on tumor growth, as compared to control mice (P<.0001). Importantly, when IDH2 silencing was combined to CFZ, there was a further significant reduction in tumor growth in relation to single treatments (CFZ vs CFZ/DOXY P=.0244; DOXY vs CFZ/DOXY P=.0238; Fig. 24D). The median overall survival of mice treated with CFZ associated to IDH2 silencing was significantly longer than vehicle-treated mice (26 vs 49 days; P=.0001), or mice treated with either drug alone (35 days for CFZ and 38 days for DOXY) (Fig. 24E). Moreover, we were able to establish a systemic mouse model of MM suitable for therapy testing (Fig. 24F-G-H). Briefly, DsRed+ KMS-28 MM cells were intravenously injected into the tail vein of NSG mice and signs of disease were monitored by nuclear magnetic resonance (NMR) overtime. Mice were euthanized at 46 days, organs collected and dismantled to obtain single cell suspensions. KMS-28 cells engraftment was detected in different organs including BM, by FACS analysis using anti-human-CD138 (Fig. 24F). To confirm if this model could be exploited to test new combination therapies, KMS28 cells expressing inducible shRNA against IDH2 were used. Following i.v. tail vein inoculation of MM cells, animals were randomized and treated with dosing regimens comparable to those described in subcutaneous MM xenograft studies. As shown in Fig. 26 G-H, FACS analysis of CD138/DsRed double positive cells indicated that MM cell engraftment was significantly impaired by DOX/CFZ combination, as compared to single treatments (Fig. 24G-H).

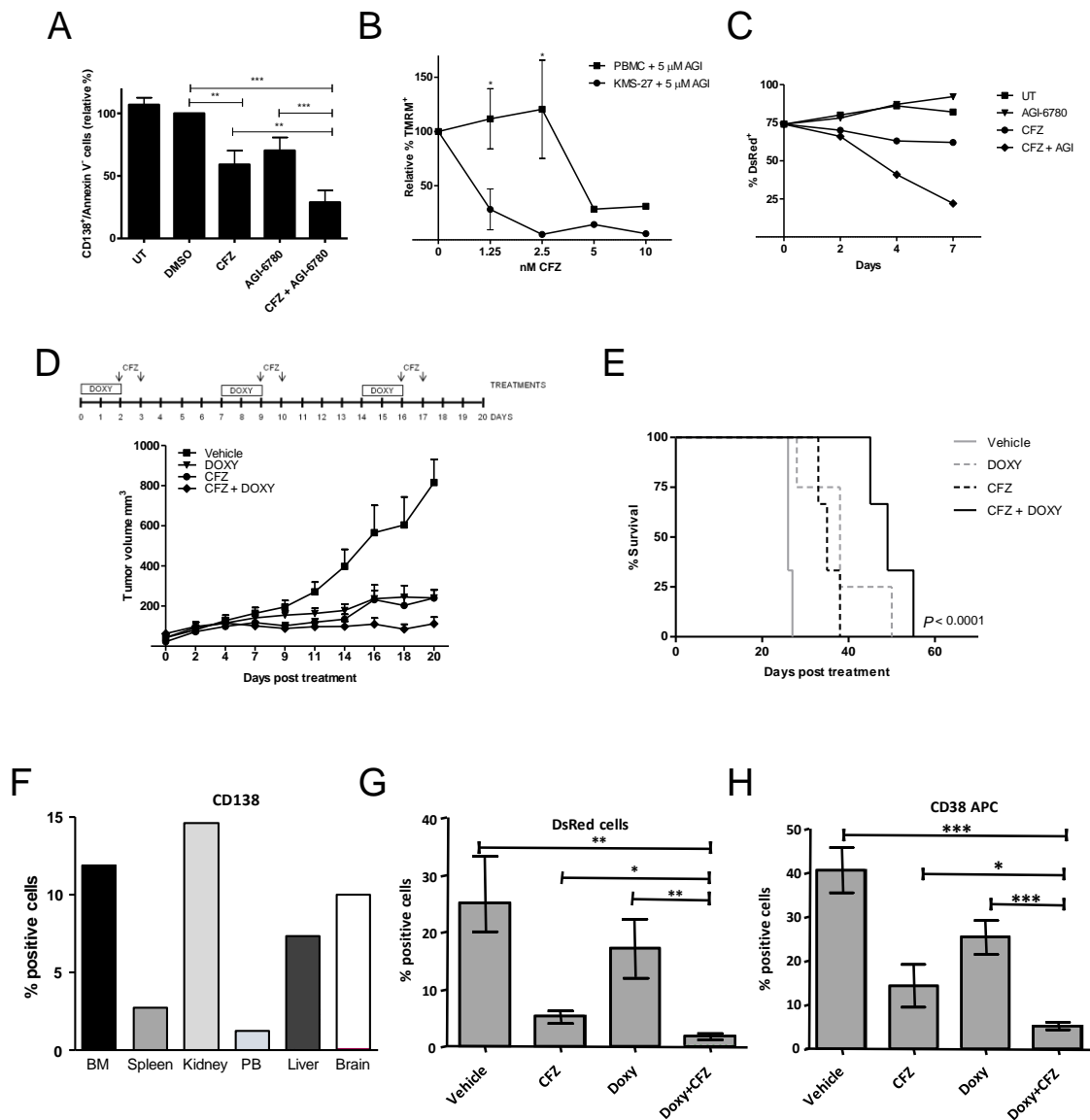


Figure 24. Targeting IDH2 and proteasome activities triggers synergistic inhibition of human MM cells growth ex-vivo and in vivo with low toxicity to normal human cells.

(A) Buffy coats derived from bone marrow aspirates of MM patients were treated with CFZ (2.5 nM) in combination or not with AGI-6780 (5 μM). Cell viability was estimated by FACS measuring Annexin V- and CD138⁺ cells 96 hours post-treatment. Histograms represent the percentage of viable cells normalized versus DMSO samples. Data are the means ± s.e.m. of nine independent MM patients. (B) Peripheral blood mononuclear cells (PBMCs) and KMS-27 were treated with DMSO, CFZ (1.25, 2.5, 5, 10 nM), AGI-6780 (5 μM), or the combination of the two drugs. PBMCs were derived from 4 healthy donors. Cell viability was measured by TMRM staining-flow cytometry 48h post-treatment. Data are the means ± s.d. (*P<.05; **P<.01; ***P<.001). (C) KMS-27-TK cells (expressing DsRed fluorescent protein) were co-cultured with HS-5 bone marrow/stroma cell line and treated with CFZ, AGI-6780, or the combination. Percentage of live DsRed⁺ cells was

measured overtime. Data are the means \pm s.d. of three independent experiments (CFZ vs CFZ+AGI-6780 $**P<.01$). (D) Growth patterns of KMS-27-TK-IDH2-A4 cells injected subcutaneously into the flanks of NOD/SCID/IL2R $\gamma^{-/-}$ (NSG) mice. Tumor masses of 0.5 cm diameter mice were randomized for treatment with vehicle (n = 6), 4 mg/kg CFZ (n = 8), 0.1 mg/mL DOXY (n = 10), or the combination of both compounds (n = 10) over 3 weeks. Administration of either agent had a substantial effect on tumor growth, as compared to control mice ($P<.0001$). Combination of IDH2 silencing with CFZ further reduced tumor growth in relation to single treatments (CFZ vs CFZ/DOXY $P=.0244$; DOXY vs CFZ/DOXY $P=.0238$). Each data point represents the average tumor volume (mean \pm standard error of the mean) for the indicated treatment condition. The timeline shows the schedule of treatment followed for in vivo treatments. (E) Kaplan–Meier survival plot showing survival for mice treated with vehicle (n = 6), 4 mg/kg CFZ (n = 6), 0.1 mg/mL DOXY (n = 8), or their combination (n = 6). CFZ plus DOXY-treated mice show significantly increased survival (49 days) in comparison with vehicle-treated mice (26 days; $P<.0001$), CFZ alone (35 days; $P=.0007$), and DOXY alone (38 days; $P=.0472$). (F) Percentage of human MM cell lines engraftment in different organs. DsRed+ cells (1×10^7) were intravenously injected in tail vein in 8-week old NSG mice and left to engraft for 46 days. Mice were euthanized, organs collected and dismantled to obtain single cell suspension. Human MM inoculated cells were identified by FACS analysis of anti-human-CD138 positive staining. (G-H). Percentage of DsRed+ (G) and CD138+ (H) cells after treating with DOXY (0.1 mg/mL biweekly) and CFZ (4 mg/kg biweekly), or control diluents by intravenously (i.v.) injection.

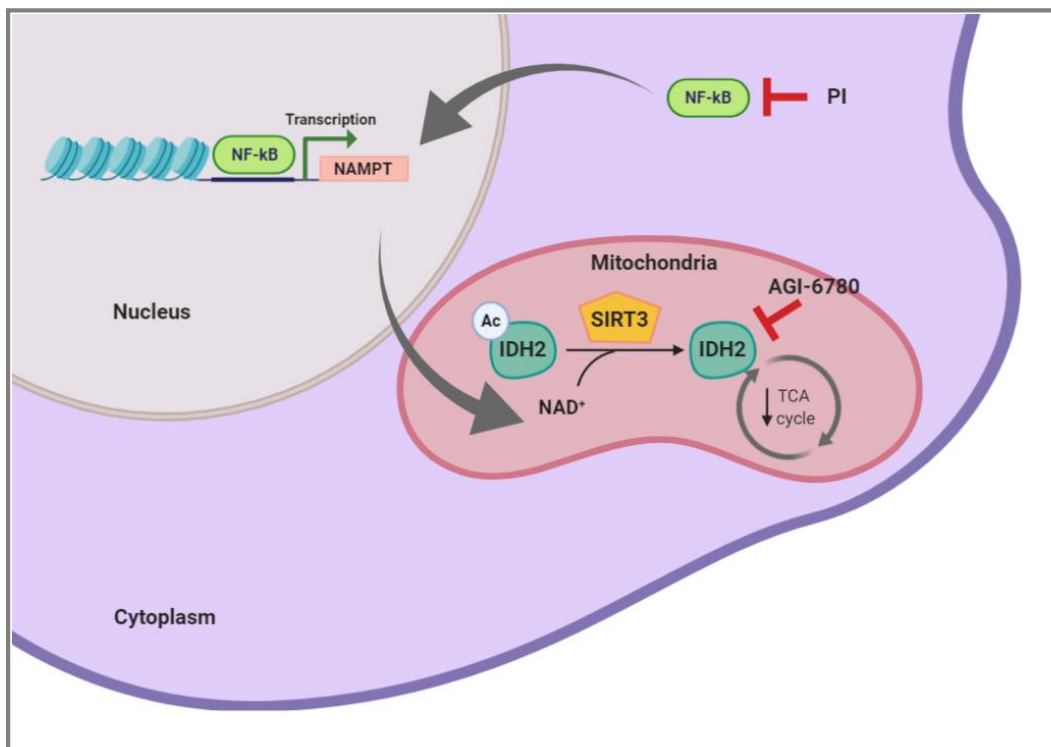


Figure 25. Graphic summary of PI/AGI-6780 synergistic effects in multiple myeloma cells. PI treatment inhibits NF-kB activity, with a consequent reduction of NAMPT expression. This leads to a decrease in NAD⁺ synthesis, decreased SIRT3 activation, and IDH2 enzymatic inhibition. Furthermore, AGI-6780 treatment directly inhibits IDH2 in the mitochondria. Taken together, PI/AGI-6780 combination significantly decreases TCA cycle activity and ATP production thus inducing cell death.

5.14. LSD1 silencing sensitizes PI-resistant MM cells to carfilzomib treatment

As discussed above, shRNA screening led to the identification of 3 top synthetic lethal genes with CFZ treatment (Fig. 9C). We then decided to validate additional genes identified by shRNA screening. In particular, we focused on lysin-specific demethylase 1 (LSD1). LSD1 is the first discovered histone demethylase, and it can act as co-activator or co-repressor by demethylating mono- or di-methylated lysine 4 or 9 of histone H3 (H3K4me1/me2 and H3K9me1/me2, respectively) depending on its interacting partners. First, we individually transduced PI-resistant cell lines KMM-1^{PIR} and U266^{PIR} with two shRNA (D9 and D10) direct against human LSD1 mRNA. LSD1 silencing was confirmed by RT-qPCR (Fig. 26A-B) and western blot (Fig. 26C). LSD1 knockdown did not affect cell viability of KMM-1^{PIR} and U266^{PIR} cell lines, but upon CFZ treatment, enhance cytotoxicity was observed in silenced cell lines compared to cells transfected with scramble shRNA (Fig. 26D-E). Taken together these data demonstrated that LSD1 inhibition can increase sensitivity to CFZ in PI-resistant cells.

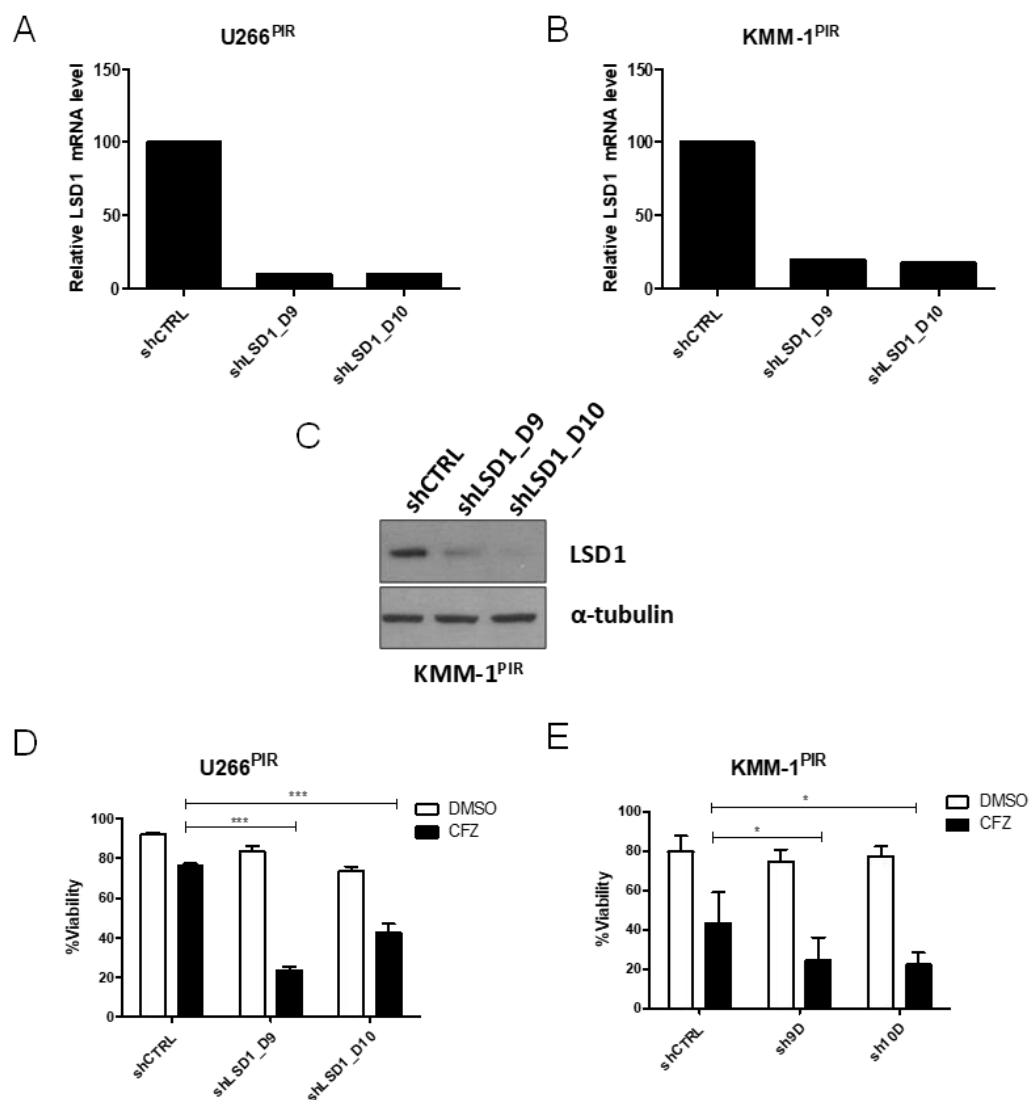


Figure 26. LSD1 silencing enhances sensitivity to CFZ treatment in PI-resistant MM cell lines. (A) KMM-1^{PIR} and (B) U266^{PIR} cells were transduced with lentiviral particles expressing two shRNA (shLSD1_D9, shLSD1_D10) targeting LSD1 or scramble shRNA (shCTRL). LSD1 silencing was monitored by RT-qPCR after puromycin selection. (C) Representative western blot showing LSD1 expression levels in KMM-1^{PIR} cells transduced with lentiviral particles expressing scramble shRNA (shCTRL) or two shRNA targeting LSD1 (shLSD1_D9 and shLSD1_D10). Vinculin protein expression was included for protein loading normalization. (D) U266^{PIR} and (E) KMM-1^{PIR} cell lines were transduced with control shRNA or with shRNA targeting LSD1 (shLSD1_D9, shLSD1_D10) and treated with CFZ (U266^{PIR} and KMM-1^{PIR}, 20 nM and 10 nM, respectively) or DMSO. Cell viability was measured by TMRM staining-flow cytometry 72 hours post-treatment (hpt). Data are the means \pm s.d. of three independent experiments (**P<.01; ***P<.001).

5.15. Synthetic lethal interaction between LSD1 silencing and CFZ treatment is recapitulated in MM-sensitive cell lines

To investigate if cytotoxic interaction between LSD1 silencing and CFZ treatment can be repeated in PI-sensitive MM cells, three myeloma cells, including KMM-1 parental cell line, were individually transfected with two shRNA sequences against LSD1 (D9 and D10). LSD1 depletion initially affected cell viability in parental KMM-1 cell line, but the effect was lost over time (Fig. 27A). In this cell line we were able to demonstrate that LSD1 inhibition enhances sensitivity to CFZ treatment (Fig. 27B). However, in KMS-28 and AMO-1 cell lines, LSD1 inhibition alone affected cell viability as compared to scramble shRNA transfected cells (Fig. 27C-D). We then generated inducible LSD1-shRNAs (LSD1-D9 and LSD1-D10) in KMS-28 and AMO-1 cell lines, as described above. We first confirmed progressive LSD1 silencing and GFP expression, upon doxycycline treatment by western blot analysis (Fig. 27E-F). Then, 96 hours post-doxycycline treatment, when LSD1 was depleted and cells were viable (data not shown), we started CFZ treatment. Remarkably, LSD1 silencing was able to enhance CFZ treatment in both cell lines (Fig. 27G-H). Together these data demonstrated that LSD1 can mediate CFZ sensitivity also in MM sensitive cell lines, and it can have a role in regulate cell viability in myeloma cells.

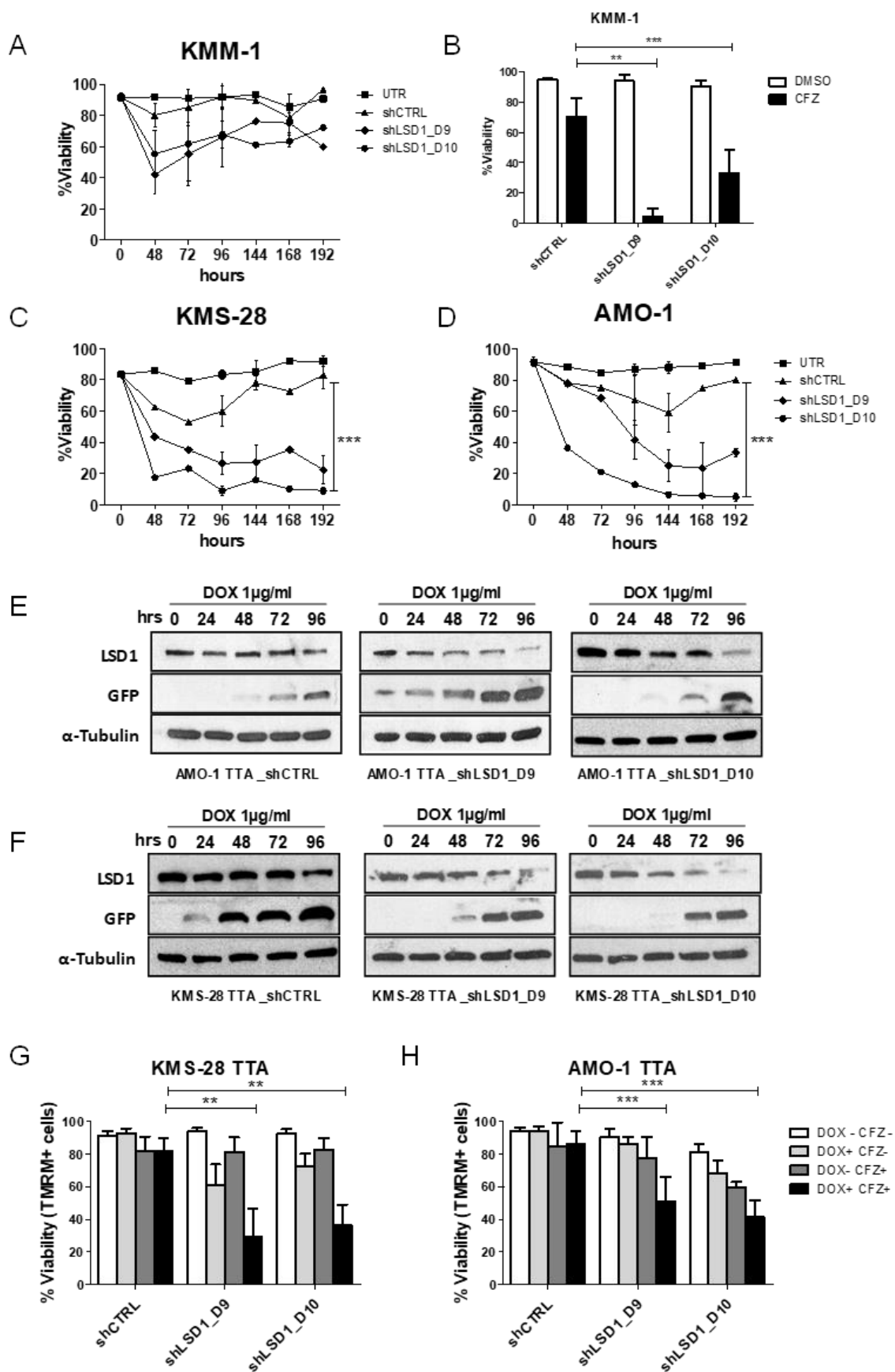


Figure 27. LSD1 silencing enhances sensitivity to CFZ in PI-sensitive MM cell lines.

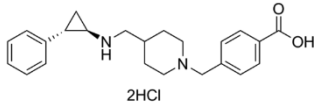
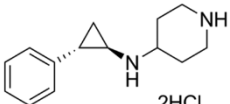
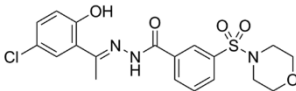
(A) KMM-1 cell line was transduced with lentiviral particles expressing two shRNA (shLSD1_D9, shLSD1_D10) targeting LSD1, scramble shRNA (shCTRL) or left untransduced (UTR). Cell viability was monitored by TMRM staining-flow cytometry at indicated time points after puromycin selection. (B) KMM-1 cell line was transduced with lentiviral particles expressing two shRNA (shLSD1_D9, shLSD1_D10) targeting LSD1 or scramble shRNA (shCTRL) and treated with 5nM CFZ. Cell viability was measured by TMRM staining-flow cytometry 72 hours post-treatment. Data are the means \pm s.d. of three independent experiments (**P<.01; ***P<.001). (C) KMS-28 and (D) AMO-1 cell lines were transduced with lentiviral particles expressing two shRNA (shLSD1_D9, shLSD1_D10) targeting LSD1, scramble shRNA (shCTRL) or left untransduced (UTR). Cell viability was monitored by TMRM staining-flow cytometry at indicated time points after puromycin selection. (E-F) Western blot showing LSD1 and GFP expression in (E) AMO-1 TTA and (F) KMS-28 TTA cell lines transduced with lentiviral particles expressing two shRNA against LSD1 (shLSD1_D9 and shLSD1_D10) or scramble shRNA (shCTRL), upon induction with doxycycline (DOX). Cells were treated with 1 μ g/ml of DOX and pellet were collected at indicated time points. α -tubulin protein expression was included for loading normalization. (G) KMS-28 TTA and (H) AMO-1 TTA were transduced with lentiviral particles expressing two shRNA against LSD1 (shLSD1_D9 and shLSD1_D10) or scramble shRNA (shCTRL) and treated or not with DOX (1 μ g/ml) for 72 hours and then with CFZ (1.25 nM). Cell viability was measured by TMRM staining-flow cytometry 72 hours post CFZ treatment. Data are the means \pm s.d. of four independent experiments (**P<.01; ***P<.001).

5.16. LSD1 inhibitors are effective in MOLM-13 AML cell line

In years, epigenetic regulators have become major targets for developing antimyeloma agents^{168,169}. Today, histone lysine demethylases (KDMs) are also emerging and they represent new therapeutic strategies. For this reason, to confirm data obtained with genetic LSD1 silencing, we tested three LSD1 inhibitors, SP2509, GSK2879552 and GSK-LSD1 for their effectiveness in MM cells (Table 2). SP2509 is a reversible and selective non-competitive LSD1 inhibitor, that has demonstrated potent activity against acute myeloid leukemia (AML), non-small cell lung cancer (NSCLC) and clear cell renal cell carcinoma (ccRCC) in vitro and in xenograft models¹⁷⁰⁻¹⁷². SP2509 was first described by Sorna et al¹⁷³ as a novel compound able to inhibit specifically LSD1, over MAO enzymes. In the work they demonstrated that SP2509 can alter the solution dynamics of LSD1 by constraining its conformational dynamics¹⁷³. Therefore, they suggest that SP2509 may disrupt key

protein-protein interaction which can regulate LSD1 activity. However, its exact mechanism of action, binding mode and pharmacokinetics are not well clarified. GSK2879552 and GSK-LSD1 are two potent, selective and irreversible inhibitors of LSD1 which covalently modify the FAD cofactor to inhibit its catalytic activity¹⁷⁴. It has been demonstrated that they are mechanism-based inhibitors as its mechanism of action involves single electron reduction of the LSD1-bound FAD cofactor, leading to homolytic cleavage of the cyclopropyl ring and ultimate covalent modification of the FAD cofactor¹⁷⁴. GSK2879552 showed antiproliferative activity in AML and small cell lung cancer (SCLC) cells, both in vitro and in vivo¹⁷⁴. While GSK-LSD1 showed antiproliferation activity against various cancer cell lines^{175,176}. Since LSD1 inhibitors have showed promising results for the treatment of AML¹⁷⁷, we first decided to test effectiveness of agents in AML cell line, MOLM-13. SP2509 was effective in inducing MOLM-13 cell death at low micromolar concentrations. In contrast, GSK2879552 and GSK-LSD1 did not affect cell viability, even at much higher concentrations (Fig. 28A). To prove effectiveness of GSK-inhibitors, we focused on cell differentiation, as previously described^{170,178}. MOLM-13 cells were treated with increasing concentration of GSK2879552 and GSK-LSD1. Both drugs induced cells to differentiate, as demonstrated by increase expression of surface CD11b protein (Fig. 28B). Finally, all drugs increased percentage of cells in G0/G1 phase of cell cycle (Fig. 28C-D-E). These data demonstrated that LSD1 inhibitors are effective in MOLM-13 AML cells.

Table 2. Overview on LSD1 inhibitors. LSD1 inhibitors chemical structure, drug mechanism of action and current clinical status are reported¹⁷⁹.

Compound	GSK2879552	GSK-LSD1	SP2509
Structure			
Mechanism of action	K_{iapp} of 1.7 μ M Irreversible inhibitor covalently modifying the FAD cofactor (23)	IC_{50} : 16 nM Irreversible inhibitor covalently modifying the FAD cofactor (23)	IC_{50} : 13 nM Reversible noncompetitive inhibitor (43)
Clinical status	Phase I studies in SCLC (NCT02034123) and AML (NCT02177812) have been terminated because the risk benefit does not favor continuation. Phase I/II study in MDS (NCT02929498)	NA	NA

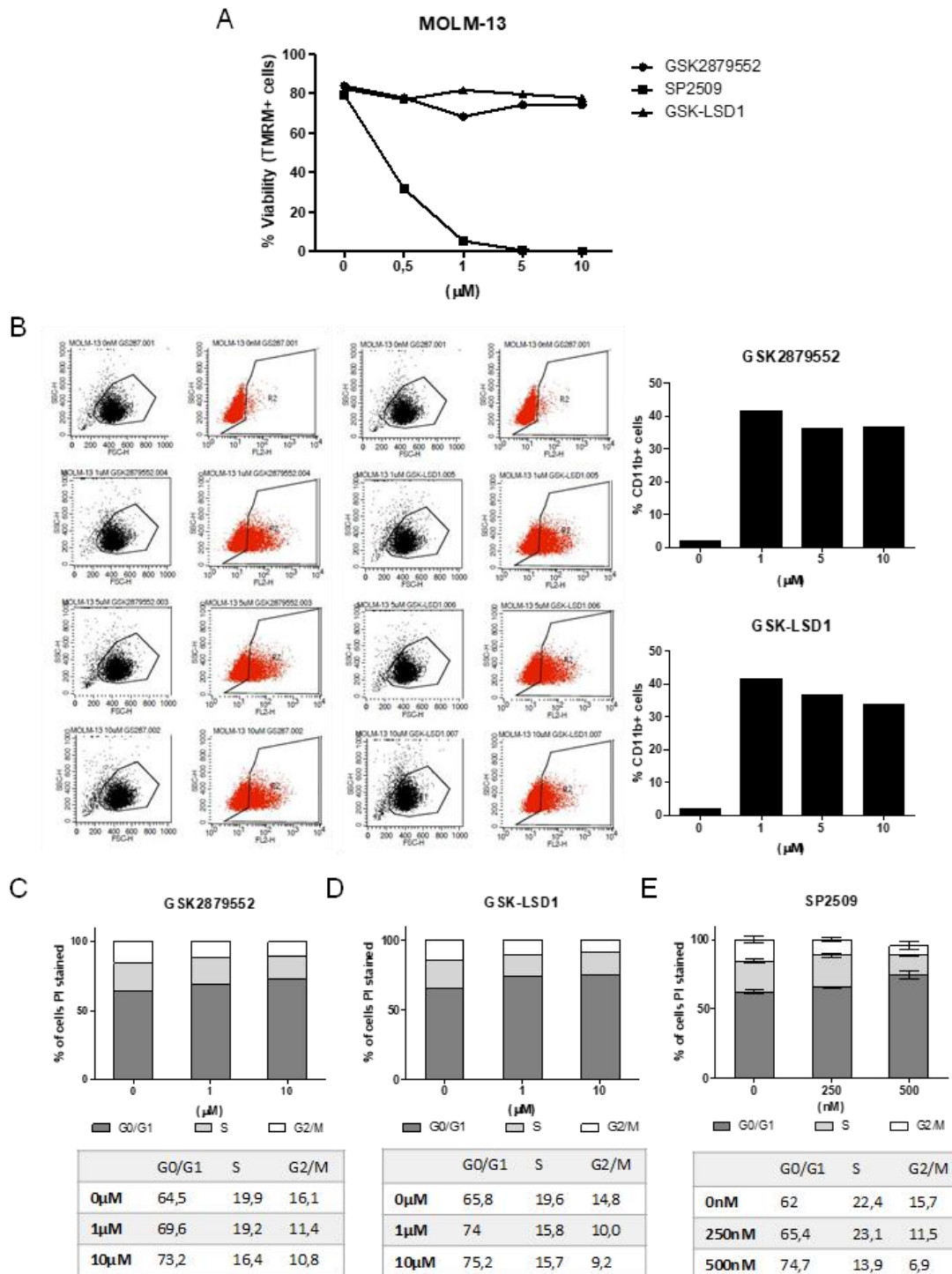


Figure 28. LSD1 inhibitors are effective in AML MOLM-13 cell line. (A) MOLM-13 cells were treated with SP2509, GSK2879552 and GSK-LSD1 at indicated concentrations. Cell viability was measured by TMRM staining-flow cytometry at 72 hours post-treatment. (B) MOLM-13 cells were treated with increasing concentrations of GSK2879552 and GSK-LSD1 every 72 hours or left untreated. (Left panel) Differentiation was measured by CD11b staining-flow cytometry 7 days post-treatment. (Right panel) Percentage of CD11b positive cells was represented by histograms. (D-E-F) MOLM-13 cells were treated with

(D) GSK2879552, (E) GSK-LSD1 and (F) SP2509 at indicated doses. Cell cycle was measured by PI staining-flow cytometry 72 hours post-treatment.

5.17. LSD1 pharmacological inhibition enhances sensitivity to CFZ treatment in MM cell lines

To confirm data of synthetic lethal interaction between LSD1 inhibition and CFZ treatment, KMM-1^{PIR} and U266^{PIR} resistant cell lines were treated with SP2509 and CFZ. Combinatorial treatment significantly increases cell death, compared to single treatments (Fig. 29A), confirming data obtained by LSD1 knockdown. To investigate whether this effect was synergistic or additive, Compusyn analysis software was used^{180,181}. KMM-1^{PIR} cells were treated with increasing concentration of SP2509 and CFZ, by maintaining the same ratio between two drugs. Effectiveness of treatments was confirmed by FACS analysis (Fig. 29B). Importantly, combined therapy with CFZ and SP2509 synergistically induced apoptosis of KMM-1^{PIR} cells, with combination indices (CI) below 1.0 for three drug treatments, as determined by isobologram analysis (Fig. 29C). Then we tested combined therapy in a panel of ten MM cell lines, with different CFZ sensitivity. Eight out of ten MM cell lines showed enhanced sensitivity to the combination therapy respect to either agent alone, with high significance for six cell lines, and minor significance for two (Fig. 29D). Moreover, two MM cell lines did not show sensitivity for neither agent alone nor combination therapy. These results demonstrated that SP2509 and CFZ display synergistic activity, and that their effects are not restricted to PI-resistant MM cell lines.

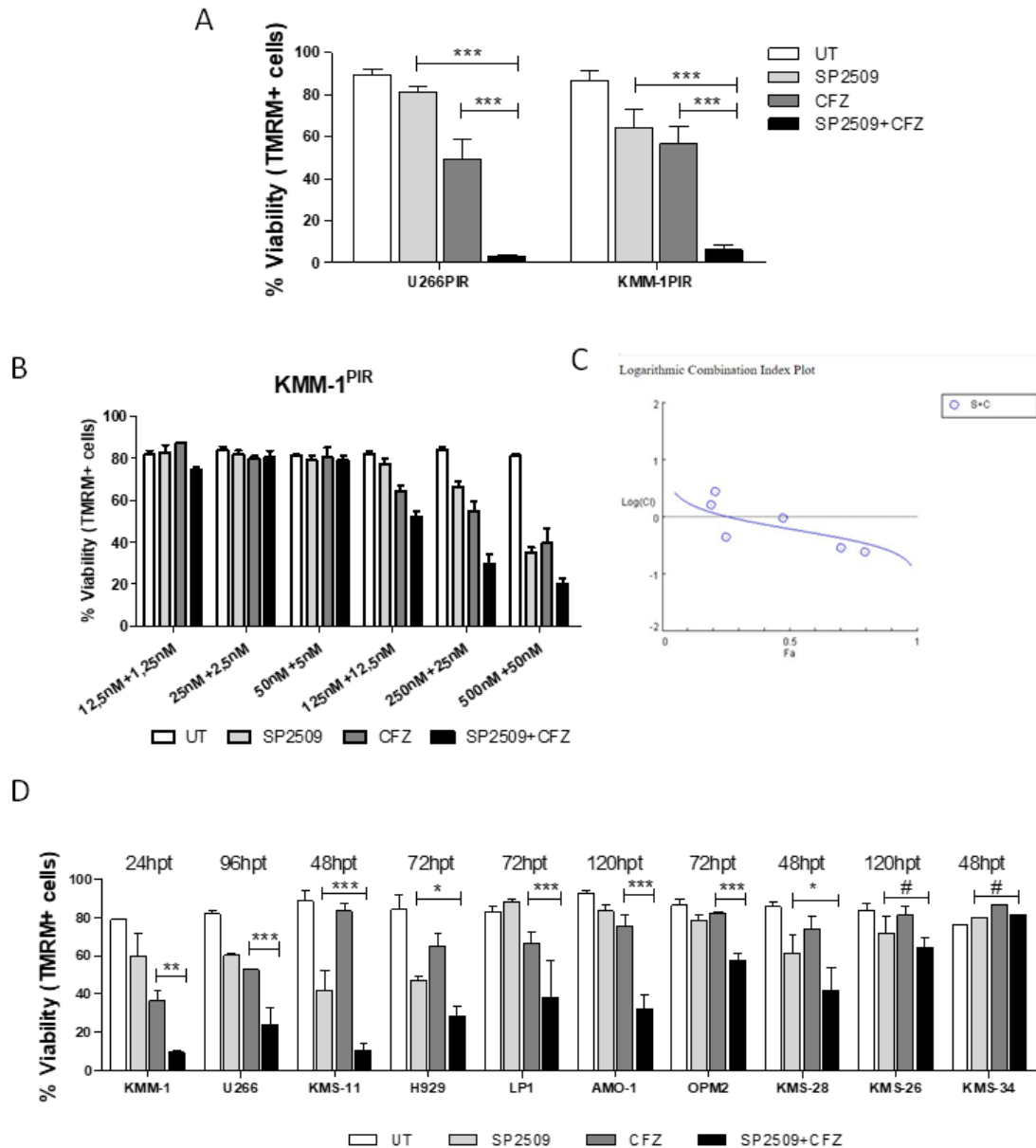


Figure 29. Pharmacological inhibition of LSD1 enhances sensitivity to CFZ in MM cell lines. (A) KMM-1^{PIR} and (B) U266^{PIR} cells were treated every 48h with 100 nM and 500nM SP2509, respectively. At day 2, cells were treated or not with 10 nM and 20 nM CFZ, respectively. Cell viability was measured by TMRM staining-flow cytometry 48 hours and 120 hours post CFZ-treatment, respectively. Data are the means \pm s.d. of three independent experiments. (B) KMM-1^{PIR} cells were treated with six increasing combinations of SP2509 and CFZ, by maintaining the same ratio between drugs (1:10, CFZ and SP2509, respectively), following the same therapeutic protocol as described in panel A. Cell viability was measured 24 hours post CFZ-treatment. Data are the means \pm s.d. of three independent experiments. (C) KMM-1^{PIR} cells were treated as described in B. Isobologram analysis was performed using Compusyn software. Combination index (CI)

less than 1.0, equal to 1.0 and major than 1.0 indicate synergistic, additive and antagonist interaction of the two agents, respectively. (D) Ten MM cell lines were treated with CFZ (1.25 nM CFZ for AMO-1, OPM2, LP1, U266; 2,5 nM for KMS-28, KMM-1; nM for KMS-11, KMS-34, KMS-26 and NCI-H929 cell lines) in combination or not with SP2509 (100 nM for KMS-11, KMS-26, KMS-34; 250 nM for KMS-28; 500 nM for AMO-1, H929, U266, KMM-1, OPM2 and LP1). SP2509 treatment was performed every 48h, and only at day 2 for CFZ. Cell viability was measured by TMRM staining-flow cytometry at indicated hours post-treatments (hpt). Data are the means \pm s.d. of at least three independent experiments (* $P < .05$; ** $P < .01$; *** $P < .001$; # $P \geq .05$).

5.18. GSK LSD1 inhibitors are not able to sensitize MM cells to CFZ treatment

Considering the reduction in cellular fitness triggered by the combined treatment between SP2509 and CFZ, we decided to test whether others LSD1 inhibitors could mediate enhanced sensitivity to CFZ treatment. We selected CFZ-resistant KMM-1^{PIR} and -sensitive LP1 cell lines and treated them with micromolar concentrations of GSK2879552 or GSK-LSD1. Surprisingly, combinatorial treatment between CFZ and GSK2879552 did not show neither synergic nor additive effects (Fig. 30A). To address the discrepancy between SP2509 and GSK2879552 effects, a third LSD1 strong inhibitor, known to inhibit its catalytic demethylase activity (GSK-LSD1), was also tested. Again, combinatorial treatment between GSK-LSD1 and CFZ, did not enhance cell death compared to either agent alone (Fig. 30B). In recent years, many reports described a new catalytic-independent LSD1 function^{181–183}. Then, these data could be explained by a nonenzymatic role of LSD1 in mediating increased sensitivity to CFZ treatment. However, further investigations are needed to confirm this hypothesis.

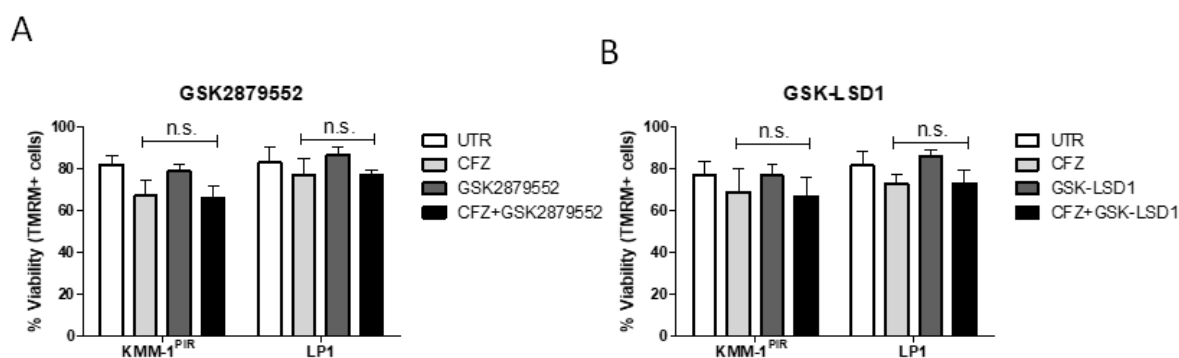


Figure 30. GSK LSD1 inhibitors doesn't enhance sensitivity to CFZ in MM cells. (A) KMM-1^{PIR} and LP1 cell lines were treated with CFZ (10 nM and 1.25 nM respectively)

and GSK2879552 (10 μ M) or (B) GSK-LSD1 (10 μ M). Cell viability was measured by TMRM staining-flow cytometry at 48 hours post-treatments. Data are the means \pm s.d. of at least three independent experiments.

5.19. Overexpression of endogenous and exogenous LSD1 as in vitro models to access SP2509 specificity

In order to address whether the effects observed following SP2509 and CFZ treatment were specifically mediated by LSD1 inhibition, we decided to force its expression to carry out rescue experiment using two strategies. Since in past years, CRISPR-Cas9 technology showed a wide ranges of applications for genome editing, including gene activation, we exploited CRISPR/gRNA-directed synergistic activation mediator (SAM) tool^{184,185}. In CRISPR-Cas9 SAM approach, a multiprotein complex is assembled and driven on the target DNA sequence. Briefly, a catalytically inactive Cas9 (dCas9) is fused with VP64 activator protein. Guide RNA (sgRNA) is modified with aptamers that allow the interaction with a set of other transcriptional activator proteins (p65 and HSF1) via MS2 adaptor. The assembly of the whole operating complex at target DNA sequence synergistically induces gene transcription, with concomitant mRNA production. (Fig. 31A). We first transduced AMO-1 with lentiviral particles expressing dCas9-VP64 and MS2-p65-HSF1 proteins. Western blot analysis confirmed expression of the exogenous proteins (Fig. 31B). Following AMO-1 transduction with activator complexes, we infected cells individually with three different sgRNA targeting LSD1 promoter. RT-qPCR of selected cells demonstrated LSD1 fold-expression with all three sgRNA, even with different efficiency (Fig. 31C). Moreover, western blot analysis confirmed LSD1 induction with two sgRNA (Fig. 31D). Therefore, we generated a multiple myeloma cell line with a sustained LSD1 expression, thanks to the described CRISPR-Cas9 SAM approach.

AMO-1 dCas9-VP64::MS2-p65-HSF1-sgRNA will help us to in vitro investigate the specificity of SP2509 action. AMO-1 with sustained LSD1 transcription will be treated with single drug (either CFZ or SP2509) or the combination of PI and LSD1 inhibitor. Viability values will be evaluated upon treatments, at different timepoints. Depending on the observations, we could be able to make hypothesis about SP2509 specificity. To give an example, in case LSD1 overexpressing cells would be more alive upon CFZ and SP2509 treatments respect to control cells, we could suggest that LSD1 enhanced expression could protect cells from the drugs' action. Therefore, we would be able to make some suggestions about SP2509 specificity. At the moment, SP2509 and/or CFZ treatments on AMO-1 dCas9-VP64::MS2-p65-HSF1-sgRNA are ongoing and data are still preliminary (data not shown).

Secondly, we decided to overexpress exogenous LSD1 by transducing cells with LSD1 ORF. We confirmed LSD1 overexpression in KMS-28 and AMO-1 cell lines transduced with increasing amount of lentivirus carrying LSD1 ORF, by RT-qPCR analysis (Fig. 31E-F). LSD1 overexpressing cells will be treated with either SP2509 and CFZ alone or in combination, to access whether LSD1 is responsible for the sensitivity to drug treatments and synergy, as described above.

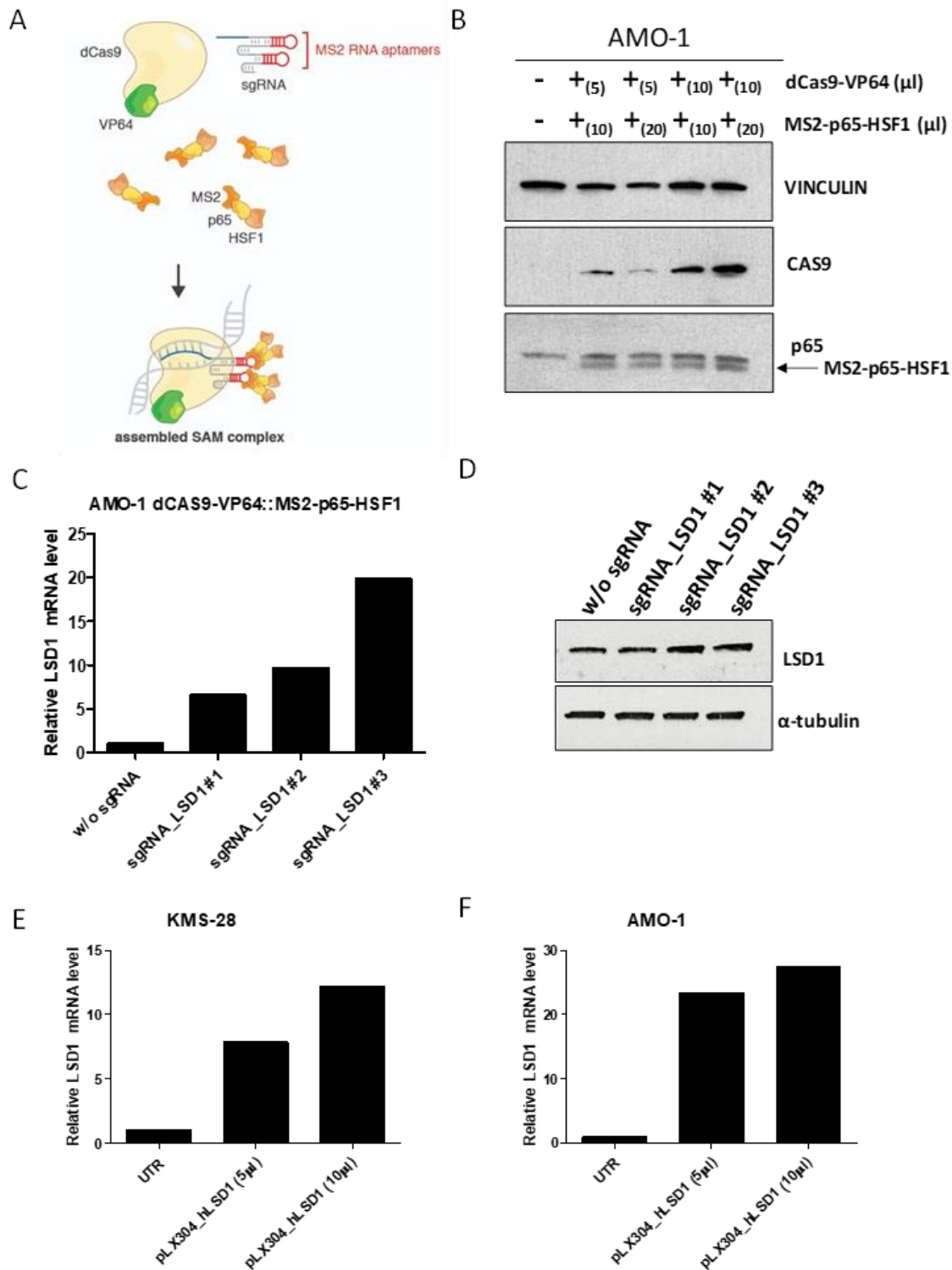


Figure 31. Two different strategies led to LSD1 overexpression. (A) Schematic representation of CRISPR-Cas9 SAM complex (B) Representative western blot showing Cas9 and MS2-p65-HSF1 expression in AMO-1 cells transduced with lentiviral particles expressing SAM activators. Vinculin protein expression was included for protein loading normalization. (C) AMO-1 cells were transduced with lentiviral particles expressing SAM activators (dCAS9-VP64 and MS2-p65-HSF1) and three sgRNA targeting LSD1 promoter

(sgRNA_LSD1 #1, sgRNA_LSD1 # and sgRNA_LSD1 #3). LSD1 activation was monitored by RT-qPCR analysis after blasticidin (4 µg/ml), hygromycin (400 µg/ml) and puromycin selection (1 µg/ml). (D) Representative western blot showing LSD1 expression in AMO-1 cells transduced with lentiviral particles expressing SAM activators. α -tubulin was included for protein loading normalization. (E-F) KMS-28 (E) and AMO-1 (F) cell lines were transduced with 5 µl and 10 µl of pLX304_hLSD1 and selected with 5 µg/ml of blasticidin every 48 hour for a total of 96 hours. Then pellets were collected and LSD1 expression was monitored by RT-qPCR.

6. Discussion and conclusion

Even though PIs have led to substantial outcome improvements in MM and MCL patients, the development of novel combination strategies is needed to overcome resistance and broaden the applicability of this class of drugs to other malignancies. The present study identified IDH2 as a new synthetic lethal target to PIs, efficacious in several hematological malignancies including MM, MCL, BL and DLBCL. We showed that the combined targeting of IDH2 and proteasome triggers synergistic inhibition of human MM ex-vivo and in vivo, with low toxicity to normal human cells. We demonstrated that the NAMPT/SIRT3/IDH2 pathway is a major determinant of PIs responsiveness, thus providing a proof of concept for new combination strategies to enhance sensitivity and broaden the application of PIs to other malignancies.

IDH2 is a mitochondrial enzyme that catalyzes the reversible oxidative decarboxylation of isocitrate to alpha-ketoglutarate, with concomitant reduction of NADP⁺ to NADPH. Hotspot mutations in IDH2 gene have been identified in acute myeloid leukemias (AML)^{186,187}, angioimmunoblastic T-cell lymphomas (AITL)¹⁸⁸, and several other malignancies^{128,129,186,189,190}. IDH2 mutations cause a loss of IDH2 activity and an enzymatic gain of function that catalyzes the conversion of alpha-ketoglutarate to (R)-hydroxyglutarate (2-HG), with consequences on metabolism, epigenetic state, and cellular differentiation^{191,192}. The appreciation of the role of IDH2 mutations in oncogenesis and their early occurrence prompted to the approval of the IDH2-mutant inhibitor enasidenib (AG-221) for the treatment of refractory/relapsed IDH2-mutated AML patients.

In contrast, the potential role of wild-type IDH2 and its clinical relevance in cancers has been poorly investigated. It is thought that the impact of IDH2 expression on neoplastic progression and drug resistance differs with respect to the site of origin and histological type¹⁹³⁻¹⁹⁸. Our study suggests the hypothesis that inhibition of wild-type IDH2 may have therapeutic potentials, regardless of IDH2 expression levels. Concordantly, we excluded that the IDH2 mutational status or its aberrant expression was associated to PIs responsiveness in MM cells. Analysis of gene expression profiling datasets did not detect significant changes of IDH2 expression in the evolution of MM disease (data not shown). However, evaluation of IDH2 enzymatic activity could be more appropriate to further dissect the relevance of IDH2 in tumor development and maintenance, as well as a possible prognostic factor.

We demonstrated that genetic and pharmacological inhibition of IDH2 synergizes with first- and second-generation PIs by enhancing tumor cells death. In contrast, induction of IDH2 enzymatic activity through glucose starvation impairs the therapeutic efficacy of PIs, confirming that pharmacological IDH2 inhibition is a suitable strategy to enhance PIs effects.

Mechanistically, we observed that CFZ significantly down-regulates NAMPT expression levels, most likely through the inhibition of NF- κ B^{159,160,198}. NAMPT is a key NAD pathway intermediate that catalyzes the transfer of a phosphoribosyl group from 5-phosphoribosyl-1-pyrophosphate (PRPP) to nicotinamide, forming nicotinamide mononucleotide (NMN). It has been previously shown that NAMPT inhibition is synthetic lethal to BTZ in MM¹⁶². Here, we demonstrated that the combination of CFZ with either NAMPT or SIRT3 inhibitors induces synergistic down-regulation of IDH2 activity through the impairment of NAMPT/SIRT3/IDH2 pathway. The strong impairment of this pathway drastically decreases IDH2 and TCA cycle activities, leading to ETC flux and mitochondrial ATP synthesis down-regulation. However, we could not exclude that additional mechanisms may contribute to the anti-tumoral effects of CFZ/AGI-6780 combination.

We showed that the combined targeting of IDH2 and proteasome activities triggers synergistic inhibition of primary human MM cells. Importantly, CFZ/AGI-6780 combination exhibits a favorable cytotoxicity profile toward peripheral blood mononuclear cells and bone marrow-derived stromal cells. Considering the efficacy of CFZ/AGI-6780 also in PI-resistant cell lines, we speculate that this combination could be successful also in relapsed and refractory MM patients. To answer this question, further studies in a cohort of patients stratified for their PI response are required. We extended the clinical relevance of our observations proving that IDH2 inhibition synergizes with PIs in several B-cell non-Hodgkin lymphoma cell lines including MM, MCL, BL, and diffuse large B-cell lymphomas. Our preclinical studies, therefore, provide the rationale for the development of novel IDH2 inhibitors directed against wild-type IDH2. These observations are in line with recent studies highlighting the importance of wild-type IDH1 as therapeutic potential^{199–201}. A further interesting expansion to the present work would be to investigate whether IDH2 synthetic lethal interaction to PIs could also take place in cancer patients with mutant IDH2, such as AML, AITL, and other malignancies.

Finally, we provided an *in vivo* proof of principle that IDH2 inhibition enhances the therapeutic efficacy of CFZ in a subcutaneous xenograft model of MM, resulting in inhibition of tumor progression and extended survival. Owing to the lack of wt-IDH2 inhibitors suitable for an *in vivo* use, we exploited a conditional shRNA system to knockdown IDH2. In contrast to *in vitro* data, *in vivo* IDH2 inhibition has a more substantial effect on tumor growth, probably as a consequence of higher gene silencing obtained with the inducible shRNA.

In conclusion, we identified IDH2 as a new synthetic lethal target to PIs, efficacious in several hematological malignancies. We demonstrated that the NAMPT/SIRT3/IDH2 pathway is a major determinant of PIs responsiveness, thus providing a proof of concept for new combination strategies to enhance sensitivity and broaden the application of PIs to other malignancies.

Then, we focused our attention on LSD1, the first lysine-specific demethylases to be discovered¹³⁰. The family of histone demethylases includes up to 21 different enzymes that modify histone tails, to promote or repress gene expression and can be divided into two groups. The larger one comprises the Jumonji C family (JMJs) that are dependent on α -ketoglutarate and Fe²⁺ and acts on tri-, di-, or mono-methylated lysine residues. The smaller LSD family consists of only two members LSD1, and its paralog LSD2 (also known as KDM1A and KDM1B, respectively). They are flavine-adenine dinucleotide (FAD)-dependent amine oxidases (AO), that demethylates di- and mono-methyl groups on H3K4. LSD1 possess also a demethylase activity for di- and mono-methylated H3K9 and for several non-histone targets. Since its discovery in 2004, LSD1 was seen as a pivotal player in regulating many cellular processes, ranging from embryonic development to adult tissue homeostasis and cellular differentiation¹³¹. LSD1 overexpression is observed in different hematological and solid tumors, including acute myeloid leukemia (AML), acute lymphoblastic leukemia (ALL), myelodysplastic syndromes, T cell non-Hodgkin and Hodgkin lymphomas, hepatocellular carcinoma, small cell lung cancer (SCLC), bladder, colon and prostate tumors¹³². Increased expression of LSD1 in different types of human hematological neoplasms, highlights its involvement in leukemogenesis, where it sustains leukemic stem cells potential and differentiation^{133,134}. Moreover, several reports have shown that LSD1 is critically involved in the regulation of the epithelial-to-mesenchymal transition (EMT), thus regulating cellular motility and invasiveness in both solid and hematological tumors^{138-140,202}. Interestingly, a conserved role of LSD1 in the control of metabolic reprogramming, across different types of cancer, was also demonstrated¹³⁵⁻¹³⁷.

Here we found LSD1 as a possible synthetic lethal target in combination with CFZ treatment, by exploiting shRNA loss-of-function screening in PI-resistant MM cell lines. First, we validated screening results, by individually silencing LSD1 expression in PI-resistant MM cells and treating them with CFZ. We demonstrated that LSD1 silencing enhanced sensitivity to CFZ in PI-resistant cells and that this effect was recapitulated in PI-sensitive MM cells.

To increase the therapeutic potential of our research, we decided to test pharmacological inhibition of LSD1 in combination with CFZ treatment. Due to the potential of LSD1 as an anti-cancer target, several LSD1 inhibitors have been explored, with some of these having entered clinical trials or even clinical use²⁰³. We decided to test three LSD1 inhibitors. GSK2879552 is both selective for LSD1 and orally bioavailable, and it acts by covalent modification of the FAD cofactor, in irreversible manner¹⁷⁴. This compound inhibits the growth of small cell lung cancer (SCLC) cells in vitro and in vivo and has entered in clinical trials for SCLC treatments¹⁷⁴. GSK-LSD1 is another potent and selective inhibitor of LSD1 catalytic demethylase activity, that showed growth inhibition effects on AML and sarcoma cell lines^{174, 204,205}. Finally, SP2509 is a reversible non-competitive LSD1 inhibitor,

that showed specificity for LSD1 over MAO enzymes¹⁷³, and effectiveness against different types of tumors^{206–209}. A clinical formulation of SP2509, SP2577, is entered a phase I trial in patients with Ewing sarcoma and, recently for advanced solid tumors (NCT03600649 and NCT03895684, respectively). We observed synergistic activity between CFZ and SP2509 in PI-resistant cell lines, and in a panel of sensitive MM cell lines. However, GSK2879552 and GSK-LSD1 were not able to reproduce these effects, despite they showed effectiveness against an AML cell line, MOLM-13. A possible explanation of the discrepancy among LSD1 inhibitors is a different mechanism of enzyme inhibition, and ultimately a non-catalytic dependent function of LSD1. Indeed, many reports described a novel paradigmatic role of LSD1 not only in cancer, based on its scaffolding activity^{182,183,209,210}. To validate this hypothesis, we will perform a rescue experiment by silencing endogenous LSD1 with shRNA against 3'UTR and consequently by expressing wild-type LSD1, AOD catalytically inactive LSD1 (K661A) and LSD1 lacking the Tower domain (LSD1 Δ Tower)²¹¹. Cell viability will be measured after CFZ treatment. However, it is noteworthy that SP2509 can induce cell death regardless of LSD1 expression²¹². Moreover, 2-hydroxyphenyl-hydrazone structural motif within SP2509 has previously been identified as a pan-assay interference compound (PAINS) that has the potential to elicit promiscuous biological activity²¹³. In order to address this evidence, we decided to overexpress LSD1 to carry out rescue experiments. By exploiting CRISPR-Cas9 SAM tool^{184,185}, we were able to induce overexpression of LSD1 with three different sgRNAs. Moreover, preliminary results demonstrated that cells that displayed higher LSD1 fold-induction, were less sensitive to both SP2509 alone and in combination with CFZ (data not shown). However, these results need to be replicated. Finally, we are testing another strategy to validate LSD1 role in mediating CFZ sensitivity, by transducing cells with exogenous LSD1 ORF, followed by CFZ treatment. Here we obtained LSD1 overexpression in two MM cell lines, KMS-28 and AMO-1, as confirmed by RT-qPCR analysis. Rescue experiments in these cell lines are in progress.

As SP2509 has shown therapeutic potential *in vivo* against AML xenograft¹⁷⁰, we will carry out *in vivo* experiment in MM xenograft, by intravenously or subcutaneously injection of MM cells, as described above. Combinatorial treatment tests will allow excluding possible side effects and environmental-mediated mechanisms of resistance. Remarkably, to access cytotoxicity profile in normal patient cell lines, peripheral blood mononuclear cells and bone marrow-derived stromal cells will be treated with either agent alone or the combination.

As we mentioned before, LSD1 is implicated in a wide range of cellular processes, in normal and cancer cell lines. Hence, it is not surprising that nearly 60 different gene regulatory proteins have been identified as interacting with LSD1 in multi-protein complexes^{214–217}. Whether LSD1 is implicated in CFZ sensitivity as a scaffold protein or as a catalytic enzyme, it is reasonable that its

inhibition/silencing in the presence of CFZ treatment could induce major transcriptional program changes. In order to find molecular mechanisms that could explain LSD1-mediated sensitivity to CFZ treatment, we will exploit more than one high-throughput approach. For instance, RNA-sequencing and chromatin immunoprecipitation (ChIP)-sequencing experiments will be carried out in MM cells in the presence of single or combined perturbations (CFZ, LSD1 inhibition or silencing). RNA-seq and ChIP-Seq data and pathway analysis will be instrumental to identify putative LSD1 partners and targets in MM cells. Immunoprecipitation (IP) experiments will confirm interacting proteins. Moreover, Reverse Phase Protein Array (RPPA) technology in cells treated with CFZ, SP2509 or the combination of both, will provide us an overview of functional proteomics changes that can explain the synergy between drugs.

All together these results shed light on the complexity of mechanisms of resistance to proteasome inhibitors. Indeed, we found a metabolic protein and, potentially, an epigenetic enzyme, that can mediate sensitivity to this class of drugs. Interestingly, we demonstrated that targeting both genes is an effective strategy to increase cell death also in non-resistant MM cells, and in other hematological malignancies, thus expanding the therapeutic potential of our research.

This study opens the way to the future development of inhibitors for the wt-IDH2, and to improve research to find on-target and powerful LSD1 inhibitors. Moreover, it aims to suggest new therapeutic options for clinical practice, to overcome resistance or enhance sensitivity to PIs in the treatment of patients with hematological and solid tumors.

7. References

1. Chapman, M. A. *et al.* Initial genome sequencing and analysis of multiple myeloma. *Nature* **471**, 467–472 (2011).
2. Greenberg, A. J., Vachon, C. M. & Rajkumar, S. V. Disparities in the prevalence, pathogenesis and progression of monoclonal gammopathy of undetermined significance and multiple myeloma between blacks and whites. *Leukemia* **26**, 609–614 (2012).
3. Presutti, R. *et al.* Pesticide exposures and the risk of multiple myeloma in men: An analysis of the North American Pooled Project. *Int. J. Cancer* **139**, 1703–1714 (2016).
4. Sergentanis, T. N. *et al.* Risk Factors for Multiple Myeloma: A Systematic Review of Meta-Analyses. *Clin. Lymphoma Myeloma Leuk.* **15**, 563-577.e3 (2015).
5. Weiss, B. M., Abadie, J., Verma, P., Howard, R. S. & Kuehl, W. M. A monoclonal gammopathy precedes multiple myeloma in most patients. *Blood* **113**, 5418–22 (2009).
6. Wadhera, R. K. & Rajkumar, S. V. Prevalence of Monoclonal Gammopathy of Undetermined Significance: A Systematic Review. *Mayo Clin. Proc.* **85**, 933–942 (2010).
7. Kumar, S. K. *et al.* Multiple myeloma is a malignancy of terminally differentiated plasma cells, and is the second most common haematological malignancy after non-Hodgkin lymphoma. *Nat. Rev. Dis. Prim.* **3**, 1–20 (2017).
8. Kyle, R. A. *et al.* Clinical Course and Prognosis of Smoldering (Asymptomatic) Multiple Myeloma. *N. Engl. J. Med.* **356**, 2582–2590 (2007).
9. Albarracin, F. & Fonseca, R. Plasma cell leukemia. *Blood Rev.* **25**, 107 (2011).
10. Kyle, R. A. *et al.* Review of 1027 Patients With Newly Diagnosed Multiple Myeloma. *Mayo Clin. Proc.* **78**, 21–33 (2003).
11. Palumbo, A. *et al.* Revised International Staging System for Multiple Myeloma: A Report From International Myeloma Working Group. *J. Clin. Oncol.* **33**, 2863–9 (2015).
12. Hideshima, T., Mitsiades, C., Tonon, G., Richardson, P. G. & Anderson, K. C. *Understanding multiple myeloma pathogenesis in the bone marrow to identify new therapeutic targets.* *Nature Reviews Cancer* **7**, 585–598 (Nature Publishing Group, 2007).
13. Mori, Y. *et al.* Anti- α 4 integrin antibody suppresses the development of multiple myeloma and associated osteoclastic osteolysis. *Blood* **104**, 2149–54 (2004).
14. Terpos, E., Ntanasis-Stathopoulos, I., Gavriatopoulou, M. & Dimopoulos, M. A. Pathogenesis of bone disease in multiple myeloma: from bench to bedside. *Blood Cancer J.* **8**, 7 (2018).
15. Lee, J. W. *et al.* IL-3 expression by myeloma cells increases both osteoclast formation and growth of myeloma cells. *Blood* **103**, 2308–15 (2004).

16. Ehrlich, L. A. *et al.* IL-3 is a potential inhibitor of osteoblast differentiation in multiple myeloma. *Blood* **106**, 1407–14 (2005).
17. Hashimoto, T. *et al.* Ability of myeloma cells to secrete macrophage inflammatory protein (MIP)-1alpha and MIP-1beta correlates with lytic bone lesions in patients with multiple myeloma. *Br. J. Haematol.* **125**, 38–41 (2004).
18. Giuliani, N. *et al.* Myeloma cells block RUNX2/CBFA1 activity in human bone marrow osteoblast progenitors and inhibit osteoblast formation and differentiation. *Blood* **106**, 2472–83 (2005).
19. Gunn, W. G. *et al.* A Crosstalk Between Myeloma Cells and Marrow Stromal Cells Stimulates Production of DKK1 and Interleukin-6: A Potential Role in the Development of Lytic Bone Disease and Tumor Progression in Multiple Myeloma. *Stem Cells* **24**, 986–991 (2006).
20. Qiang, Y.-W. *et al.* Myeloma-derived Dickkopf-1 disrupts Wnt-regulated osteoprotegerin and RANKL production by osteoblasts: a potential mechanism underlying osteolytic bone lesions in multiple myeloma. *Blood* **112**, 196–207 (2008).
21. Xu, L. *et al.* Cell Adhesion Molecule CD166 Drives Malignant Progression and Osteolytic Disease in Multiple Myeloma. *Cancer Res.* **76**, 6901–6910 (2016).
22. Alsayed, Y. *et al.* Mechanisms of regulation of CXCR4/SDF-1 (CXCL12)-dependent migration and homing in multiple myeloma. *Blood* **109**, 2708–17 (2007).
23. Vacca, A. *et al.* Bone Marrow Neovascularization, Plasma Cell Angiogenic Potential, and Matrix Metalloproteinase-2 Secretion Parallel Progression of Human Multiple Myeloma. *Blood* **93**, (1999).
24. Tjin, E. P. M., Derksen, P. W. B., Kataoka, H., Spaargaren, M. & Pals, S. T. Multiple myeloma cells catalyze hepatocyte growth factor (HGF) activation by secreting the serine protease HGF-activator. *Blood* **104**, 2172–5 (2004).
25. Dankbar, B. *et al.* Vascular endothelial growth factor and interleukin-6 in paracrine tumor-stromal cell interactions in multiple myeloma. *Blood* **95**, (2000).
26. Chretien, M.-L. *et al.* Understanding the role of hyperdiploidy in myeloma prognosis: which trisomies really matter? *Blood* **126**, 2713–9 (2015).
27. Smadja, N.-V. *et al.* Chromosomal analysis in multiple myeloma: cytogenetic evidence of two different diseases. *Leukemia* **12**, 960–969 (1998).
28. Prideaux, S. M., Conway O'Brien, E. & Chevassut, T. J. The genetic architecture of multiple myeloma. *Adv. Hematol.* **2014**, 864058 (2014).
29. Vallespinós, M. *et al.* B Lymphocyte commitment program is driven by the proto-oncogene c-Myc. *J. Immunol.* **186**, 6726–36 (2011).
30. Walker, B. A. *et al.* A compendium of myeloma-associated chromosomal copy number abnormalities and their prognostic value. *Blood* **116**, e56–e65 (2010).

31. Mani, M. *et al.* BCL9 Promotes Tumor Progression by Conferring Enhanced Proliferative, Metastatic, and Angiogenic Properties to Cancer Cells. *Cancer Res.* **69**, 7577–7586 (2009).
32. Walker, B. A. *et al.* Mutational Spectrum, Copy Number Changes, and Outcome: Results of a Sequencing Study of Patients With Newly Diagnosed Myeloma. *J. Clin. Oncol.* **33**, 3911–20 (2015).
33. Heuck, C. J. *et al.* Myeloma is characterized by stage-specific alterations in DNA methylation that occur early during myelomagenesis. *J. Immunol.* **190**, 2966–75 (2013).
34. Harada, T. *et al.* HDAC3 regulates DNMT1 expression in multiple myeloma: therapeutic implications. *Leukemia* **31**, 2670–2677 (2017).
35. Morgan, G. J., Walker, B. A. & Davies, F. E. The genetic architecture of multiple myeloma. *Nat. Rev. Cancer* **12**, 335–348 (2012).
36. Rajkumar, S. V. & Kumar, S. Multiple Myeloma: Diagnosis and Treatment. *Mayo Clin. Proc.* **91**, 101–19 (2016).
37. Krishnan, A. *et al.* Autologous haemopoietic stem-cell transplantation followed by allogeneic or autologous haemopoietic stem-cell transplantation in patients with multiple myeloma (BMT CTN 0102): a phase 3 biological assignment trial. *Lancet. Oncol.* **12**, 1195–203 (2011).
38. Bruno, B. *et al.* A comparison of allografting with autografting for newly diagnosed myeloma. *N. Engl. J. Med.* **356**, 1110–20 (2007).
39. Kyle, R. A. & Rajkumar, S. V. Multiple myeloma. *Blood* **111**, 2962–72 (2008).
40. Palumbo, A. *et al.* Continuous lenalidomide treatment for newly diagnosed multiple myeloma. *N. Engl. J. Med.* **366**, 1759–69 (2012).
41. Glickman, M. H. & Ciechanover, A. The Ubiquitin-Proteasome Proteolytic Pathway: Destruction for the Sake of Construction. *Physiol. Rev.* **82**, 373–428 (2002).
42. Thibaudeau, T. A. & Smith, D. M. A Practical Review of Proteasome Pharmacology. *Pharmacol. Rev.* **71**, 170–197 (2019).
43. Arendt, C. S. & Hochstrasser, M. Identification of the yeast 20S proteasome catalytic centers and subunit interactions required for active-site formation. *Proc. Natl. Acad. Sci. U. S. A.* **94**, 7156–61 (1997).
44. Voges, D., Zwickl, P. & Baumeister, W. The 26S Proteasome: A Molecular Machine Designed for Controlled Proteolysis. *Annu. Rev. Biochem.* **68**, 1015–1068 (1999).
45. Crawford, L. J., Walker, B. & Irvine, A. E. Proteasome inhibitors in cancer therapy. *J. Cell Commun. Signal.* **5**, 101–10 (2011).
46. Kane, R. C., Bross, P. F., Farrell, A. T. & Pazdur, R. Velcade: U.S. FDA approval for the treatment of multiple myeloma progressing on prior therapy. *Oncologist* **8**, 508–13 (2003).
47. Park, J. E., Miller, Z., Jun, Y., Lee, W. & Kim, K. B. Next-generation proteasome inhibitors for cancer therapy.

- Transl. Res.* **198**, 1–16 (2018).
48. Zaal, E. A. *et al.* Bortezomib resistance in multiple myeloma is associated with increased serine synthesis. *Cancer Metab.* **5**, 7 (2017).
 49. Kim, K. B. & Crews, C. M. From epoxomicin to carfilzomib: chemistry, biology, and medical outcomes. *Nat. Prod. Rep.* **30**, 600–4 (2013).
 50. Kuhn, D. J. *et al.* Potent activity of carfilzomib, a novel, irreversible inhibitor of the ubiquitin-proteasome pathway, against preclinical models of multiple myeloma. *Blood* **110**, 3281 (2007).
 51. Manasanch, E. E. & Orłowski, R. Z. Proteasome inhibitors in cancer therapy. *Nat. Rev. Clin. Oncol.* **14**, 417–433 (2017).
 52. Chauhan, D. *et al.* In vitro and in vivo selective antitumor activity of a novel orally bioavailable proteasome inhibitor MLN9708 against multiple myeloma cells. *Clin. Cancer Res.* **17**, 5311–21 (2011).
 53. Spencer, A. *et al.* A phase 1 clinical trial evaluating marizomib, pomalidomide and low-dose dexamethasone in relapsed and refractory multiple myeloma (NPI-0052-107): final study results. *Br. J. Haematol.* **180**, 41–51 (2018).
 54. Bota, D. A. *et al.* Marizomib activity as a single agent in malignant gliomas: Ability to cross the blood brain barrier. *J. Clin. Oncol.* **33**, e12644–e12644 (2015).
 55. Miller, M. T. Thalidomide embryopathy: a model for the study of congenital incomitant horizontal strabismus. *Trans. Am. Ophthalmol. Soc.* **89**, 623–74 (1991).
 56. D’Amato, R. J., Loughnan, M. S., Flynn, E. & Folkman, J. Thalidomide is an inhibitor of angiogenesis. *Proc. Natl. Acad. Sci. U. S. A.* **91**, 4082–5 (1994).
 57. Kazandjian, D. & Landgren, O. A look backward and forward in the regulatory and treatment history of multiple myeloma: Approval of novel-novel agents, new drug development, and longer patient survival. *Semin. Oncol.* **43**, 682–689 (2016).
 58. Zhu, Y. X., Kortuem, K. M. & Stewart, A. K. Molecular mechanism of action of immune-modulatory drugs thalidomide, lenalidomide and pomalidomide in multiple myeloma. *Leuk. Lymphoma* **54**, 683–7 (2013).
 59. Ito, T. *et al.* Identification of a primary target of thalidomide teratogenicity. *Science* **327**, 1345–50 (2010).
 60. Zhu, Y. X. *et al.* Cereblon expression is required for the antimyeloma activity of lenalidomide and pomalidomide. *Blood* **118**, 4771–9 (2011).
 61. Krönke, J. *et al.* Lenalidomide causes selective degradation of IKZF1 and IKZF3 in multiple myeloma cells. *Science* **343**, 301–5 (2014).
 62. Lu, G. *et al.* The Myeloma Drug Lenalidomide Promotes the Cereblon-Dependent Destruction of Ikaros Proteins. *Science (80-.)*. **343**, 305–309 (2014).
 63. Shaffer, A. L. *et al.* IRF4 addiction in multiple myeloma. *Nature* **454**, 226–231 (2008).

64. Gandhi, A. K. *et al.* Immunomodulatory agents lenalidomide and pomalidomide co-stimulate T cells by inducing degradation of T cell repressors Ikaros and Aiolos via modulation of the E3 ubiquitin ligase complex CRL4(CRBN). *Br. J. Haematol.* **164**, 811–21 (2014).
65. Davies, F. E. *et al.* Thalidomide and immunomodulatory derivatives augment natural killer cell cytotoxicity in multiple myeloma. *Blood* **98**, 210–6 (2001).
66. Muller, G. W. *et al.* Structural modifications of thalidomide produce analogs with enhanced tumor necrosis factor inhibitory activity. *J. Med. Chem.* **39**, 3238–40 (1996).
67. Gupta, D. *et al.* Adherence of multiple myeloma cells to bone marrow stromal cells upregulates vascular endothelial growth factor secretion: therapeutic applications. *Leukemia* **15**, 1950–61 (2001).
68. Mitsiades, N. *et al.* Apoptotic signaling induced by immunomodulatory thalidomide analogs in human multiple myeloma cells: therapeutic implications. *Blood* **99**, 4525–30 (2002).
69. Hanaizi, Z. *et al.* The European medicines agency review of pomalidomide in combination with low-dose dexamethasone for the treatment of adult patients with multiple myeloma: summary of the scientific assessment of the committee for medicinal products for human use. *Oncologist* **20**, 329–34 (2015).
70. Zhu, Y. X. *et al.* Identification of lenalidomide resistance pathways in myeloma and targeted resensitization using cereblon replacement, inhibition of STAT3 or targeting of IRF4. *Blood Cancer J.* **9**, 19 (2019).
71. Lee, H. C. & Weber, D. M. Advances and practical use of monoclonal antibodies in multiple myeloma therapy. *Hematol. Am. Soc. Hematol. Educ. Progr.* **2016**, 512–520 (2016).
72. Laubach, J. P., Tai, Y.-T., Richardson, P. G. & Anderson, K. C. Daratumumab granted breakthrough drug status. *Expert Opin. Investig. Drugs* **23**, 445–452 (2014).
73. de Weers, M. *et al.* Daratumumab, a novel therapeutic human CD38 monoclonal antibody, induces killing of multiple myeloma and other hematological tumors. *J. Immunol.* **186**, 1840–8 (2011).
74. Krejcik, J. *et al.* Daratumumab depletes CD38+ immune regulatory cells, promotes T-cell expansion, and skews T-cell repertoire in multiple myeloma. *Blood* **128**, 384–94 (2016).
75. Abramson, H. N. Monoclonal Antibodies for the Treatment of Multiple Myeloma: An Update. *Int. J. Mol. Sci.* **19**, (2018).
76. Hsi, E. D. *et al.* CS1, a potential new therapeutic antibody target for the treatment of multiple myeloma. *Clin. Cancer Res.* **14**, 2775–84 (2008).
77. Collins, S. M. *et al.* Elotuzumab directly enhances NK cell cytotoxicity against myeloma via CS1 ligation: evidence for augmented NK cell function complementing ADCC. *Cancer Immunol. Immunother.* **62**, 1841 (2013).
78. Ishibashi, M. *et al.* Clinical impact of serum soluble SLAMF7 in multiple myeloma. *Oncotarget* **9**, 34784–34793 (2018).
79. Atadja, P. Development of the pan-DAC inhibitor panobinostat (LBH589): Successes and challenges. *Cancer*

- Lett.* **280**, 233–241 (2009).
80. Mithraprabhu, S., Kalff, A., Chow, A., Khong, T. & Spencer, A. Dysregulated Class I histone deacetylases are indicators of poor prognosis in multiple myeloma. *Epigenetics* **9**, 1511–20 (2014).
 81. Growney, J. D. *et al.* Efficacy of Panobinostat (LBH589) in Multiple Myeloma Cell Lines and In Vivo Mouse Model: Tumor-Specific Cytotoxicity and Protection of Bone Integrity in Multiple Myeloma. *Blood* **110**, (2007).
 82. Laubach, J. P., Moreau, P., San-Miguel, J. F. & Richardson, P. G. Panobinostat for the Treatment of Multiple Myeloma. *Clin. Cancer Res.* **21**, 4767–4773 (2015).
 83. Catley, L. *et al.* Aggresome induction by proteasome inhibitor bortezomib and alpha-tubulin hyperacetylation by tubulin deacetylase (TDAC) inhibitor LBH589 are synergistic in myeloma cells. *Blood* **108**, 3441–9 (2006).
 84. Kawaguchi, Y. *et al.* The deacetylase HDAC6 regulates aggresome formation and cell viability in response to misfolded protein stress. *Cell* **115**, 727–38 (2003).
 85. García-Guerrero, E. *et al.* Panobinostat induces CD38 upregulation and augments the antimyeloma efficacy of daratumumab. *Blood* **129**, 3386–3388 (2017).
 86. Fandy, T. E., Shankar, S., Ross, D. D., Sausville, E. & Srivastava, R. K. Interactive Effects of HDAC Inhibitors and TRAIL on Apoptosis Are Associated with Changes in Mitochondrial Functions and Expressions of Cell Cycle Regulatory Genes in Multiple Myeloma. *Neoplasia* **7**, 646–657 (2005).
 87. Moore, D. Panobinostat (Farydak): A Novel Option for the Treatment of Relapsed Or Relapsed and Refractory Multiple Myeloma. *P T* **41**, 296–300 (2016).
 88. Matsui, W. *et al.* Clonogenic Multiple Myeloma Progenitors, Stem Cell Properties, and Drug Resistance. *Cancer Res.* **68**, 190 (2008).
 89. Schwarzenbach, H. Expression of MDR1/P-Glycoprotein, the Multidrug Resistance Protein MRP, and the Lung-Resistance Protein LRP in Multiple Myeloma. *Med. Oncol.* **19**, 87–104 (2002).
 90. Abraham, J., Salama, N. N. & Azab, A. K. The role of P-glycoprotein in drug resistance in multiple myeloma. *Leuk. Lymphoma* **56**, 26–33 (2015).
 91. Wang, L., Lin, N. & Li, Y. The PI3K/AKT signaling pathway regulates ABCG2 expression and confers resistance to chemotherapy in human multiple myeloma. *Oncol. Rep.* **41**, 1678–1690 (2019).
 92. Buda, G. *et al.* Polymorphisms in the multiple drug resistance protein 1 and in P-glycoprotein 1 are associated with time to event outcomes in patients with advanced multiple myeloma treated with bortezomib and pegylated liposomal doxorubicin. *Ann. Hematol.* **89**, 1133–40 (2010).
 93. Shah, S. P. *et al.* Bortezomib-induced heat shock response protects multiple myeloma cells and is activated by heat shock factor 1 serine 326 phosphorylation. *Oncotarget* **7**, 59727–59741 (2016).
 94. Tonelli, C., Chio, I. I. C. & Tuveson, D. A. Transcriptional Regulation by Nrf2. *Antioxid. Redox Signal.* **29**, 1727–1745 (2018).

95. Sun, Y., Abdul Aziz, A., Bowles, K. & Rushworth, S. High NRF2 expression controls endoplasmic reticulum stress induced apoptosis in multiple myeloma. *Cancer Lett.* **412**, 37–45 (2018).
96. Bravo, R. *et al.* Endoplasmic Reticulum and the Unfolded Protein Response: Dynamics and Metabolic Integration. *Int. Rev. Cell Mol. Biol.* **301**, 215 (2013).
97. Ling, S. C. W. *et al.* Response of myeloma to the proteasome inhibitor bortezomib is correlated with the unfolded protein response regulator XBP-1. *Haematologica* **97**, 64–72 (2012).
98. Leung-Hagesteijn, C. *et al.* Xbp1s-Negative Tumor B Cells and Pre-Plasmablasts Mediate Therapeutic Proteasome Inhibitor Resistance in Multiple Myeloma. *Cancer Cell* **24**, 289 (2013).
99. Nikesitch, N. *et al.* Predicting the response of multiple myeloma to the proteasome inhibitor Bortezomib by evaluation of the unfolded protein response. *Blood Cancer J.* **6**, e432 (2016).
100. Hong, S. Y. & Hagen, T. Multiple myeloma Leu167Ile (c.499C>A) mutation prevents *XBPI* mRNA splicing. *Br. J. Haematol.* **161**, 898–901 (2013).
101. Barrio, S. *et al.* Spectrum and functional validation of PSMB5 mutations in multiple myeloma. *Leukemia* **33**, 447–456 (2019).
102. Papanagnou, E.-D. *et al.* Molecular responses to therapeutic proteasome inhibitors in multiple myeloma patients are donor-, cell type- and drug-dependent. *Oncotarget* **9**, 17797 (2018).
103. Kortüm, K. M. *et al.* Targeted sequencing of refractory myeloma reveals a high incidence of mutations in CRBN and Ras pathway genes. *Blood* **128**, 1226–33 (2016).
104. Xu, J. *et al.* Molecular signaling in multiple myeloma: association of RAS/RAF mutations and MEK/ERK pathway activation. *Oncogenesis* **6**, e337 (2017).
105. Nijhof, I. S. *et al.* CD38 expression and complement inhibitors affect response and resistance to daratumumab therapy in myeloma. *Blood* **128**, 959–70 (2016).
106. Postelnek, J. *et al.* Effects of Elotuzumab on Soluble SLAMF7 Levels in Multiple Myeloma. *Blood* **126**, (2015).
107. Nijman, S. M. B. Synthetic lethality: general principles, utility and detection using genetic screens in human cells. *FEBS Lett.* **585**, 1–6 (2011).
108. DOBZHANSKY, T. Genetics of natural populations; recombination and variability in populations of *Drosophila pseudoobscura*. *Genetics* **31**, 269–90 (1946).
109. Thompson, J. M., Nguyen, Q. H., Singh, M. & Razorenova, O. V. *Approaches to identifying synthetic lethal interactions in cancer.* *Yale Journal of Biology and Medicine* **88**, 145–55 (2015).
110. Kaelin, W. G. The concept of synthetic lethality in the context of anticancer therapy. *Nat. Rev. Cancer* **5**, 689–98 (2005).
111. Tiedemann, R. E. *et al.* Identification of molecular vulnerabilities in human multiple myeloma cells by RNA interference lethality screening of the druggable genome. *Cancer Res.* **72**, 757–68 (2012).

112. Cho, Y.-Y. RSK2 and its binding partners in cell proliferation, transformation and cancer development. *Arch. Pharm. Res.* **40**, 291–303 (2017).
113. Zhu, Y. X. *et al.* RNA interference screening identifies lenalidomide sensitizers in multiple myeloma, including RSK2. *Blood* **125**, 483–91 (2015).
114. Acosta-Alvear, D. *et al.* Paradoxical resistance of multiple myeloma to proteasome inhibitors by decreased levels of 19S proteasomal subunits. *Elife* **4**, e08153 (2015).
115. Shalem, O. *et al.* Genome-scale CRISPR-Cas9 knockout screening in human cells. *Science* **343**, 84–87 (2014).
116. Wang, T., Wei, J. J., Sabatini, D. M. & Lander, E. S. Genetic Screens in Human Cells Using the CRISPR-Cas9 System. *Science (80-.)*. **343**, 80–84 (2014).
117. Liu, J. *et al.* A genome-scale CRISPR-Cas9 screening in myeloma cells identifies regulators of immunomodulatory drug sensitivity. *Leukemia* **33**, 171–180 (2019).
118. Shi, C.-X. *et al.* CRISPR Genome-Wide Screening Identifies Dependence on the Proteasome Subunit PSMC6 for Bortezomib Sensitivity in Multiple Myeloma. *Mol. Cancer Ther.* **16**, 2862–2870 (2017).
119. Turcotte, S. *et al.* A Molecule Targeting VHL-Deficient Renal Cell Carcinoma that Induces Autophagy. *Cancer Cell* **14**, 90–102 (2008).
120. Chan, D. A. *et al.* Targeting GLUT1 and the Warburg Effect in Renal Cell Carcinoma by Chemical Synthetic Lethality. *Sci. Transl. Med.* **3**, 94ra70-94ra70 (2011).
121. Jacquemont, C., Simon, J. A., D’Andrea, A. D. & Taniguchi, T. Non-specific chemical inhibition of the Fanconi anemia pathway sensitizes cancer cells to cisplatin. *Mol. Cancer* **11**, 26 (2012).
122. Siegel, M. B. *et al.* Small molecule inhibitor screen identifies synergistic activity of the bromodomain inhibitor CPI203 and bortezomib in drug resistant myeloma. *Oncotarget* **6**, 18921–18932 (2015).
123. O’Neil, N. J., Bailey, M. L. & Hieter, P. Synthetic lethality and cancer. *Nat. Rev. Genet.* **18**, 613–623 (2017).
124. Dang, L., Yen, K. & Attar, E. C. IDH mutations in cancer and progress toward development of targeted therapeutics. *Ann. Oncol.* **27**, 599–608 (2016).
125. Upadhyay, V. A., Brunner, A. M. & Fathi, A. T. Isocitrate dehydrogenase (IDH) inhibition as treatment of myeloid malignancies: Progress and future directions. *Pharmacol. Ther.* **177**, 123–128 (2017).
126. Yan, H. *et al.* IDH1 and IDH2 Mutations in Gliomas. *N. Engl. J. Med.* (2009). doi:10.1056/NEJMoa0808710
127. Mardis, E. E. R. E. *et al.* Recurring mutations found by sequencing an acute myeloid leukemia genome. *N. Engl. J. Med.* (2009). doi:10.1056/NEJMoa0903840
128. Amary, M. F. *et al.* IDH1 and IDH2 mutations are frequent events in central chondrosarcoma and central and periosteal chondromas but not in other mesenchymal tumours. *J. Pathol.* **224**, 334–43 (2011).
129. Borger, D. R. *et al.* Frequent mutation of isocitrate dehydrogenase (IDH)1 and IDH2 in cholangiocarcinoma identified through broad-based tumor genotyping. *Oncologist* **17**, 72–9 (2012).

130. Shi, Y. *et al.* Histone demethylation mediated by the nuclear amine oxidase homolog LSD1. *Cell* **119**, 941–53 (2004).
131. Majello, B., Gorini, F., Saccà, C. D. & Amente, S. Expanding the role of the histone lysine-specific demethylase Lsd1 in cancer. *Cancers (Basel)*. **11**, 1–15 (2019).
132. Hino, S., Kohroggi, K. & Nakao, M. Histone demethylase LSD1 controls the phenotypic plasticity of cancer cells. *Cancer Sci.* **107**, 1187–92 (2016).
133. Harris, W. J. J. *et al.* The Histone Demethylase KDM1A Sustains the Oncogenic Potential of MLL-AF9 Leukemia Stem Cells. *Cancer Cell* **21**, 473–487 (2012).
134. Wada, T., Koyama, D., Kikuchi, J., Honda, H. & Furukawa, Y. Overexpression of the shortest isoform of histone demethylase LSD1 primes hematopoietic stem cells for malignant transformation. *Blood* **125**, 3731–46 (2015).
135. Qin, Y. *et al.* LSD1 sustains pancreatic cancer growth via maintaining HIF1 α -dependent glycolytic process. *Cancer Lett.* **347**, 225–232 (2014).
136. Kosumi, K. *et al.* Lysine-specific demethylase-1 contributes to malignant behavior by regulation of invasive activity and metabolic shift in esophageal cancer. *Int. J. Cancer* **138**, 428–439 (2016).
137. Sakamoto, A. *et al.* Lysine Demethylase LSD1 Coordinates Glycolytic and Mitochondrial Metabolism in Hepatocellular Carcinoma Cells. *Cancer Res.* **75**, 1445–1456 (2015).
138. Ferrari-Amorotti, G. *et al.* Inhibiting interactions of lysine demethylase LSD1 with snail/slug blocks cancer cell invasion. *Cancer Res.* **73**, 235–45 (2013).
139. Lin, T., Ponn, A., Hu, X., Law, B. K. & Lu, J. Requirement of the histone demethylase LSD1 in Snai1-mediated transcriptional repression during epithelial-mesenchymal transition. *Oncogene* **29**, 4896–904 (2010).
140. McDonald, O. G., Wu, H., Timp, W., Doi, A. & Feinberg, A. P. Genome-scale epigenetic reprogramming during epithelial-to-mesenchymal transition. *Nat. Struct. Mol. Biol.* **18**, 867–74 (2011).
141. Gilbert, L. A. *et al.* Genome-Scale CRISPR-Mediated Control of Gene Repression and Activation. *Cell* **159**, 647–61 (2014).
142. Wiznerowicz, M. & Trono, D. Conditional suppression of cellular genes: lentivirus vector-mediated drug-inducible RNA interference. *J. Virol.* **77**, 8957–61 (2003).
143. Schmittgen, T. D. & Livak, K. J. Analyzing real-time PCR data by the comparative CT method. *Nat. Protoc.* **3**, 1101–1108 (2008).
144. Schadt, E. E., Li, C., Ellis, B. & Wong, W. H. Feature extraction and normalization algorithms for high-density oligonucleotide gene expression array data. *J. Cell. Biochem. Suppl.* **Suppl 37**, 120–5 (2001).
145. Tusher, V. G., Tibshirani, R. & Chu, G. Significance analysis of microarrays applied to the ionizing radiation response. *Proc. Natl. Acad. Sci. U. S. A.* **98**, 5116–21 (2001).

146. Urban, D. J. *et al.* Assessing inhibitors of mutant isocitrate dehydrogenase using a suite of pre-clinical discovery assays. *Sci. Rep.* **7**, 12758 (2017).
147. Wang, F. *et al.* Targeted inhibition of mutant IDH2 in leukemia cells induces cellular differentiation. *Science* **340**, 622–6 (2013).
148. Obrist, F., Manic, G., Kroemer, G., Vitale, I. & Galluzzi, L. Trial Watch: Proteasomal inhibitors for anticancer therapy. *Mol. Cell. Oncol.* **2**, e974463 (2015).
149. Gandolfi, S. *et al.* The proteasome and proteasome inhibitors in multiple myeloma. *Cancer Metastasis Rev.* (2017). doi:10.1007/s10555-017-9707-8
150. Hideshima, T. *et al.* The proteasome inhibitor PS-341 inhibits growth, induces apoptosis, and overcomes drug resistance in human multiple myeloma cells. *Cancer Res.* **61**, 3071–6 (2001).
151. Pasqualucci, L. & Dalla-Favera, R. Genetics of diffuse large B-cell lymphoma. *Blood* **131**, 2307–2319 (2018).
152. Babicki, S. *et al.* Heatmapper: web-enabled heat mapping for all. *Nucleic Acids Res.* **44**, W147–W153 (2016).
153. Someya, S. *et al.* Sirt3 mediates reduction of oxidative damage and prevention of age-related hearing loss under caloric restriction. *Cell* **143**, 802–12 (2010).
154. Yu, W., Dittenhafer-Reed, K. E. & Denu, J. M. SIRT3 protein deacetylates isocitrate dehydrogenase 2 (IDH2) and regulates mitochondrial redox status. *J. Biol. Chem.* **287**, 14078–86 (2012).
155. Molenaar, R. J., Maciejewski, J. P., Wilmink, J. W. & van Noorden, C. J. F. Wild-type and mutated IDH1/2 enzymes and therapy responses. *Oncogene* **37**, 1949–1960 (2018).
156. Maharjan, S., Oku, M., Tsuda, M., Hoseki, J. & Sakai, Y. Mitochondrial impairment triggers cytosolic oxidative stress and cell death following proteasome inhibition. *Sci. Rep.* **4**, 5896 (2014).
157. Lipchick, B. C., Fink, E. E. & Nikiforov, M. A. Oxidative stress and proteasome inhibitors in multiple myeloma. *Pharmacol. Res.* **105**, 210–5 (2016).
158. Garten, A. *et al.* Physiological and pathophysiological roles of NAMPT and NAD metabolism. *Nat. Rev. Endocrinol.* **11**, 535–546 (2015).
159. Audrito, V. *et al.* Nicotinamide Phosphoribosyltransferase (NAMPT) as a Therapeutic Target in BRAF-Mutated Metastatic Melanoma. *JNCI J. Natl. Cancer Inst.* **110**, 290–303 (2018).
160. Audrito, V. *et al.* Extracellular nicotinamide phosphoribosyltransferase (NAMPT) promotes M2 macrophage polarization in chronic lymphocytic leukemia. *Blood* **125**, 111–23 (2015).
161. Zhang, L. Q., P. Heruth, D. & Qing Ye, S. Nicotinamide Phosphoribosyltransferase in Human Diseases. *J. Bioanal. Biomed.* **03**, 13–25 (2011).
162. Cagnetta, A. *et al.* Intracellular NAD⁺ depletion enhances bortezomib-induced anti-myeloma activity. *Blood* **122**, 1243–55 (2013).
163. Outeiro, T. F. *et al.* Sirtuin 2 inhibitors rescue alpha-synuclein-mediated toxicity in models of Parkinson's

- disease. *Science* **317**, 516–9 (2007).
164. Popovici-Muller, J. *et al.* Discovery of the First Potent Inhibitors of Mutant IDH1 That Lower Tumor 2-HG in Vivo. *ACS Med. Chem. Lett.* **3**, 850–5 (2012).
165. Ho, T.-T. *et al.* Targeting non-coding RNAs with the CRISPR/Cas9 system in human cell lines. *Nucleic Acids Res.* **43**, e17–e17 (2015).
166. Piva, R. *et al.* Gene expression profiling uncovers molecular classifiers for the recognition of anaplastic large-cell lymphoma within peripheral T-cell neoplasms. *J. Clin. Oncol.* (2010). doi:10.1200/JCO.2008.20.9759
167. Spaccarotella, E. *et al.* STAT3-mediated activation of microRNA cluster 17~92 promotes proliferation and survival of ALK-positive anaplastic large cell lymphoma. *Haematologica* (2014). doi:10.3324/haematol.2013.088286
168. Issa, M. E. *et al.* Epigenetic strategies to reverse drug resistance in heterogeneous multiple myeloma. *Clin. Epigenetics* **9**, 1–13 (2017).
169. Alzrigat, M., Párraga, A. A. & Jernberg-Wiklund, H. Epigenetics in multiple myeloma: From mechanisms to therapy. *Semin. Cancer Biol.* **51**, 101–115 (2018).
170. Fiskus, W. *et al.* Highly effective combination of LSD1 (KDM1A) antagonist and pan-histone deacetylase inhibitor against human AML cells. *Leukemia* **28**, 2155 (2014).
171. Zhu, L. *et al.* LSD1 inhibition suppresses the growth of clear cell renal cell carcinoma via upregulating P21 signaling. *Acta Pharm. Sin. B* **9**, 324 (2019).
172. Lu, Y., Liu, Y., Oeck, S. & Glazer, P. M. Hypoxia Promotes Resistance to EGFR Inhibition in NSCLC Cells via the Histone Demethylases, LSD1 and PLU-1. *Mol. Cancer Res.* **16**, 1458 (2018).
173. Sorna, V. *et al.* High-throughput virtual screening identifies novel N'-(1- phenylethylidene)-benzohydrazides as potent, specific, and reversible LSD1 inhibitors. *J. Med. Chem.* **56**, 9496–9508 (2013).
174. Mohammad, H. P. P. *et al.* A DNA Hypomethylation Signature Predicts Antitumor Activity of LSD1 Inhibitors in SCLC. *Cancer Cell* **28**, 57–69 (2015).
175. Wang, Z. Z.-N. *et al.* Inhibition of H3K4 demethylation induces autophagy in cancer cell lines. *Biochim. Biophys. Acta - Mol. Cell Res.* **1864**, 2428–2437 (2017).
176. Magliulo, D., Bernardi, R. & Messina, S. Lysine-specific demethylase 1A as a promising target in acute myeloid leukemia. *Front. Oncol.* **8**, (2018).
177. Chou, T.-C. Theoretical basis, experimental design, and computerized simulation of synergism and antagonism in drug combination studies. *Pharmacol. Rev.* **58**, 621–81 (2006).
178. Smitheman, K. N. *et al.* Lysine specific demethylase 1 inactivation enhances differentiation and promotes cytotoxic response when combined with all-trans retinoic acid in acute myeloid leukemia across subtypes. *Haematologica* **104**, 1156–1167 (2019).

179. Romo- Morales, A., Aladowicz, E., Blagg, J., Gatz, S. A. & Shipley, J. M. Catalytic inhibition of KDM1A in Ewing sarcoma is insufficient as a therapeutic strategy. *Pediatr. Blood Cancer* **66**, (2019).
180. Chou, T.-C. T.-C. Drug Combination Studies and Their Synergy Quantification Using the Chou-Talalay Method. *Cancer Res.* **70**, 0008-5472.CAN-09–1947 (2010).
181. Barth, J. *et al.* LSD1 inhibition by tranilcypromine derivatives interferes with GFII-mediated repression of PU.1 target genes and induces differentiation in AML. *Leukemia* **33**, 1411–1426 (2019).
182. Hatzi, K. *et al.* Histone demethylase LSD1 is required for germinal center formation and BCL6-driven lymphomagenesis. *Nat. Immunol.* **20**, 86–96 (2019).
183. Vinyard, M. E. *et al.* CRISPR-suppressor scanning reveals a nonenzymatic role of LSD1 in AML. *Nat. Chem. Biol.* **15**, 529–539 (2019).
184. Zhang, Y. *et al.* CRISPR/gRNA-directed synergistic activation mediator (SAM) induces specific, persistent and robust reactivation of the HIV-1 latent reservoirs. *Sci. Rep.* **5**, 1–14 (2015).
185. Silvana Konermann^{1, 2, 3, 4,*}, Mark D. Brigham^{1, 2, 3, 4,*}, Alexandro E. Trevino^{1, 2, 3, 4}, Julia Joung^{1, 4}, Omar O. Abudayyeh^{1, 2, 3, 4}, Clea Barcena^{1, 2, 3, 4}, Patrick D. Hsu^{1, 2, 3, 4}, Naomi Habib¹, Jonathan S. Gootenberg^{1, 2, 3, 4, 5}, Hiroshi Nishimasu, and F. *et al.* Genome-scale transcriptional activation by an engineered CRISPR-Cas9 complex. *Nature* **517**, 583–8 (2015).
186. Figueroa, M. E. *et al.* Leukemic IDH1 and IDH2 mutations result in a hypermethylation phenotype, disrupt TET2 function, and impair hematopoietic differentiation. *Cancer Cell* **18**, 553–67 (2010).
187. Molenaar, R. J. *et al.* Clinical and biological implications of ancestral and non-ancestral IDH1 and IDH2 mutations in myeloid neoplasms. *Leukemia* **29**, 2134–42 (2015).
188. Wang, C. *et al.* IDH2R172 mutations define a unique subgroup of patients with angioimmunoblastic T-cell lymphoma. *Blood* **126**, 1741–52 (2015).
189. Yan, H. *et al.* IDH1 and IDH2 Mutations in Gliomas. *N. Engl. J. Med.* **360**, 765–773 (2009).
190. Pansuriya, T. C. *et al.* Somatic mosaic IDH1 and IDH2 mutations are associated with enchondroma and spindle cell hemangioma in Ollier disease and Maffucci syndrome. *Nat. Genet.* **43**, 1256–61 (2011).
191. DiNardo, C. D. *et al.* IDH1 and IDH2 mutations in myelodysplastic syndromes and role in disease progression. *Leukemia* **30**, 980–984 (2016).
192. Yang, H., Ye, D., Guan, K.-L. & Xiong, Y. IDH1 and IDH2 mutations in tumorigenesis: mechanistic insights and clinical perspectives. *Clin. Cancer Res.* **18**, 5562–71 (2012).
193. Chen, X. *et al.* The clinical significance of isocitrate dehydrogenase 2 in esophageal squamous cell carcinoma. *Am. J. Cancer Res.* **7**, 700–714 (2017).
194. Guirguis, A. *et al.* Use of gene expression profiles to stage concurrent endometrioid tumors of the endometrium and ovary. *Gynecol. Oncol.* **108**, 370–6 (2008).

195. Altenberg, B. & Greulich, K. O. Genes of glycolysis are ubiquitously overexpressed in 24 cancer classes. *Genomics* **84**, 1014–20 (2004).
196. Wu, D. Isocitrate dehydrogenase 2 inhibits gastric cancer cell invasion via matrix metalloproteinase 7. *Tumour Biol.* **37**, 5225–30 (2016).
197. Lv, Q. *et al.* Altered expression levels of IDH2 are involved in the development of colon cancer. *Exp. Ther. Med.* **4**, 801–806 (2012).
198. Tian, G.-Y. *et al.* Isocitrate Dehydrogenase 2 Suppresses the Invasion of Hepatocellular Carcinoma Cells via Matrix Metalloproteinase 9. *Cell. Physiol. Biochem.* **37**, 2405–14 (2015).
199. Calvert, A. E. *et al.* Cancer-Associated IDH1 Promotes Growth and Resistance to Targeted Therapies in the Absence of Mutation. *Cell Rep.* **19**, 1858–1873 (2017).
200. Wahl, D. R. *et al.* Glioblastoma Therapy Can Be Augmented by Targeting IDH1-Mediated NADPH Biosynthesis. *Cancer Res.* **77**, 960–970 (2017).
201. Zarei, M. *et al.* Posttranscriptional Upregulation of IDH1 by HuR Establishes a Powerful Survival Phenotype in Pancreatic Cancer Cells. *Cancer Res.* **77**, 4460–4471 (2017).
202. Lin, Y. *et al.* The SNAG domain of Snail1 functions as a molecular hook for recruiting lysine-specific demethylase 1. *EMBO J.* **29**, 1803–16 (2010).
203. Chandhok, N. S. & Prebet, T. Insights into novel emerging epigenetic drugs in myeloid malignancies. *Ther. Adv. Hematol.* **10**, 2040620719866081 (2019).
204. The Structural Genomics Consortium. GSK-LSD1. A chemicalprobe for LSD1. *Chemical Probes 2014* Available at: <https://www.thesgc.org/chemical-probes/GSK-LSD1>. (Accessed: 11th September 2019)
205. Mohammad, H. *et al.* Inhibition Of LSD1 As a Therapeutic Strategy For The Treatment Of Acute Myeloid Leukemia. *Blood* **122**, (2013).
206. Sankar, S. *et al.* Mechanism and relevance of EWS/FLI-mediated transcriptional repression in Ewing sarcoma. *Oncogene* **32**, 5089–5100 (2013).
207. Theisen, E. R. *et al.* Reversible inhibition of lysine specific demethylase 1 is a novel anti-tumor strategy for poorly differentiated endometrial carcinoma. *BMC Cancer* **14**, 752 (2014).
208. Gupta, S. *et al.* Reversible lysine-specific demethylase 1 antagonist HCI-2509 inhibits growth and decreases c-MYC in castration- and docetaxel-resistant prostate cancer cells. *Prostate Cancer Prostatic Dis.* **19**, 349–357 (2016).
209. Sehrawat, A. *et al.* LSD1 activates a lethal prostate cancer gene network independently of its demethylase function. *Proc. Natl. Acad. Sci. U. S. A.* **115**, E4179–E4188 (2018).
210. Maiques-Diaz, A. *et al.* Enhancer Activation by Pharmacologic Displacement of LSD1 from GFI1 Induces Differentiation in Acute Myeloid Leukemia. *Cell Rep.* **22**, 3641–3659 (2018).

211. Chen, Y. *et al.* Crystal structure of human histone lysine-specific demethylase 1 (LSD1). *Proc. Natl. Acad. Sci. U. S. A.* **103**, 13956–61 (2006).
212. Sonnemann, J. *et al.* LSD1 (KDM1A)-independent effects of the LSD1 inhibitor SP2509 in cancer cells. *Br. J. Haematol.* **183**, 494–497 (2018).
213. Mould, D. P., McGonagle, A. E., Wiseman, D. H., Williams, E. L. & Jordan, A. M. Reversible Inhibitors of LSD1 as Therapeutic Agents in Acute Myeloid Leukemia: Clinical Significance and Progress to Date. *Med. Res. Rev.* **35**, 586–618 (2015).
214. Luka, Z., Moss, F., Loukachevitch, L. V., Bornhop, D. J. & Wagner, C. Histone Demethylase LSD1 Is a Folate-Binding Protein. *Biochemistry* **50**, 4750–4756 (2011).
215. Kooistra, S. M. & Helin, K. Molecular mechanisms and potential functions of histone demethylases. *Nat. Rev. Mol. Cell Biol.* **13**, 297–311 (2012).
216. Perillo, B. *et al.* DNA Oxidation as Triggered by H3K9me2 Demethylation Drives Estrogen-Induced Gene Expression. *Science (80-.)*. **319**, 202–206 (2008).
217. Amente, S. *et al.* LSD1-mediated demethylation of histone H3 lysine 4 triggers Myc-induced transcription. *Oncogene* **29**, 3691–3702 (2010).